AD-A178 299 CHAOTIC BEHAVIOUR IN QUANTUM DYNAMICS(U) CENTRO DI CULTURA SCIENTIFICA A VOLTA COMO (ITALY) G CASATI ET AL. DEC 86 R/D-4183-PH DAJA45-83-C-0050 1/2

UNCLASSIFIED F/G 20/10 NL

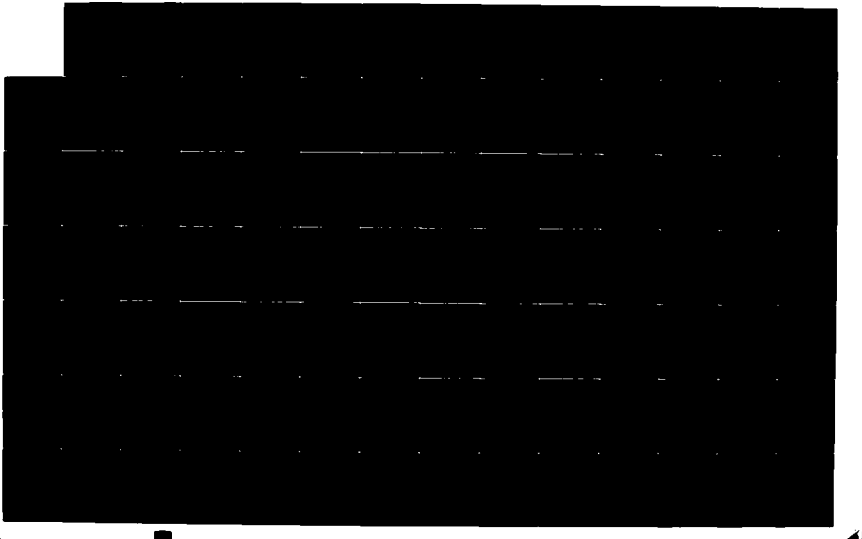

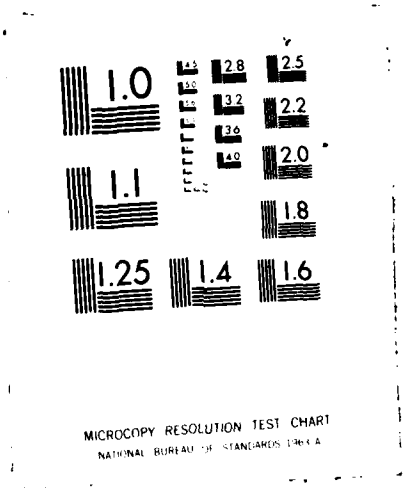
1.0
1.1
1.25
1.4
1.6
2.8
3.2
3.6
4.0
2.5
2.2
2.0
1.8
MICROCOPY RESOLUTION TEST CHART
NATIONAL BUREAU OF STANDARDS 1963 A

(9)

AD

CHAOTIC BEHAVIOUR IN QUANTUM DYNAMICS

Final Technical Report

by

Giulio Casati and Italo Guarneri

December, 1986

United States Army
EUROPEAN RESEARCH OFFICE OF THE U.S. ARMY

London England

CONTRACT NUMBER DAJA45-83-C-0050

Giulio Casati

AD

CHAOTIC BEHAVIOUR IN QUANTUM DYNAMICS

Final Technical Report

by

Giulio Casati and Italo Guarneri

December, 1986

United States Army
EUROPEAN RESEARCH OFFICE OF THE U.S. ARMY

London England

CONTRACT NUMBER DAJA45-83-C-0050

Giulio Casati

UNCLASSIFIED

SECURITY CLASSIFICATION OF THIS PAGE *(When Data Entered)*

RAD 4183-PH

REPORT DOCUMENTATION PAGE		READ INSTRUCTIONS BEFORE COMPLETING FORM
1. REPORT NUMBER	2. GOVT ACCESSION NO. AD-A175 299	3. RECIPIENT'S CATALOG NUMBER
4. TITLE *(and Subtitle)* Chaotic Behaviour in Quantum Dynamics		5. TYPE OF REPORT & PERIOD COVERED Final Technical Report Sept '83 - Nov '86
		6. PERFORMING ORG. REPORT NUMBER
7. AUTHOR(s) Giulio Casati and Italo Guarneri		8. CONTRACT OR GRANT NUMBER(s) DAJA45-83-C-0050
9. PERFORMING ORGANIZATION NAME AND ADDRESS Centro di Cultura Scientifica A. Volta Villa Olmo, Como, Italy		10. PROGRAM ELEMENT, PROJECT, TASK AREA & WORK UNIT NUMBERS 61102A 1L161102BH57-07
11. CONTROLLING OFFICE NAME AND ADDRESS USARDSG-UK Box 65, FPO NY 09510-1500		12. REPORT DATE December, 1986
		13. NUMBER OF PAGES 74
14. MONITORING AGENCY NAME & ADDRESS *(if different from Controlling Office)*		15. SECURITY CLASS. *(of this report)* Unclassified
		15a. DECLASSIFICATION/DOWNGRADING SCHEDULE

16. DISTRIBUTION STATEMENT *(of this Report)*

Approved for Public Release; distribution unlimited

17. DISTRIBUTION STATEMENT *(of the abstract entered in Block 20, if different from Report)*

18. SUPPLEMENTARY NOTES

19. KEY WORDS *(Continue on reverse side if necessary and identify by block number)*

Quantum Chaos, Energy Level Statistics. Quantum Kicked Rotator. Anderson Localization. Microwave Excitation of Hydrogen Atoms. Keldish Parameter. Quantum Diffusion.

20. ABSTRACT *(Continue on reverse side if necessary and identify by block number)*

We present analytical and numerical results on the mechanism of excitation and ionization of hydrogen atoms under microwave fields. In particular we predict the existence of a critical value of the microwave field, *the quantum delocalization border*, above which the quantum packet delocalizes

DD FORM 1 JAN 73 1473 EDITION OF 1 NOV 65 IS OBSOLETE

UNCLASSIFIED

SECURITY CLASSIFICATION OF THIS PAGE *(When Data Entered)*

and strong excitation and ionization takes place.

Below the quantum border, the packet is localized even though the corresponding classical system is chaotic and obeys a diffusion equation.

Our studies reveal some other unexpected new features of quantum dynamics which also could be observed in laboratory experiments and provides a quantum theory for subthreshold ionization.

1. Background: Review of Basic Concepts

This final report illustrates the results of a three-years research program on Quantum Chaos. When our program was started this subject was still in a native stage, dominated by the pioneering work of a restricted number of scientists. By now, instead, it has grown into a most active field of research, and keeps drawing increasing attention by scientists working in widely different areas, ranging from pure theoretical to experimental ones. International conferences and workshops on Quantum Chaos have been held, and others are being announced, witnessing the liveliness and the interest of the topic.

Curiously enough, despite this great development the very definition of Quantum Chaos is still a controversial point. A very neutral statement is that quantum chaos is concerned with the properties of quantum systems that are chaotic in the classical limit. In order to get a more precise formulation of the problems involved and to give a clear exposition of our contributions, we shall first review some basic concepts and keywords.

1.1 Classical Chaos.

Chaos is today a protagonist in all problems that can be treated by classical mechanics. The appearance of chaos is connected with an extreme type of instability that often appears in nonlinear classical systems. Chaotic systems are in many senses the very opposite of integrable systems. The orbits in phase space of one integrable system are bound to smooth surfaces whose dimension equals the number of freedoms, called invariant tori. For this reason, integrable systems are

very stable; a small error in specifying the initial data involves an error in predicting the state at a later time that grows linearly with time, so that finite-precision algorithms allow for a reliable computation of orbits. Integrable systems are well known, being the sole class of nonlinear systems that are amenable to analytical solution.

Generic Hamiltonian systems can be regarded as perturbations of integrable systems - i.e., their Hamiltonian is obtained by adding some correction to an integrable Hamiltonian. It is now known that in this case some orbits are still confined (and densely fill) on some invariant surfaces that can be looked upon as distorted remnants of the supply of invariant tori that is available in the unperturbed case. The celebrated KAM theorem characterizes this surviving set of 'regular' orbits, that becomes narrower as the perturbation strength-or just the energy, in the conservative case-increases.

Chaos became a keyword in classical mechanics when the behaviour of the other orbits - i.e., those that are no longer confined to smooth "tori"-was studied in some detail. Indeed, it turned out that these orbits are usually exponentially unstable - i.e., errors in the initial data propagates exponentially in time. This makes hopeless the prediction of individual orbits by finite precision algorithms. If the state of the system moving along a typical chaotic orbit is recorded with a finite precision at a prescribed sequence of instants, one gets a string of data that is indistinguishable from a random string - i.e., from a string of numbers generated by a random device. Analysis of single orbits is therefore meaningless; instead, the behaviour of ensembles of orbits turns out to be describable, in statistical terms, and it is found that the ensemble evolution is, in a suitable approximation, a diffusion process. Whereas regular orbits lie on invariant tori and are therefore confined forever to a negligible region of phase space chaotic orbits have a tendency to explore the whole available phase space in a diffusive way. Bounds on this pervasive behaviour are however posed by the survival of some tori, that can substantially slow down or even stop the diffusion.

1.2 Model systems - Billiards and the kicked Rotator

The onset of chaos in Hamiltonian systems is in most cases unambiguously detected by numerical simulation, but the theoretical

analysis of this process is still far from being complete. For this reason, in order to understand at least the qualitative features of chaotic dynamics it has proved very useful to consider simplified models. Not being modelled after any actual phenomenological situation, they are abstract constructions; yet, they exhibit the essential features of chaos, bare of complications that are usually superimposed in realistic cases. A first example is provided by billiards, i.e., particles bouncing elastically inside suitable plane regions. Rigorous mathematical results have shown that, if the boundary of the billiard is suitably shaped, then the simple Hamiltonian system so defined displays strongly chaotic properties. Unlike generic Hamiltonian systems in which both chaotic and regular orbits coexist, the latter becoming negligible only by suitably increasing the energy, billiards are fully chaotic - i.e., regular orbits have zero measure - at any energy.

As we shall emphasize later, the most impressive phenomenological manifestations of chaos are offered by Hamiltonian systems subject to external perturbations periodic in time. Within this class, one model system dominates the scene: the δ-kicked rotator, also called standard, or Chirikov's map, by more mathematically oriented authors. This is the 1-dim. Hamiltonian system described by the time-dependent Hamiltonian

$$H = P^2/2 + k\cos\theta \sum_n \delta(t - nT); \quad 0 \leq \leq 2\pi$$

Physically, it is a pendulum whose weight is 'turned up' in an impulsive, δ-like way, at regularly operated instants of time. It can obviously be looked upon, as a perturbation of a free rotator ($k=0$) and indeed, the whole scenery of KAM theory is here realized. The object of interest here is the discrete-time orbit $p(nT)$, $\theta(nT)$, which, in the unperturbed case is generically bound and densely fills a regular curve. As k is increased, the set of 'regular' orbits shrinks and, for $kT>1$, almost all orbits become chaotic. A remarkable indication of the stochatic nature of the motion in this case is offered by the behaviour of the kinetic energy $T(nT) = \langle P^2(nT)/2 \rangle$ averaged over the phase θ; this grows in a diffusive way $\sim Dn$ with $D \approx (kT)^2/2$.

1.3 Phenomenological Relevance of Classical Chaos

The appearance of irregular orbits may dramatically change the phenomenological behaviour of a given system. Indeed, a major impulse to the study of chaotic dynamics was given by the necessity of predicting the precise conditions under which dangerous instabilities develop in physical situations that are amenable to a classical description, such as, e.g., beams of accelerated particles or confined plasmas. A vivid illustration of the effect of chaos on real physics is provided by the very problem that was the most important part of the research described here : an hydrogen atom in an external microwave field. Deferring a detailed analysis to a later section, we shall give here a qualitative explanation why chaos is essential in the classical behaviour of such an atom. The unperturbed atom is obviously an integrable system. As soon as the external perturbation is turned on (the microwave field), some of the orbits become irregular and start wandering away. For not too large perturbation strength, residual invariant tori persist that prevent this diffusion from leaving the 'bound' state subspace of the whole phase space. However, for any given initial (bound) state of the atom, a value of the external field will be found, for which the orbit leaving from this state will no longer meet any such impediment and will therefore diffuse away until the atom ionizes. This simple picture leads to predict that for atoms prepared in a fixed initial state under a field of fixed frequency there is a threshold in the field strength, across which the ionization rate changes abruptly due to the onset of unbounded diffusion.

1.4 Quantum Limitations to Classical Chaos in Conservative Systems. Level Statistics.

Why should a quantum physicist care about classical chaos? In the light of the above sketched picture of the microwave ionization of hydrogen atoms, this question has at least one immediate answer because just the failure of certain classical predictions about the hydrogen atoms was one starting point in the edification of quantum mechanics. Nevertheless, on account of the correspondence principle, one can predict that by going up to sufficiently high quantum numbers

quantum and classical predictions will agree. It was however apparent since the beginning of studies on chaotic dynamics that the correspondence between a quantum system and its classical limit may have some subtle aspect when the latter is chaotic. For example, a chaotic conservative classical system with a bounded configuration space (such as a billiard) display a highly non-recurrent behaviour: by this we mean that, even though it comes infinitely often arbitrarily close to its initial state (Poincare recurrence), nevertheless there is no upper bound on the return times, that will take arbitrarily large values as the system moves along a given orbit. The quantum analog of any such system will have a pure point energy spectrum; the quantum evolution will then be quasi-periodic, hence recurrent. On the other hand, the correspondence principle requires that the recurrent quantum behaviour goes into the highly non recurrent classical one as $h \to 0$!

An obvious way out to this apparent contradiction is that recurrence (or non-recurrence) is a long-time property, and the classical limit $\hbar \to 0$ can be non uniform in time. In other words, for a given quantum state which is quasi-classical one can expect at best that quantum dynamics looks like the classical over just a finite time scale $\tau(\hbar)$ so that $\tau(\hbar) \to \infty$ as $\hbar \to 0$. One has then a sort of chaos confined to a bounded time scale, so that "Transient Chaos" or "Pseudochaos" appear more appropriate expressions.

Despite this severe limitation placed by quantum mechanics on classical chaos in the conservative case - the nonconservative case will be discussed below - there are still reasons why quantized conservative chaotic systems should be made the object of a careful investigation. Integrable systems played a central role in the early stages of quantum mechanics. Indeed, the Bohr-Sommerfeld quantization procedure is only applicable to integrable systems.

Instead, the present-day form of quantum mechanics does no longer suffer from such a limitation, and we can safely quantize any conservative Hamiltonian system, regardless of its integrable or chaotic nature. Nevertheless, semiclassical quantization rules still play an important role, in that they are often the only reasonable way to get quantitative informations about the higher part of the energy spectrum. These rules are today rigorously deduced from the Schroedinger equation in the form of the EWBK rules. Again, this theory works only under the explicit assumption that the system at hand has an integrable classical

limit! A natural problem is then whether semiclassical methods can be used also in the non-integrable case in order to get infromation about the semiclassical part of the spectrum.

It was suggested by Berry [1] that the integrable or non-integrable character of classical dynamics is mirrored by the statistical type of the corresponding energy spectra. Given a spectrum whatsoever, one can define the associated level spacing distribution function P(s,E) as follows. Given a $\Delta>0$, one takes only those eigenvalues $E_n(\hbar)$ that lie between $E-\Delta$ and $E+\Delta$ and forms the string s_n of the spacings $E_{n+1} - E_n$, measured in units of their average value. These numbers s_n will be distributed according to an hystogram $N(s,\hbar,E)$ giving, for any s the relative frequency of occurence, within the string, of spacings between s and s+ds. Letting then $\hbar->0$, $N(s,\hbar,E)$ would tend to a limit P(s,E).

On account of numerical computations and analytical arguments, it is currently assumed that, if the system has an integrable classical limit, P(s,E) is given by the Poisson distribution e^{-S}. Instead, if the system has a chaotic classical limit, P(s) should be the same as the Wigner distribution valid for eigenvalues of random matrices in the Gaussian orthogonal ensemble, that is given almost exactly by

$$P(s) = (\Pi/2)S \exp(-\Pi s^2/4)$$

The most obvious difference between these two forms of P(s) is that, in the latter, one has level repulsion - i.e., the frequency of small spacings is vanishingly small.

1.5 Quantum Chaos for Periodically Perturbed Hamiltonian Systems.

In the section 4 above a reason was pointed out, why the long -time behaviour of quantum and classical conservative systems in the presence of chaos cannot be expected to be the same. However, the physically most interesting cases such as the H-atom of sec. 1.3, do not belong to this class, because their Hamiltonian is periodic in time.

In that case, quantum dynamics is no longer defined by an energy spectrum, but rather by the quasi-energy (q.e.) spectrum. While in the conservative case the energy spectrum was known to be pure point, there

is now no reason to expect that the q.e. spectrum should be pure point in all cases; the question of persistence of chaos or of some of its effects in quantum mechanics in this nonconservative case must then be started afresh.

The first results were obtained by Casati et al. [4] who subjected the quantum version of the δ kicked rotor sketched in sec. 1.2 to a numerical analysis,with the following remarkable results. It will be recalled that the character of the classical motion is defined by the quantity K=kT. In the quantum case, the dynamics depends on two parameters $k_q=k\hbar^{-1}$ and $T_q=T\hbar$. If T_q is a rational multiple of 4π ($T_q= 4\pi\ m/n$, m, n integers) the quantum rotor behaves resonantly, and its average kinetic energy $E(t)=\langle\psi(t)\left|-(\hbar^2/2)d^2/d\theta^2\right|\psi(t)\rangle$ increases with time according to an asymptotically t^2 law. This resonance has no classical analog and is not therefore related to classical chaos. Therefore, the search for quantum chaos must resort to <u>irrational</u> values of $(4\pi)^{-1}T_q$. The response of computer experiments was that E(t) follows the classical diffusive law $E(t)\propto t$ only up to some time t_β, after which it enters a steady oscillatory state. In other words, according to numerical experiments one has a <u>quantum suppression of chaotic diffusion.</u>

1.6 Relevance of Classical Analisys to the Problem of Microwave Ionization

The other nonconservative system discussed in this report - the H-atom in a microwave field - had never been subjected to quantum analisys, neither theoretical nor computational, up to the start of our program. Nevertheless, it presented a unique occasion to check the possible survival of chaotic effects in quantum mechanics, because laboratory experiments on microwave ionization for highly excited H-atoms had been performed since 1974 by Bayfield and Koch, [12] who succeeded in exposing a relevant ionization for low fields and frequencies well below the 1-photon threshold. No satisfactory quantum analysis was available for this phenomenon. After the work of Jensen [19,20] the idea took place, that quantitative predictions in agreement with experiments might be provided by a classical theory; indeed,

experiments carried out in parallel with classical analysis gave an overall satisfactory response. According to such results, quantum mechanics does indeed follow classical mechanics so closely, as to reproduce even chaotic effects.

2. Statement of Problems

The rapid overview of the state of the art we gave in the previous section should have put in evidence that current problems in Quantum Chaos belong to two main areas: those involving the spectral properties of conservative systems and those investigating the dynamics of *externally perturbed systems*.

In this report we shall present a number of contributions we have given to both fields.

2.1 The conservative case

Our starting point here was Berry's hypothesis, that the statistics of energy levels should be essentially different in the integrable and in the chaotic case. Numerical work by Bohigas and other authors [1] supports the generally accepted conclusion, that the level statistics for a quantum system which is chaotic in the classical limit is well described by random matrix theory: in particular, under the assumption of time reversal invariance one can assume that fluctuation properties in the spectrum will obey the same statistics as in the case of random matrices in the so called Gaussian Orthogonal ensemble. This contention was tested, by analyzing "1st order" statistics- i.e., statistical properties involving pair correlations between different levels, such as the spacing distribution P(s), and also higher order statistics, involving multiple correlations, such as the Δ-3 statistics to be defined later. Therefore, chaotic systems display *a remarkable universality* in their spectral statistics.

Is there any universal statistics for the integrable case? Early results suggested an affirmative answer; indeed, Berry gave an argument

according to which 'generic' integrable systems have a Poisson distribution of spacings. On the grounds of this argument it has been conjectured that the fluctuation properties of the 'integrable' spectrum should be the same as for a Poisson process. According to this conjecture, the energy levels of an integrable system, despite their predictability by more or less simple semiclassical rules, should make up a completely random sequence!

Even though this conjecture was supported by numerical results insofar as the level spacing distribution was involved, there was neither theoretical nor numerical evidence that also higher order statistics should be Poisson-like. Therefore, we posed the following problem:
to analyze higher order statistical properties - in particular, the δ-3 statistics - of the sequence of energy levels of an integrable system, in order to check whether Poisson statistics is still obeyed.

2.2 The Time Dependent Case

Our current understanding of the interaction between matter and radiation is provided by quantum mechanics, the development of which was indeed prompted by the incapability of classical mechanics to account for the response of microsystems to radiation fields. In simple cases, a sufficient approximation for the behaviour of an atom or a molecule to an external electromagnetic field can be obtained by considering the latter as a classical field; in these cases, the quantum dynamics is described by a time dependent Schroedinger equation.

When the intensity of the fields is sufficiently small, this can be handled by time-dependent perturbation theory, that leads to describe the interaction with radiation in terms of multiphoton processes. However, the present state of physical research often confronts us with situations in which it is important to predict the response of atoms or molecules to intense fields; moreover, experimental results indicate that the dynamics in such cases may be qualitatively very different than one would guess on the grounds of perturbatively based intuitions. A typical example is Bayfield and Koch's experiment, which exposed strong ionization in a situation in which ~ 100 photons would be required.

In the absence of a method whatsoever, by which the Schroedinger

equation can be at least approximately solved for the large fields required, the best one can do in order to get some theoretical indication is just coming back to classical mechanics, and indeed in physically relevant cases such as microwave ionization of hydrogen atom in an external field shows that a chaotic threshold exist. For field strength exceeding this threshold, a qualitative change in the dynamics occurs, that leads to intense ionization due to a diffusive-like motion of the electron in the external field. Numerical simulation of the classical model is easily feasible, and a partial comparison of numerical data gotten in this way with results of experiments on real atoms has shown a certain degree of agreement. This fact seems to indicate that in a semiclassical regime, the predictions of classical chaotic dynamics are essentially respected by quantum dynamics. Shall we conclude that classical chaos in time-dependent problems is basically surviving quantization? Certainly not; and the reason is that we know of at least one quantum system - the δ-kicked rotator - in which the fully developed chaos of the classical model is completely suppressed. What are then the reasons why quantum mechanics reacts so differently to classical chaos in these two cases? Answering this question is an essential task, because the existence of a quantum regime lying beyond the perturbative regime in which the motion has some 'diffusive' features would open a new field of immense potential interest. We threfore need some theory that may be able to set precise quantitative conditions for the applicability of semiclassical approximations when the classical motion is chaotic. The following program should then be fulfilled:

1) To build a simple model for a H atom in a microwave field, that is amenable to both classical and quantum solution by computer simulation

2) to compare the classical and quantum motion in different parameter regions, ranging from extreme semiclassical to pure quantum ones in order to assess the modifications imposed by quantum mechanics on the classical chaotic behaviour

3) to identify under what conditions these modifications take the form of a complete suppression of classical chaotic effects.

3. Semiclassical Theory of Electron Excitation.

3.1. Classical Dynamics of Electron Excitation

In this section we will develop the classical theory of the excitation of an hydrogen atom in a linearly polarized monochromatic electric field.

Here and in the following we will use atomic units, in which the Hamiltonian takes the form:

$$H = P^2/2 - 1/r + \epsilon z \cos\omega t \qquad (1a)$$

where ϵ and ω are the field strength and frequency respectively and the z-coordinate is measured along the direction of the external field. The classical dynamics associated with (1a) is conveniently studied in parabolic coordinates since the unperturbed dynamics is separable in these coordinates. Accordingly, action-angle variables (n_1, n_2, m, λ_1, λ_2,ψ) can be introduced /30/, in which the Hamiltonian takes the form:

$$H = -1/2n^2 + \epsilon z\,(n_1, n_2, m, \lambda_1, \lambda_2)\cos\omega t\,; \qquad n = n_1 + n_2 + |m|. \qquad (1b)$$

Owing to axial symmetry, m (which is the z-component of the angular momentum) is an integral of the motion; therefore, (1) describes an essentially 2-dimensional model.

The function $z(n_1, n_2, m, \lambda_1, \lambda_2)$ can be expanded in a double Fourier series in the angle variables λ_1, λ_2:

$$z = \sum_{k_1 k_2} z_{k_1 k_2}(n_1, n_2, m)\, e^{i(k_1\lambda_1 + k_2\lambda_2)} \qquad (1c)$$

The coefficients $z_{k_1 k_2}$ can be found as shown in Appendix I, and are given by/18/:

$$z_{k_1k_2} = [n^2/(k_1 + k_2)]\,[\mu_2 J_{k_1}(\mu_1 k_1 + k_2)J'_{k_2}(\mu_2(k_1 + k_2)) - \mu_1 J'_{k_1}(\mu_1(k_1 + k_2))J_{k_2}(\mu_2(k_1 + k_2))]\,; \qquad \text{for } k_1 + k_2 \neq 0 \tag{1d}$$

$$z_{k_1,-k} = \begin{cases} 0 & \text{for } k \neq 0 \\ 3n(n_1 - n_2)/2 & \text{for } k = 0 \end{cases}$$

Here J_k are Bessel functions of the first kind and J'_k their derivates. The dependence of $z_{k_1k_2}$ on n_1, n_2, m is embodied in the parameters μ_1, μ_2, which are defined by

$$\mu_{1,2} = (n_{1,2})^{1/2}\,(n_{1,2} + |m|)^{1/2}/n\,. \tag{1e}$$

According to standard semiclassical approximation theory /28/, $z_{k_1k_2}$ give semiclassical values of dipole matrix elements for transitions $n_{1,2} \rightarrow n'_{1,2} = n_{1,2} + k_{1,2}$. The element $z_{0,0}$, which is just the average of z over the unperturbed torus labelled by n_1, n_2, m, yields the standard quantum mechanical expression for the linear Stark effect.

If the electron is initially in an "almost one-dimensional" state, i.e., in a state with $n_1 \gg n_2$, $n_1 \gg m$, then in (1a-1e) we can assume $\mu_1 = 1$, $\mu_2 = 0$. In that case, the dynamics will be described in first approximation by the one-dimensional Hamiltonian

$$H = -1/2\,n^2 + \epsilon n^2 \cos\omega t\,[3/2 - 2\textstyle\sum_k J'_k(k)\,k^{-1}\cos k\lambda] \tag{2}$$

which is just the Hamiltonian, in action-angle variables, for an electron moving along the positive z axis/17,20/:

$$H = p^2/2 - 1/z + \epsilon z \cos\omega t\,. \qquad z \geq 0 \tag{2a}$$

We start our analysis with this simplified Hamiltonian (2). Later in

this section we shall discuss the validity of this one-dimensional approximation, i.e. we shal discuss to what extent the one-dimensional hamiltonian (2) is adequate in order to describe the evolution of quasi one-dimensional initial states under the full Hamiltonian (1).

Under appropriate conditions, the classical system described by the Hamiltonian (2) undergoes a transition to chaotic dynamics. By this we mean that a deep change occurs in the nature of orbits, which, above a certain perturbation strength, become extremely sensitive and complicated and wander erratically in phase space. This irregular motion, if described in the unperturbed actions space, has a diffusive character and leads to fast ionization. Quantitative conditions for the onset of chaotic dynamics can be obtained by means of the resonance overlapping criterion /17,20/. The starting point of this analysis is realizing that the external field will more effectively perturb the undisturbed motion at first order resonances, i.e., at values n of the unperturbed actions such that the external frequency ω resonates with some harmonic of the unperturbed electron motion. These values of n are such that $s\Omega(n) = \omega$ with s an integer and $\Omega(n)$ the angular frequency (Kepler frequency) of the unperturbed motion:

$$\Omega(n) = dH_0/dn = 1/n^3$$

First order resonances are then given by $n_s = (s\omega^{-1})^{1/3}$. However, despite the the fact that for these values n_s the perturbation is very effective, as soon as it manages to drive the motion away from one unperturbed resonant orbit its effect becomes weaker, and nonlinear stabilization may occur. In that case, the motion keeps in a neighborhood (a "resonance region") of the original unperturbed orbit.

However, if the perturbation is sufficiently strong, the motion can be driven so far away from the original resonant value of the action, that it can fall under the influence of another nearby resonance. There, the same process may repeat, so that the orbit may wander in action space in a diffusive way.

A quantitative estimate of the perturbation strength which is necessary in order that this may happen is gotten by evaluating the

width of the various resonance regions and then by requiring that nearby regions overlap /17/.

The analysis just outlined can be applied to model (2); it is then found that for $\omega_0 = \omega n_0^3 > 1$ (where n_0 is the initial value of the action) and for field strength exceeding a critical value ϵ_{cr}

$$\epsilon_0 = \epsilon n_0^4 > \epsilon_{cr} \approx 1/(50\ \omega_0^{1/3}) \qquad (3)$$

all resonance regions corresponding to $n_s \geq n_0$ do overlap. Then an orbit leaving with action n_0 in a region of phase space where both $\omega_0 > 1$ and (3) are satisfied will diffuse indefinitely and eventually ionize.

Notice that in (3) we have introduced rescaled values $\epsilon_0 = \epsilon n_0^4$ for field and $\omega_0 = \omega n_0^3$ for frequency. The usefulness of this scaling is due to the fact that classical dynamics depends on n_0 only via these variables since, as can be readily checked, changing the initial n_0 by some factor will change the solution $n(t)$ at any later time by the same factor, provided ϵ_0 and ω_0 are kept constant, and time is measured in periods of the field (see also /15/).

We emphasize that estimate (3) is valid only for $\omega_0 > 1$. Indeed for $\omega_0 < 1$, i.e. in that phase space region where ω is smaller than the Kepler frequency, there are no first-order resonant values of n, and the motion is therefore more stable. A transition to chaotic behaviour can still occur/17,20/ due to the finite width of the resonance region associated with $\omega_0 = 1$ but, in order to compute the ϵ_{cr} in this region, also higher-order resonances $s\Omega = p\omega$, $p > 1$ must be taken into account. It is then found that the critical field increases with decreasing ω_0; however, for very low ω_0 static field ionization occurs when $\epsilon_0 > .13$.

Of course, higher order resonances play a role in the chaotic transition also for $\omega_0 > 1$ and, indeed, an approximate account of them is already taken in (3) via the choice of the numerical factor 1/50. /17/. A proper second order analysis/29/ leads to but a small increase in this numerical factor.

In the chaotic regime, $\epsilon_0 > \epsilon_{cr}$, $\omega_0 > 1$ the process of diffusive excitation is conveniently described in statistical terms. Indeed, an equation of the Fokker-Planck type can be derived /17/ :

$$\partial f/\partial \tau = 1/2\ \partial/\partial n\ (D\ \partial f/\partial n) \qquad (4)$$

where $f(n, \tau)$ is the distribution function and τ is the dimensionless time, measured as the number of periods $\tau = \omega t/2\pi$ of the external field. The diffusion coefficient D in quasi-linear approximation is given by

$$D = d\langle(\delta n)^2\rangle/d\tau \approx 2\epsilon_0^2\ n^3/(\omega_0^{7/3}\ n_0) = 2\ \epsilon^2\ n^3/\omega^{7/3} \qquad (5)$$

((4) and (5) were also derived in /20/).(*)

Since D increases with n according to a power law, it is possible to find an exact solution of (4). In order to do this, we must take notice that the stochastic diffusion ruled by (4) can take place only in that part of phase space where the chaotic transition has occurred. Going down to lower and lower action values, one will eventually meet an invariant curve which has not been destroyed; we must therefore look for a solution of (4) satisfying the boundary condition $\partial f/\partial n\,|_{n=\bar{n}} = 0$ of zero flux across the boundary $n=\bar{n}$ of the region of stability. In order to do that, the change of variables $y = n/n_0$, $\bar{\tau} = \tau\epsilon_0^2\omega_0^{-7/3}$ is convenient. Then, as shown in app. II, for $\bar{\tau}\sqrt{y} \ll 1$ and letting $\bar{y} = \bar{n}/n_0$, the solution assumes a sufficiently simple form:

$$f(y,\bar{\tau}) \simeq \{\exp[-(1/\sqrt{y} - 2/\sqrt{\bar{y}} + 1)^2/\bar{\tau}\,] + \exp[-(1/\sqrt{y} - 1)^2/\bar{\tau}\,]\}/[2y^{3/4}\sqrt{(\pi\bar{\tau})}] \qquad (5a)$$

(*) The numerical coefficient 2 in (5) corresponds to the frequency range $1 < \omega_0 < 3$. For $\omega_0 \gg 3$, the asymptotic value of this coefficient must be used, which is near to 3.

As will be seen in section 3, this formula compares with the results of numerical integration of the equations of motion with remarkable success.

The possibility of using this statistical description will play an important role in our subsequent analysis of the ionization process. Indeed, due to the rapid growth with n of the diffusion coefficient, stochastic orbits diffuse so fast towards high values of n that in practice we can assume that they actually ionize- i.e. n becomes infinite- in a finite time. A rough estimate of the ionization time adequate for our present purposes can be gotten from eq. (5):

$$\tau_I \sim n_0^2/D \sim \omega_0^{7/3}/(2\,\epsilon_0^2)\,. \qquad (6)$$

In later sections we'll use expression (6) in order to roughly estimate the diffusive ionization rate $P_I \sim \tau_I^{-1}$.

In the remainder of this section we discuss the validity of the one-dimensional approximation (2). Let's consider first the case when $n_1 \gg n_2$, $n_1 \gg m$ and therefore $\mu_2 \ll 1$. Then, since $z_{k_1,k_2} \sim \mu_2^{|k_2|}$ for large $|k_2|$, the main contribution to the variation of n_2 will be given by terms in (1c,d) with $k_2 = \pm 1$. (Notice that z_{k_1,k_2} give semiclassical matrix elements for transitions with $\Delta n_2 = \pm k_2$. The fast decrease of these matrix elements with small μ_2 when k_2 is large was already remarked in /31/).

For $\epsilon_0 > \epsilon_{cr}$, the phase λ_1 begins to vary chaotically, and this leads to a diffusive change in n_2 also. The diffusion rate for n_2 in quasi-linear approximation can be derived, as shown in /17/, by retaining in (1c) only terms with $k_2 = \pm 1$. One finds that:

$$D_2 \approx n_2\, D(n_2 + |m|)/n^2 \qquad (7)$$

This estimate shows that over the ionization time (6) the change in n_2: $(\Delta n_2)^2 \sim n_2\,(n_2 + |m|) \sim n^2$ appears to be small. This fact indicates that the onset of stochasticity doesn't lead to significant

violations of the one-dimensional approximation.

Along similar lines, we can show that a suitable one-dimensional approximation is valid also in cases when $n_1 \sim |m| >> n_2$. Indeed from (1e) it follows that, in such cases also, $\mu_2 << 1$. Then, upon neglecting μ_2 in (1c,d) we obtain the one-dimensional dynamics for the variable $n_1 = n - |m|$, described by the Hamiltonian

$$H = -1/2n^2 + \epsilon\, n \cos \omega t \left[3(n-|m|)/2 - 2\mu_1 n \sum_k J'_k(\mu_1 k)\, k^{-1} \cos k\, \lambda_1\right] \qquad (8)$$

with $\mu_1 \approx (1-|m|/n)^{1/2}$. We can now apply to this one-dimensional dynamics the resonance analysis, just as was done for (2). From the asymptotic properties of $J_k'(k\mu_1)$ for $k \to \infty$ /32/ it follows that high-k harmonics in (8) become exponentially small as soon as k is so high that $(3/k)^{2/3} \leq m/n$. This means that the resonances of the field with such high harmonics (which take place when $\omega_0 = k$ with $(3/k)^{2/3} \leq m/n$), cannot significantly contribute in the chaotization process. Therefore, when $\omega_0 >> 1$ the transition to chaotic motion is possible only for $m \lesssim m_{cr}$, with

$$m_{cr} = n_0\, (3/\omega_0)^{2/3} \qquad \text{for } \omega_0 >> 1. \qquad (9)$$

For $\omega_0 \sim 1$ we may take $m_{cr} \approx n_0$. At this point we might start afresh the analysis for the Hamiltonian (8) in order to determine the critical field and the diffusion rate under condition (9). However a comparison of (8) with (2) suggests that the results of this analysis shouldn't deviate more than a factor 2 from formulas (4) and (5).

Again, the one-dimensional approximation (8) is not significantly violated over the ionization time; this can be seen at once, because the diffusion rate for n_2 is still given by (7), so that an estimate for the variation Δn_2 similar to the previously established one for (2) holds for the present case.

Further details on the classical dynamics of excitation for the

model (2) will be given in Sec. 3.2, where we shall also discuss the results of numerical simulation of this model.

3.2. Theory of Quantum Localization

The main result of the classical analysis carried out in the previous section was that for sufficiently strong field the classical model (2) exhibits a transition to chaotic motion. After this, the classical distribution $f(n, \tau)$ spreads diffusively in action space, and ionization takes place in a finite time.

We will now tackle the basic question, of what modifications would be imposed on this picture by quantum mechanics. In particular, we will study the behaviour of the quantum probability distribution over the unperturbed levels, which is the quantum analog of $f(n, \tau)$.

Previous studies on periodically perturbed quantum systems that become chaotic in the classical limit - in particular, on the kicked rotator model - brought into the light the localization phenomenon as a typical occurrence. The quasi-energy spectrum is typically a pure point one, and quantum effects lead to a limitation of the classical diffusion and to exponential localization of the probability distribution around the initially excited level n_0 ; which means that in the average, and apart from fluctuations (that may even be rather big ones) the distribution looks like:

$$\bar{\Gamma}_n \propto \exp\left(-2\left|n-n_0\right|/l\right) \tag{10}$$

Here $\bar{\Gamma}_n$ is the time-averaged population on the unperturbed level corresponding to a value n of the quantized action, and l is the localization length.

In the light of these previous findings, it is natural to assume that a similar picture applies also in the present case. Specifically, we will assume that even in the semiclassical region, and when the classical motion is chaotic, a mechanism of quantum limitation of the

chaotic diffusion is working, and that, under suitable conditions, this mechanism will produce a situation analogous to the rotator case. Under such conditions, the part of the q.e. spectrum relevant to our analysis will be quasi-discrete; the small line breadth of its levels will be negligeable on a time scale short in comparison with the very long one associated with multi-photonic ionization. While it remains true that the quantum atom described by (2) will eventually ionize, no matter how small ϵ, nevertheless on the time scale involved by actual experiments the localization phenomenon discussed here will give it a remarkable stability in contrast with the properties of chaotic motion. The obvious premise that localization in hydrogen atom is related to a finite time scale, should not be forgotten throughout this paper.This assumption will be fully supported by the results of our numerical experiments.

Under such assumptions, we shall presently determine the localization length by the simple method described in /3/. In this way, we will be able also to determine the quantitative conditions under which the localization picture actually applies. To this end, let us start with the case of homogeneous classical diffusion, that is, we overlook the variation of D with n.

In the semiclassical regime, the evolution of a quantum state initially coinciding with one unperturbed eigenstate n_0 will initially follow to some extent the classical development of $f(n,\tau)$. Therefore, over the time scale in which this semiclassical approximation holds, the spread of the wave packet over the unperturbed eigenstates will grow in time according to $\Delta n(\tau)\approx(D\tau)^{1/2}$.

However, the discrete character of the quasi-energy spectrum will prevent this diffusive growth from going on indefinitely, as it would in the classical case. The time τ_D after which the discreteness of the quasi-energy spectrum will become manifest can be estimated by $\tau_D \sim N$, where N is the number of q.e. eigenstates significantly excited by the original unperturbed eigenstate; indeed $2\pi/N$ is just the average spacing of q.e. eigenvalues significantly contributing to the packet evolution. Then, the number of unperturbed levels excited by

the wave packet after the time τ_D is $\Delta n(\tau_D) \approx (D\tau_D)^{1/2}$. This means that one unperturbed level contains $N \sim \Delta n(\tau_D)$ q.e. levels and that, *vice-versa*, one q.e. eigenstate "contains" $\sim \Delta n(\tau_D)$ unperturbed levels. The latter number, however, is the maximum spread attainable by the wave-packet, i.e., it coincides with the localization length l. Therefore we get an equation for τ_D:

$$\tau_D \approx \alpha \Delta n(\tau_D) \approx \alpha (D\tau_D)^{1/2} \approx \alpha\, l$$

where we have introduced an undetermined numerical factor α, to be found by numerical experiments /10/. For the rotator model, it was found $\alpha \approx 1$. The same choice for α in the hydrogen atom case would yield

$$l \approx D(n_0) \approx \tau_D \qquad (11)$$

where $D(n_0)$ is given by (5): $D(n_0) = 2\varepsilon_0^2 n_0^3/\omega_0^{-7/3}$.

However this result was obtained under the assumption that D=const., which is justified only in that region where $l \ll n_0$. Instead, for $l \sim n_0$, the dependence of D on n may substantially modify the localization picture, and, if the field strength exceeds some critical value, it may even turn out that localization is *not possible at all*. (A similar "delocalization" phenomenon was investigated and explained on a simple example in Refs. /3,10/).

In order to clarify how delocalization occurs, we need to modify the above method for determining l, in such a way that the dependence of D on n is explicitly taken into account. Therefore, in place of $\Delta n(\tau) \approx (D/n_0)\,\tau)^{1/2}$ *we must substitute* the dependence of Δn on τ that is enforced by the Fokker-Planck equation (4). In this way we find, as a result of the calculations developed in Appendix III, that $\Delta n(\tau)$ is given by:

$$\Delta n(\tau) = [(1 - 2\varepsilon_0^2 \omega_0^{-7/3}\,\tau)^{-2} - 1]^{1/2}\, n_0/\sqrt{3} \qquad (12)$$

By the same argument as above, we can now find τ_D and l from the localization condition $\Delta n(\tau_D) = \tau_D$. However, if ϵ_0 is large enough, the curve $\Delta n(\tau)$ will never intersect the straight line $\alpha\tau$ before exploding at $\tau = \omega_0^{7/3}/3\epsilon_0^2$. When this happens, no localization is possible and this implies unbounded diffusion for the electron. More specifically, in App. III we show that the solution of $\Delta n(\tau_D) = \alpha\tau_D$ gives the localization length l in the form:

$$l \approx \alpha^{-1}(\omega_0^{7/3}/\epsilon_0^2)\, u\, /3 \qquad (13)$$

where u is the least of the two solutions of the equation (*)

$$3\alpha^2(\omega_0^{-7/6}\, n_0^{1/2}\, \epsilon_0)^4 = g(u) \equiv u(1-u)^2/(2-u) \qquad (14)$$

such that $0<u<1$. Numerical data indicate that here too, like in the rotator case, $\alpha \approx 1$ is to be chosen (see e. g. fig. 10 and related comments in sec. 3). Therefore, since the function g(u) in the interval (0,1), has a maximum $\approx 1/12$ at $u = (3-\sqrt{5})/2$, it follows that for

$$\epsilon_0 > \epsilon_q^{(1)} = \omega_0^{7/6}/\sqrt{(6n_0)} \qquad (15)$$

eq. (14) has no solution.

Thus $\epsilon_q^{(1)}$ defines the threshold for quantum delocalization. Of course, in order that delocalization may occur, it is also necessary that ϵ_0 exceeds the threshold for classical chaos (3), just because the semiclassical estimate (12) holds under the assumption that chaotic diffusion takes place in the classical system. According to the argument just outlined, across the threshold $\epsilon_q^{(1)}$ a qualitative change

---

(*) The slight difference in numerical coefficients between (13) and the analogous formula of ref. /21/ is due to the fact that in /21/ a value of α somewhat lesser than 1 was introduced in I=>0.

occurs, and the localization picture is no longer justified. We should then expect that above this threshold here is no quantum limitation to the classical diffusion and, indeed, this will clearly appear from numerical results.

The above one-dimensional analysis can now be modified, so as to apply also in the 2-dim case for quasi-1-dim. states. Indeed, even though we know from Sec. 2.1 that the 1-dim. approximation is not violated for such states, still we cannot *a priori* exclude that the presence of an additional degree of freedom can destroy the localization of these quasi, but not strictly, 1-dim. states. However, we can answer this question by the same method used in the 1-dim. case. Indeed since classical diffusion will now take place both for n_1 and n_2 , the number of unperturbed levels excited at time τ will be

$$N \approx \Delta n_1(\tau)\ \Delta n_2(\tau)$$

For $\Delta n_1(\tau)$ we will now take eq. (12); moreover, since $\Delta n_2(\tau)$ can be assumed to be small (see sec. 2.1) , we will take $\Delta n_2(\tau) \sim (D_2\tau)^{1/2}$ with D_2 as in formula (7). Imposing now the delocalization condition $N \geq \tau$ /3/6/10/11/18/21/ one easily get the estimate for the two-dimensional delocalization threshold:

$$\epsilon_0 > \epsilon_0^{(2)} = \beta\, \omega_0^{7/6}/(n_0\,[n_2\,(n_2 + |m|)]^{1/2}\,)^{1/2} \qquad (16)$$

where again an undetermined numerical factor $\beta \sim 1$ was introduced.*

The estimate (16) clearly indicates that 2-dimensionality sharply decreases the delocalization threshold. Nonetheless, for states with $m \sim n_2 \sim 1$ the 2-dim. threshold is almost the same as the 1-dim. one.

(*)Actually a more refined analysis shows that in the 2-dim. case here considered one has localization on an exponentially large scale (See ref. 43 and eq. (4.4) of ref. 6), so that delocalization takes place only slightly above (16).

We are therefore justified in assuming that for such quasi-1-dim. states, the localization-delocalization picture remains valid.

The decrease of the delocalization threshold in the 2-dim. model yields one reason (another one will be given in Sec.3.3) why some agreement was found between experiments on excitation of H atoms from states with $n \sim 66$ with field frequency $\omega/2\pi \sim 10$ GHz /12/ and the results of numerical simulation of this process on the *classical* model /15/26/. Indeed, in numerical experiments the initial distribution of states with n=66 was nearly microcanonical, so that the above discussed 2-dim effects played an essential role in lowering the delocalization threshold.

In closing this section, a couple of remarks concerning the validity of the quantum system described by the Hamiltonian (2) as a physically realistic model are in order. In the first place, in the quantum theory discussed above we considered the electric field as classical. This approximation holds if the full number N of field quanta inside the microwave cavity of volume V :

$$N = V\epsilon^2/(4\pi\hbar\omega) \sim 3.10^{23}\epsilon_0^2/(n_0^5\omega_0)$$

is sufficiently large. For istance, for $\epsilon_0 = .05$, $\omega_0 = 1$, $n_0 = 100$, $V = 1cm^3$, which are typical for the range explored in our investigations, we get $N \sim 10^{11}$.

Also the question may be raised whether the diffusive excitation process, that is made possible by the delocalization phenomenon, should not be significantly reduced by the spontaneous radiation process. However, the rate Γ_s of the latter process is much less than the diffusion rate Γ_D. Indeed even for orbital quantum number $l \sim 1$ the rate $\Gamma_s \sim (c^3 n_0^3 l^2)^{-1} \leq c^{-3} n_0^{-3}$ /33/. Estimating Γ_D by the inverse of the classical ionization time i.e., by $t_1^{-1}\omega/2\pi$, with t_1 as in (6), we obtain:

$$\Gamma_2/\Gamma_1 \sim 3\omega_0^{4/3}/(\epsilon_0^2) \sim 10^{-3}$$

where the numerical estimate is given for the typical values $\omega_0=1$, $\epsilon_0=.05$; notice also that the ratio does not depend on n_0. Actually, this ratio is even smaller because the extended state contains l up to $\sim\sqrt{n_0}$ $>>1$.

3.3. Ionization in the Presence of Localization

According to the theory developed in the previous section, as long as the one-dimensional approximation is valid, the dependence of ionization on the field strength should have a more or less marked threshold character, defined by the quantum delocalization border (15). However, a microcanonical distribution of initial states looks fairly typical in many physical situations, so that it is interesting to investigate what should be in that case the dependence of ionization probability on the field intensity. Indeed, since the two-dim. localization border (16) depends on both quantum numbers n_1, n_2, in that case we should expect that for any (not too "high") field, a fraction of the states, depending on the field strength, will be delocalized, while others will be localized and will therefore give no contribution to the ionization rate.

We will derive this dependence, under the assumption that the interaction time τ_{int} of the atom with the field is large enough for the classical system to undergo complete ionization i.e., that the classical ionization probability $P_1^{cl}=1$. Besides that, however, τ_{int} must not be so large that direct quantum ionization from the stationary distribution (10) into the continuous spectrum becomes effective(see the comments in sec. 2.2).

Let's first assume that we have initially a homogeneous distribution of states with a fixed value of n_0 and of the magnetic quantum number m. Then, after the time τ_{int}, all atoms initially in states with $\epsilon_0 > \epsilon_q^{(2)}(n_2,m)$ will be ionized.These are precisely the atoms initially in states with $n_2 > n_2^{cr}$ with n_2^{cr} given by the equation $\epsilon_0=\epsilon_q^{(2)}$

(n_2^{cr},m). Then, recalling that $n_1+n_2 = n_0-|m|$, we see that the fraction of atoms in the ensemble which will not be ionized at time τ_{int} is equal to $2n_2^{cr}/(n_0-|m|)$ (the factor 2 is due to symmetry for exchanges $n_1 \quad n_2$). Computing n_2^{cr} from eq. (16), we get:

$$n_2^{cr} = [(m^2+n_0^2A^2)^{1/2}-|m|]/2 \qquad (17)$$

The ionization probability is therefore given by:

$$P_I = 1 - 2n_2^{cr}/(n_0-|m|) =$$
$$= 1 - \{[m^2+n_0^2A^2]^{1/2}-|m|\}/(n_0-|m|)$$

where

$$A = 2\beta^2\omega_0^{7/3}\epsilon_0^{-2}n_0^{-2}. \qquad (18)$$

Now let's assume that the initial distribution is microcanonical, i.e., that all quantum states with a fixed n_0 are equally represented in it. The full number of such states is n_0^2. For any given value of m, the number of non-ionized states at time τ_{int} for the given ϵ_0 is just $n_2^{cr}(m,\epsilon_0)$. We must then sum over the different values of m; in doing this, however, we must remember that there is a classical value m^{cr} above which there is no ionization (9). Replacing the sum by an integral, we find that the fraction of non-ionized atoms at time τ_{int} for the given ϵ_0 is given by:

$$1 - P_I \approx (4/n_0^2)\int n_2^{cr}(m,\epsilon_0)\,dm$$

The factor 4 in the above formula is due to symmetry with respect to exchanges $m \quad -m$, $n_1 \quad n_2$. The latter symmetry must be taken into account also in inserting the appropriate expression for n_2^{cr} in the integrand. Indeed, n_2^{cr} cannot exceed $(n_0-|m|)/2$; otherwise, since the argument is symmetric in n_1, n_2, a supercritical value of n_2 would enforce a subcritical value of $n_1 = n_0-|m|-n_2$. Therefore, n^{cr} in the above integral is actually the infimum between (17) and $(n_0-|m|)/2$, i.e., it is given by (17) for $|m| < m_1 = n_0\sqrt{(1-A^2)}$, while, for $m > m_1$ it is equal to $(n-|m|)/2$.

Then, assuming $n_{cr} \cong n_0$ (which, as we have already remarked, is legitimate for $\omega_0 \approx 1$), and evaluating the integral, we finally get the dependence of P_1 on the field ϵ_0 in the following form:

$$P_1 = \sqrt{(1-A^2)} - A^2 \ln\{ [1+\sqrt{(1-A^2)}]/A^2 \} \qquad (19)$$

where A is given by eq. (18).

Unfortunately, it would not be correct to use available experimental data as a check of (19), for the following reasons.

In the first place, whereas experimental data concern the frequency region $\omega_0<1$, the above described theory of localization was derived in the frequency region $\omega_0>1$, where 1st order resonances exist (the peculiarities of the excitation process for $\omega_0 <1$ will be discussed in sec. 3.2).

Second, according to numerical data /15/, in experiments the condition $P_1^{cl}=1$ was not fulfilled after time τ_{int} ; indeed, by increasing τ_{int} a further increase of P_1^{cl} was gotten. This fact makes impossible the comparison of available experimental data with (19).

3.4. Comparison of Diffusive and One-Photon Ionization

In the delocalization region $\epsilon_0>\epsilon_q$ the quantum mechanism of suppression of classical diffusion is not at work and therefore one expects that the quantum electron will diffuse and ionize like the classical one. This fact has been numerically checked and will be discussed in section 3. The resulting diffusive excitation can hardly be described within the framework of conventional multiphoton theory; moreover, it usually takes place in a very different range of frequencies than considered there. In order to appreciate the effectiveness of this new ionization process, it is interesting to compare it with the familiar one-photon process.

To obtain a quantitative estimate for one-photon ionization, we shall first observe that any normalized energy eigenfunction for the unperturbed one-dimensional hydrogen atom (i.e. for the Hamiltonian (2) with $\epsilon=0$) can be written as $u(z) = z\,R(z)$, where $R(z)$ is a radial eigenfunction for the 3-dim. atom with orbital quantum number $l=0$. Therefore, the matrix element for the photoelectric transition from the n-th unperturbed level of the 1-dim. model (2) to the continuum state having energy $P^2/2 = -1/2n^2 + \omega$ is given by

$$R^{p,0}_{n,0} = \int dz\, z^3 R_{n_0}(z)\, R_{p0}(z) \qquad (20)$$

where R_{n0}, R_{p0} are radial eigenfunctions for the 3-dimensional atom with orbital quantum number $l=0$ (We assume R_{p0} to be normalized on the energy scale).

For highly excited states $n>>1$ the integral (20) can be evaluated by semiclassical methods. In Ref. /33/ the following semiclassical value of dipole matrix elements for transitions from states (n,l) to (p, l±1) was found for $l<<n$, $p<<1$ (notice the difference in normalization between (20) and ref./33/):

$$R^{p,l\pm1}_{n,l} \approx -\,l^2\,[K_{2/3}(\omega l^3/3) \pm K_{1/3}(\omega\, l^3/3)]\,/(3^{1/2}\pi\omega n^{3/2})$$

where $K_\nu(\xi)$ are Mac Donald functions. Considering that the 2nd term in square brackets is negligible for small l, and that for $\xi \to 0$, $K_{2/3}(\xi) \approx 0.459(3\pi)^{1/2}(3\xi/2)^{-2/3}$, we find the following semiclassical value for (20):

$$R^{p,0}_{n,0} \approx R^{p,1}_{n0} \approx 0.459\;\; 2^{\,2/3}\;\; (-1)\, n^{\,-3/2}\, \omega^{-5/3}/\sqrt{n}$$

Then the transition probability for unit time is:

$$\Gamma_\phi = (\,\pi/2)\,\epsilon^2\;\left|R^{p,0}_{n,0}\right|^2 \approx 0.265\;\epsilon^2/(\omega^{10/3}\, n_0^{\,3}\,) \qquad (21)$$

and the ionization probability in one period of the external field is

$$\Gamma_\Phi = 1.2\pi(\omega_0)\,\Gamma_\Phi \simeq 1.6\,\varepsilon_0^2\,n_0^{2/3}\,\omega_0^{-1/3} \qquad (22)$$

(for $\omega_0 \geq n_0/2$). This value is 3/2 times larger than in ref. /33/ due to averaging over solid angle.

In order to compare the 1-photon ionization and the diffusive ionization we shall choose the optimal regime of each process. Then for 1-photon ionization we take $\omega \approx (2n_0^2)^{-1}$, so that $\Upsilon_\Phi \approx 34\,\varepsilon_0^2\,n_0^{-7/3}$. Instead, for diffusive ionization we take $\omega \approx n_0^{-3}$ ($\omega_0 \approx 1$), and we estimate the ionization probability per period as $\Upsilon_D \approx \tau_1^{-1}$ with τ_1 as in (6): $\Upsilon_D \sim 2\varepsilon_0^2$.

In this way we see that diffusive ionization, which takes place for a much lower frequency than 1-photon ionization, is a much more effective process than the latter:

$$\Upsilon_D/\Upsilon_\Phi \sim n_0^{7/3}/17 \qquad (23)$$

In real physical time this ratio changes as each Υ is multiplied by its own optimal frequency which gives:

$$\Gamma_D/\Gamma_\Phi \sim n_0^{4/3}/8 \qquad (24)$$

This ratio is still large for $n_0 \gg 1$.

A detailed analysis of the dependence of the ionization probability on frequency will be discussed in sec. 3.4

3.5 Ionization by Tunneling and Keldysh parameter.

We shall now discuss some peculiarities of the excitation and ionization for quasi-classical states in the classically stable region $\epsilon_0<\epsilon_{cr}$, $\omega_0 > 1$. In this case the classical motion from one resonance to the next one is forbidden by the presence of smooth invariant curves between them.

Due to this fact, excitation and ionization can take place only thanks to tunneling through the classically forbidden region. A distinction can then be made between the two opposite cases, when the number of levels coupled by the field in one period, $\Delta n \sim D^{1/2} \sim \epsilon_0 n_0/\omega_0^{7/6}$ is small or large. In the former case, perturbation theory holds. Therefore, the probability of transition from the initially excited level $n_0>>1$ to nearby levels is small, and the ionization probability depends algebraically on ϵ_0:

$$W_I \propto (n_0 \epsilon_0/\omega_0^{7/6})^{2k} \qquad (25)$$

where $k \sim n_0$ is the number of photons required for the transition into the chaotic component. In the opposite case when $\Delta n>>1$ but still $\epsilon_0<\epsilon_{cr}$, tunneling becomes dominant, and we can reasonably expect W_I to depend on ϵ_0 according to

$$W_I \propto \tau_I^{-1} \exp[-cn_0 (\epsilon_{cr} - \epsilon_0)/\epsilon_0] \qquad (26)$$

where c is a numerical constant of the order of unity, τ_I^{-1} represents the ionization rate from the chaotic component, and the exponential factor is assumed to describe tunneling into the classically forbidden region, on account of its analogy with the formula describing tunneling in a static field. The condition for applicability of (26) is

$$\epsilon_0 \omega_0^{7/6}/n_0 << \epsilon_0 - \epsilon_{cr} \simeq 1/(50\omega_0^{1/3}) \qquad (27)$$

In order that (27) holds, levels $n_0 >> 50\omega_0^{3/2}$ are required; e.g., for

$\omega_n = 1$ levels with $n_0 \geq 50$ must be considered.

It is interesting to compare these results with Keldysh's theory for tunneling/34/ in which an "adiabatic parameter" $\Upsilon = \omega/(\epsilon n_0) = \omega_0/\epsilon_0$ is introduced, discriminating the perturbative regime ($\Upsilon >> 1$) from the tunneling regime ($\Upsilon << 1$). In the present case, (27) shows that in order that tunneling ionization according to (26) can take place it is necessary that $\Upsilon = \omega_0/\epsilon_0 >> 1$ while for $\Upsilon << 1$ one falls into the region where diffusive ionization occurs. For instance, for $\omega_n = 1$, $\epsilon_0 = 0{,}01$, $n_0 >> 100$ eq. (27) is satisfied but $\Upsilon \approx 100$. Therefore, we see that here also, like in /34/, the multiphoton regime occurs for weak field in the perturbative region ($\epsilon_0 << \epsilon_p$), whereas tunneling takes place in the opposite case of strong field ($\epsilon_0 >> \epsilon_p$). In conclusion, due to the phenomenon of diffusive excitation, the Keldish parameter loses its usual meaning and a new parameter Υ_H must be introduced in order to discriminate between the perturbative regime ($\Upsilon_H >> 1$) and the tunneling regime ($\Upsilon_H << 1$). According to the previous discussion the new parameter Υ_H will have the expression

$$\Upsilon_H = \omega_0^{7/6}/(n_0\epsilon_0) = \omega^{7/6}/(\epsilon n_0^{3/2}) \qquad (28)$$

4. Numerical Results

4.1. Methods of Numerical Simulation

In this section we shall describe the numerical methods and the checking procedures we used in our computer simulation of the classical and quantum dynamics of the 1-dim. model.

Reducing to one the dimension of the problem sharply decreases the computation time in the quantum case, and this allows for a more precise investigation of the excitation dynamics.
The main computations were carried out on the CRAY-XMP Computer.

The numerical solution of the classical equations was carried out in action-angle variables (n, λ) .As in /18/, in order to circumvent the singularity at $z=0$ a change was made to new variables (n, ξ) and to a new time η , which allowed to write the equations in the following form:

$$\begin{aligned} dn/d\eta &= -\epsilon n^2 \cos \omega t \sin \xi \\ d\xi/dt &= n^{-3} + 2\epsilon n \cos \omega t \,(1 - \cos \xi) \\ dt/d\eta &= 1 - \cos \xi \;; \qquad \lambda = \xi - \sin \xi \end{aligned} \tag{29}$$

A similar method for avoiding the singularity at the origin was used in /29/. Eqs. (29) were then numerically integrated by the Runge-Kutta method. The initial distribution of classical trajectories was taken on a line in phase space with $n=n_0$ and uniformly distributed phases λ; this choice corresponds to the initial condition used in the quantum case (only one level excited with $n=n_0$). The full number of classical trajectories was taken 250 or 1000.

An absorption mechanism was introduced for trajectories being excited above $n = 4n_0$. A change in the border of absorption only weakly affected the excitation probability.

The investigation of quantum dynamics described by the Hamiltonian (2) was carried out by two distinct methods. In the first one, following /16/, a base of discrete unperturbed eigenstates was used, and the equations were solved for the amplitudes c_n of the expansion

of the state vector over these eigenstates:

$$i\dot{c}_n = -(1/2n^2)\, c_n + \epsilon(t) \sum z_{nn'} c_{n'} \qquad (30)$$

The value of n_{min} was approximately 20-40 levels lesser than the initially excited state n_0 . A further decrease of n_{min} did not appreciably influence the dynamics, owing to the exponential decrease of the distribution $f_n = |c_n|^2$ in the region $n<n_0$ where the classical motion is stable. A typical value for the full number of levels for which eqs. (30) were solved was ND= $n_{max} - n_{min}$ =192.

In order to numerically integrate (30) the time dependence of the field was approximated by $\epsilon(t) = \Delta t\, \epsilon \cos \omega t \sum_k \delta(t - k\Delta t)$ with $\Delta t = 2\pi/\omega L$, where L is the number of integration steps per period. This scheme of integration is physically equivalent to introducing supplementary fields with frequencies $\omega_k = kL\omega$, k=1,2, ... Since in our computations $\omega \sim 1/n_0^3$ and the number L of steps was chosen between 100 and 500, then even the frequency $\omega_1 \approx 100\omega$ was much larger than all frequencies for transitions between intermediate levels. Therefore, the influence of the fictitious frequencies ω_k can be considered to be small.

The integration of the numerical scheme thus obtained can be carried out exactly; indeed, it reduces to successive applications of a matrix to a vector $\mathbf{c}(t)$:

$$\mathbf{c}(t + \Delta t) = \mathbf{T} \exp[- i\epsilon_0 (\cos \omega t_k)\Delta t\, z]\, \mathbf{c}(t)$$
$$= \mathbf{T}\, \mathbf{Q}\, \mathbf{Z}\, \mathbf{Q}^{-1}\, \mathbf{c}(t)$$

where $\mathbf{T}$ and $\mathbf{Z}$ are unitary diagonal matrices, with $T_{n,n} = \exp(i\Delta t/(2n^2))$ and $Z_{n,n} = \exp[-i\epsilon_0 (\cos \omega t_k)\Delta t\, z_n]$, z_n are the eigenvalues of the matrix $z_{n,n'}$, and $\mathbf{Q}$ is a unitary matrix that carries the same matrix into diagonal form. With this procedure, the normalization $W=\sum |c_n|^2$ = 1 is conserved to a very high accuracy ($\sim 10^{-7}$). In /18/21/ the operator $\exp(-i\Delta t\epsilon_0 z\cos\omega t_k)$ was computed, by means of its expansion in powers of Δt (up to the 5th order), which led to an effective damping on higher levels and to a poorer conservation of

normalization. The new method used here appears significantly more efficient, in that it permits to decrease the number of steps per period.

The main inconvenience with the just described integration scheme is that the continuous spectrum is completely neglected. Even though a number of arguments can be put forth /18/21/, suggesting that the continuous spectrum would not essentially modify the dynamics of excitation over discrete levels, nevertheless it is important to build a numerical model free of this shortcoming.

As far as we know, no numerical experiments were up to now performed, giving a precise account for continuous spectrum/51/. A partial consideration of transitions into the continuum, has been given in ref. /36/. However no account was there taken for continuum-continuum transitions, which, generally speaking, do not appear negligible as compared with transitions to and from the continuum. Moreover, the number of equations to be solved sharply increases with the level number n_0 and this does not allow for investigation of excited states with $n_0 \approx 60$.

A more efficient account for continuum can be given by means of the so called Sturm base. This base is introduced by considering the following eigenvalue equation:

$$-1/2\, d^2u/dz^2 - (\beta/z)\, u = Eu \qquad z>0,\ E<0,\ \beta>0 \quad . \tag{31}$$

For $\beta=1$, (31) is just the Schrodinger equation for the stationary states of the unperturbed 1-dim. hydrogen atom . By changing variables according to $\xi=2z$, $u(z)= (\xi/2)^{1/2} v(\xi)$, eq. (31) becomes

$$S_\xi v \equiv d/d\xi\, (\xi\, dv/d\xi) + [(E/2)\, \xi - 1/(4\xi)]\, v = -\beta v \tag{32}$$

The Sturm base is generated, by considering (32) as defining eigenvalues $-\beta$ for the operator S_ξ, where $E<0$ is an arbitrary fixed parameter.

Instead, considering in (32) β as parameter and E as the eigenvalues, one would resort to the usual base, including continuum eigenfunctions.

It is known /28/ that S_E is a self-adjoint operator with a purely discrete spectrum $\beta_s=(s+1)(-2E)^{1/2}$, with $s\geq 0$ an integer. Eigenfunctions for S_E are given by

$$f_s(\xi)=[(s+1)!\,(-2E)^{1/2}]^{1/2}\,F(-s,\,2,\,\xi(-2E)^{1/2})\,[\xi(-2E)^{1/2}]^{1/2}\exp[-(\xi/2)(-2E)^{1/2}]$$

and are orthonormal:

$$\int_0^\infty d\xi\; f_s(\xi)f_{s'}(\xi)=\delta_{ss'}$$

Here, and below, F with three variables will indicate the confluent hypergeometric function. In the following, we shall choose $E=-1/2n_0^2$, n_0 being the initially excited level. Then, $\xi^{1/2}\,f_{n_0-1}(\xi/2)$ is, apart from a normalization constant, the n_0-th unperturbed eigenfunction.

We also need matrix elements for ξ and ξ^2. For ξ^2 they are given in /28/, where they are used in order to calculate the 2nd order Stark effect. Matrix elements for ξ can be obtained by direct computation.

Non zero elements for ξ and ξ^2 are then given by:

$$\begin{aligned}
&\xi_{s,s}=2n_0(s+1)\\
&\xi_{s-1,s}=\xi_{s,s-1}=-n_0[s(s+1)]^{1/2}\\
&(\xi^2)_{s,s}=6n_0^2\,(s+1)^2\\
&(\xi^2)_{s,s-1}=(\xi^2)_{s-1,s}=-2n_0^2(2s+1)[s(s+1)]^{1/2}\\
&(\xi^2)_{s,s-2}=(\xi^2)_{s-2,s}=n_0^2\sqrt{(s^2-1)}
\end{aligned}\qquad (33)$$

Let now $\Phi(t)=\sqrt{2}\,\Psi(t)$ be the solution of the Schroedinger equation with the Hamiltonian (2), and $\tau=\xi/2$. Then, $1/4\int_0^\infty \xi\,|\Psi|^2 d\xi=1$. Since the f_s's make up a complete orthonormal set, Ψ can be expanded in the form

$$\psi(t)=\sum_{s=0}^{\infty} A_s(t)e^{-iE_0t} f_s$$

with $E_0 = -1/2n_0^2$ and $\psi(0)=(\sqrt{2}/n_0)f_{n_0-1}$ corresponding to the initially excited level n_0. By using the orthonormality of the f_s and the expression (33) for matrix elements, from the Schroedinger equation we obtain equations for the amplitudes $A_s(t)$:

$$\begin{aligned}
&2(s+1)\dot{A}_s - [s(s+1)]^{1/2}\dot{A}_{s-1} - [(s+1)(s+2)]^{1/2}\dot{A}_{s+1} = \\
&= -i\{[2(s+1-n_0)/n_0^2]A_s + 3\epsilon(t)n_0(s+1)^2 A_s + \\
&- \epsilon(t)n_0[(2s+1)(s(s+1))^{1/2} A_{s-1} + (2s+3)((s+1)(s+2))^{1/2} A_{s+1}] + \\
&+ (n_0/2)\epsilon(t)[s\sqrt{(s^2-1)}\,A_{s-2} + (s+2)\,((s+2)^2-1)]^{1/2} A_{s+2}]\}
\end{aligned} \tag{34}$$

This infinite system of equations is exact and, even though only a discrete base was used, it completely takes into account the continuum. Indeed, each Sturm function is a superposition of several eigenfunctions from the unperturbed base, including eigenfunctions belonging to the continuous spectrum.

Once eqs. (34) have been solved for A_s, the original amplitudes $c_n(t)$ of the expansion of $\psi(t)$ over the unperturbed eigenstates

$$u_n(z) = 2zn^{-3/2} e^{-z/n} F(-n+1, 2, 2z/n)$$

can be recovered by

$$c_n(t) = \sum_s B_{ns} A_s(t)$$

where the transformation matrix B_{ns} from the Sturm to the unperturbed base is given by

$$B_{ns} = 1/2 \int_0^{\infty} d\xi (\xi/2)^{1/2} f_s(\xi)\, u_n(\xi/2) = \tag{35}$$

$$= 4(s+1-n_0)\,[2(s+1)n]^{1/2}(n_0-n)^{s+n-2}(n_0n)^{-s-1}\,[(n_0+n)^{s+n+2}]^{-1} \times$$

$$\times \quad F(-s, -(n-1), 2, -4n_0n/(n-n_0)^2)$$

Here F is Gauss' hypergeometric function. A similar computation, for continuous spectrum unperturbed eigenfunctions can be made, by simply substituting 1/p in place of n, p being the electron momentum (an analogous method was used, e.g., in /33/). A method for computing F with large s, n is given in appendix IV.

The numerical integration of eqs. (35) was performed as follows. One level $s_n=n_0-1$ was initially excited, so that $A_s(0)=(\sqrt{2}/n_0)\ \delta_{s,n_0-1}$. Then eqs. (34) were solved for $s_{min} \leq s \leq s_{max}$. As a rule, $s_{min} \approx 10\text{-}30$, and the full number NS of Sturm levels ranged from 256 to 576. The dependence of the field on time was taken in the same way as in the previously described method, with approximately the same number of steps per period: $100<L<500$. Just as in the 1st method, the introduction of delta functions into the numerical scheme made it possible to exactly integrate the truncated set of equations (34) by repeated applications of matrices. For the same reason, the loss of normalization was very small ($\sim 10^{-7}$). Unlike the 1st method, here the presence of high frequencies $\omega_k = kL\omega$ led to direct transitions into the continuum; however, for the chosen values of L the probability of such transitions was negligibly small. For instance, for $n_0=60$, $\omega_0=1$, $\epsilon_0=0.1$, $L=100$ we get $\omega_1 n_0^3 = 50$ and $\Upsilon_\Phi \approx 3.10^{-6}$ to be compared with $\Upsilon_D \sim 2\epsilon_0^2 = .02$. Therefore the small δ-function kicks introduced by the numerical simulation of the monochromatic perturbation do not have any effect on the physics of the problem; moreover, their influence can be kept under control by varying the integration step.

In our opinion, monochromaticity of the perturbation is important for this problem, and substituting a δ-like perturbation $\sum_k \delta(t-2\pi k/\omega)$ in place of $\epsilon \cos\omega t$ /37/38/ can lead to a significant modification of the physical picture of multiphotonic excitation. The role of multiphoton transition in the 2-dim model with a δ-like perturbation was studied in ref. /37/.

The values of $A_s(\tau)$ obtained by integrating (34) were used to find the amplitudes $c_n(\tau)$ over the unperturbed discrete base by means of the transformation matrix B_{ns}. In this way $c_n(\tau)$ were found for approximately 200 levels. Since the total probability was conserved with high accuracy, it was then possible to determine the probability

of excitation above a given level, and also the probability of transition into the continuum, which is included in the former. (The particularities of the distribution in the continuum will be investigated in another paper).

Several characteristics of the excitation were computed by the described numerical method. Among them, the most important were the distribution over unperturbed levels $f_n = |c_n|^2$, the 1st moment $M_1 = (<n>-n_0)/n_0$, the 2nd moment $M_2 = <(\Delta n)^2> = <(n-<n>)^2>/ n_0^2$, and the probability of excitation to high levels. In order to describe the latter we considered the probability $W_{1.5}$ of excitation to states with $n \geq [1.5n_0]$, where [ ] means the integral part. For computations in Sturm base, this probability included also the probability of ionization, namely $W_{1.5}$ is the total probability in states $n \geq 1.5\ n_0$ plus the probability in the continuous part of the spectrum. In order to eliminate fluctuations, we also determined the distribution f_n averaged over $\Delta\tau$ periods of the field; as a rule, $\Delta\tau$ was chosen 40 or 60. Finally, we determined the average distance of the electron from the nucleus, <z>.

The accuracy of the numerical results was checked as follows. First, in order to check that continuous spectrum was being properly taken into account, we performed a series of experiments with frequencies larger than the 1-photon ionization threshold, $\omega_0 > n_0/2$. In the absence of resonances within the discrete spectrum, the probability on discrete levels with $n \geq 1.5\ n_0$ was then negligibly small, so that the probability of ionization $W_i \approx W_{1.5}$. An example of dependence of W_i on time is shown in Fig. 1. In Fig. 2 we show a comparison of the theoretical ionization rate with the numerically obtained one. As can be seen, there is an excellent agreement with the theory of 1-photon ionization (*22*), which indicates that computations in Sturm base efficiently reproduce continuum effects.

A different type of check was gotten by increasing the number L of integration steps per period. The relative changes of the characteristics of excitation produced in this way were very small. For instance, in the 1st method (unperturbed base, *UB*) with $n_0 = 66$, $\omega_0 = 1.5$, $\epsilon_0 = 0.04$, a change of L from 200 to 300 for $\tau = 120$ led to a relative change $\Delta W_{1.5}/W_{1.5} \approx 10^{-3}$, $\Delta<z>/<z> \approx 5\ 10^{-4}$. Of the

same orders were also the changes in Sturm base (SB), even for rather small values of $W_{1.5}$. For instance, for $n_0 = 66$, $\omega_0 = 2$, $\varepsilon_0 = 0.03$, $t = 120$, $W_{1.5} \approx 4.10^{-4}$, upon changing L from 100 to 200 the relative change in probability and in $\langle z \rangle$ were $\Delta\langle z \rangle/\langle z \rangle \approx \Delta W_{1.5}/W_{1.5} \approx 5.10^{-3}$. We can therefore assume that for sufficiently large L the effects of numerical discretization in the integration of (30) and (34) become negligibly small, and have no influence on the physics of the problem.

A further check consisted in changing the total number of levels both in the Sturm and in the unperturbed base, and also in matching the excitation characteristics obtained by the two different methods.

One such comparison is shown in Fig. 3a, where it can be seen that there is a good agreement between results of computations in UB and in SB, and also that an increase in the number of Sturm levels does not change significantly the excitation probability (which includes continuum).

Such an agreement not only takes place for integrated characteristics, but also for the distribution over unperturbed levels (Fig. 4). It is then possible to conclude that continuum effects do not lead to substantial modifications of the excitation dynamics, at least for not too strong fields and high frequencies. Moreover, the Sturm base used in our computations appears large enough to provide a satisfactory model for quantum dynamics, including continuum.

Of course, a numerical scheme whatsoever necessarily involves a discretization of the continuum, and shall therefore fail under sufficiently fine tests. Our own method, as discussed above, correctly describes the continuum spectrum at least in so far as one-photon effects are involved. A more delicate task would be, for instance, reproducing tunneling in a static field; this is an important problem for the computer simulation of actual experiments on microwave ionization as we shall discuss in sec. 4. Here, we may need more sophisticated techniques. While this is a real problem for future investigations, the really important question now is whether our scheme was good enough, that the localization-delocalization mechanism, which is the central object of the present work, can be considered an effective phenomenon and not just an artefact of numerical simulation. In this respect, the agreement we found between

classical and quantum computations in the delocalized regime, as we shall discuss in the next section, provides, in our opinion, the most convincing element in support of our methods.

The dynamics of quantum excitation was investigated for n_0 = 30, 45, 66, 100, and the field ranged in the interval $0.01 < \epsilon_0 < 0.34$. In order to facilitate conversion to physical units, we note that for n_0 = 100 the frequency $\omega/2\pi$ = 10GHz corresponds to $\omega_0 = \omega n_0^3 = 1.51998$, and $\epsilon_0 = \epsilon n_0^4 = 0.1$ corresponds to ϵ = 5.14485 V/cm.

For clarity's sake we have grouped our numerical results following the order of the previous theoretical analysis. Therefore we shall now discuss, in turn, the results on the classical model, the results demonstrating the localization phenomenon, and the results illustrating the dependence of the excitation probability on the field frequency.

4.2 Numerical results on the Classical Model.

The dependence of the excitation probability of the classical system on the frequency ω_0 and intensity ϵ_0 of the field is shown in Fig. 5. Here the excitation probability $W_{1.5}$ is computed after $t=40\omega_0$ periods of the external field. We recall that the initial value n_0 is irrelevant due to the scaling property of the classical motion.The characteristic oscillations with minima near integer values of ω_0 are connected with the presence of nonlinear resonances, the strongest of which correspond to integer ω_0. In fact, the destruction of the centers of resonance regions occurs for larger field than their overlapping (*).

Then, for not too strong fields, a part of the trajectories from the initial distribution, which is uniform in space, upon entering the chaotic region, diffuse to higher values of n, but the rest fall into the central stable region of resonance, where they remain giving no contribution to $W_{1.5}$.

The characteristic dip for $\omega_0 = 0.5$, which was also observed in numerical experiments on 2-dim. atoms /40/ corresponds to a 2nd order (half-integer) resonance. The sharp maximum of $W_{1.5}$ for $\omega_0 \approx 0.7$ (weakly depending on ϵ_0) is due to the fact that for this frequency most trajectories fall into the stochastic layer of the separatrix of the big fundamental resonance $\omega_0 = 1$. Already after half a turn around the resonance they pass into the high-n region, where excitation is significantly stronger. An analogous excitation mechanism, connected with the 2nd order resonance at $\omega_0 = 0.5$, explains also the maximum at $\omega_0 = 0.43$.

In the classical system diffusive excitation takes place only when the field strength exceeds the critical value for which the last KAM

(*)The values of the field at which the centers of resonance regions are destroyed were numerically determined in /29/.

invariant curve is destroyed and there is a transition to global stocasticity (see e.g., /5/). From Fig. 5 we see that the actual value of ϵ_{cr} for $\omega_0 \simeq 1$ is near to 0.02, which satisfactorily agrees with the theoretical value (3) obtained by the resonance overlap criterion /5/.
Fig. 5 gives an overall idea of the classical behaviour. Other numerical results such as the comparison with the solution of the diffusion equation or with the quantum distribution on the unperturbed levels will be given in the following sections.

4.3 The Distribution over the Unperturbed Levels

Here we shall describe the features of the numerically computed quantum distribution over the unperturbed levels in the various parameter regions which have been discussed in our previous theoretical analysis. In this way we shall show that numerical results support the theoretical estimates given above.

For high levels (e.g. $n_0 \approx 100$) and $\epsilon_0 \approx \epsilon_{cr} \approx 0.02$ the perturbation strength $V = (3/2)\, n^2 \epsilon$ is significantly larger than the level separation: $V/\Delta E \approx (3/2)\, \epsilon_0\, n > 1$, so that the field would be expected to connect a number of unperturbed levels. Yet, even for $\epsilon_0 n >> 1$ no diffusive excitation will be observed if $\epsilon < \epsilon_{cr}$. (The opposite case $\epsilon_0\, n << 1$ corresponds to the region below the "quantum stability border" /35/). This is illustrated in Fig. 6, where an example of stationary distribution in the region of stability $\epsilon < \epsilon_{cr}$ is shown. This distribution remains essentially unchanged upon further increasing the computation time. Classically, this fact is due to the stability of the motion, and quantum mechanically to the very small probability of tunneling into regions classically forbidden by smooth invariant curve (Sec. 2.5). However, for a reliable detection of the tunneling described in Sec. 2.5 particularly accurate investigations are required. It is also desirable to increase n_0 , because even for $n_0 = 100$ the tunneling region appears rather narrow (see eq.27). Nevertheless, we think that tunneling excitation can be investigated both in numerical and in laboratory experiments, where at the present time it is possible to prepare states with $n_0 \simeq 300$ /25/. We

also note, that clear experimental observations of tunneling excitation in alternating fields are still lacking.

For field strength exceeding the critical value (3), diffusive excitation takes place in the classical system. However, in the quantum case, for field strength lesser than the delocalization border (15) the phenomenon of quantum localization is observed, in consequence of which the distribution over the unperturbed levels reaches the stationary form (10) and then does not change upon increasing the time of interaction with the field. In this situation, the ionization probability is very small, and can be neglected for the given interaction time. A typical example of quantum localization is shown in Fig. 7. Here we see that classically there is a diffusive excitation, so that the classical distribution obtained by the numerical simulation satisfactorily agrees with the theoretical formula (5a) (the classical border of stability was here chosen at $\bar{n} = 55$ according to numerical results). The quantum distribution was obtained by the Sturm base method with NS = 576; here, as well as in Fig. 4, there is a good agreement with the results of computations by the unperturbed base method. In contrast with the classical result, in the quantum case an exponential drop followed by a multiphoton plateau is observed, almost unchanged under a change of τ from 120 to 600. The quantum limitation of chaos also led to a significantly lesser excitation probability in the quantum than in the classical case (see also Fig. 3).

Another convincing manifestation of localization was the saturation of the diffusive growth of the moment of the quantum distribution (Fig. 8). The agreement between quantum and classical dynamics here holds only over a small initial time interval $\tau_p \approx 5$. The smallness of τ_p is due to the smallness of the classical diffusion rate.

In Fig. 9 it is shown how the normalized average distance $RL = \langle z(t) \rangle / n_0^2$ of the electron from the nucleus depends on time. In the classical system this distance grows and the electron moves far away from the nucleus. Instead, in the quantum case, owing to quantum localization, the electron keeps oscillating around its initial position.

The regime of quantum localization was investigated for initial levels

n_0 = 30, 45, 66, 100, for frequencies $1 < \omega_0 < 3$ and field intensities $0.03 < \epsilon_0 < 0.12$, and localization length $l \gg 1$ (which is the condition for applicability of the estimate (11)). Numerical values for the localization length were determined directly from the stationary quantum distribution. Comparison of these numerical data with the theoretical values (Eqs. 13,14) yields good agreement (Fig. 10). The observed dispersion of points is apparently connected with the presence of islands of stability in the classical system. Also, the presence of a typically quantum resonance structure may play a role in this respect.

If the field exceeds the quantum delocalization border (15) then the quasi classical diffusion over the levels is sufficiently fast and no localization takes place. In this regime the evolution of the distribution function can be approximately described by the diffusion equation (4). An example of distribution in the delocalization regime is shown in Fig. 11a, where it can be seen that the quantum distribution agrees with the solution (5a) of the Fokker-Planck equation.

In order to check the validity of the estimate (15) for the delocalization border, we investigated the dependence of the excitation probability on ϵ_0 for different values of n_0 and of ω_0. This dependence on the rescaled field $\tilde{\epsilon}_0 = \epsilon_0/\epsilon_q^{(1)}$ is shown in Fig. 13. For each value of n_0, ω_0, the excitation probability $W_{1.5}$ was also rescaled to the corresponding classical value taken for $\epsilon_0 = \epsilon_q^{(1)}$; in other words, in Fig. 13 we actually plotted $\tilde{W}_{1.5}(\tilde{\epsilon}_0) = W_{1.5}^{q}(\epsilon_0)/W_{1.5}^{cl}(\epsilon_0)\big|_{\epsilon_0 = \epsilon q^{(1)}}$.
In case that delocalization should actually take place for $\epsilon_0 \approx \epsilon_q^{(1)}$, and that in the delocalization regime the excitation probability should keep close to its classical value, then all the lines showing the dependence of $\tilde{W}_{1.5}(\tilde{\epsilon}_0)$ for different values of n_0, ω_0 would be expected to meet for $\tilde{\epsilon}_0 = 1$ at the value $\tilde{W}_{1.5} = 1$. As can be seen from Fig. 13, this is just what actually happens.

An interesting feature of Fig. 13 is that the dependence of the ionization probability on the field strength at fixed n_0, ω_0 is not always monotonic. For example, the data corresponding to $n_0 = 66$, $\omega_0 = 3$ clearly indicate a "bump" occurring in the ionization curve. The existence of

similar "bumps" in experimentally obtained ionization curves was recently pointed out in /47/ and a theoretical explanation was put forth in /48/.

In the localization regime, the dependence of the excitation probability on field intensity can be approximately described by $W_{1.5} \propto \tilde{\epsilon}_0^{2k}$. Fig. 13 also clearly indicates that the experimental value of k changes substantially with n_0, ω_0, so that joining of all lines at a single point for $\tilde{\epsilon}_0 = 1$ is not a trivial occurrence, and can be considered as a confirmation for our estimate (15). This diversity in the values of k is connected with the different number of photons which are required for excitation in states with $n \geq [1.5\ n_0]$. However, the experimentally determined value k_E is, typically, substantially lesser than the number k_0 of photons theoretically required for direct transition from n_0 to $n \approx 1.5\ n_0$, which is $k_0 = 1 + [5n_0/18\omega_0]$. For instance, for $n_0 = 66$, $\omega_0 = 1$, one has $k_E \approx 7$, $k_0 = 19$.

In our opinion this difference is due to two effects. The first is that multiphoton transitions do not necessarily start from the initial unperturbed state, but may start from anywhere inside the stationary distribution (10) which sets up after a while. In other words, when $l > 1$ excitation may start from levels $n \sim n_0 + l$, and this reduces the multiphotonic degree k. The other reason is the appearance, for high levels $n > n_0$, of a multiphoton plateau of equidistant resonances /21/. Examples of distributions $\bar{f}_n$ which clearly exhibit this multiphoton plateau are given in Fig. 14a,b (see, also Fig. 4). The differences in unperturbed energies $E_n = -1/2n^2$ between consecutive peaks of the distribution are equal to the field frequency; therefore, the sequence of peaks can be naturally explained as the result of a chain of one-photon transitions.

In the cases illustrated by Figs. 14a, b these transitions start directly from the initial state n_0, and the peaks can be enumerated simply by the number of photons. However, the situation is not always that simple; in a series of cases, the chain of peaks does not start from n_0, but rather from somewhere inside the localized distribution (see Fig. 2 in Ref.

/21/), and it is even possible to observe two or three distinct chains within the same distribution.

On the high levels the amplitudes of the peaks become roughly the same and they build up an equidistant plateau. Increasing n still further, the peak amplitudes do not decrease; this seems to be due to the fact that on high levels the field is strong enough for the probability of transitions between nearby peaks to be significant (saturated transitions). This is the second reason why $K_\xi < K_D$.

Upon increasing the field, the multiphoton plateau rises as a whole (Fig. 14). The resonant peaks become broader, but in a number of cases they do not disappear, even in very strong fields and in the delocalization region. However, this can usually take place only for large ω_0 (compare delocalization in Fig. 11a and 14b, for $n_0 = 100$, $\omega_0 = 1.5$ and 3, respectively).

In our opinion, the appearance of the multiphoton plateau below the ionization threshold is in its substance akin to the appearance of peaks in the energy distribution of photoelectrons which is observed above the ionization threshold /41/42/. Indeed, for large n the distance between nearby levels is very small: $\Delta E \ll \omega$, and the spectrum in this region behaves like a quasi-continuum. It is then reasonable to expect that the peak structure observed in the discrete part of the spectrum will persist also in the continuum.

It is possible that a theoretical explanation of the multiphotonic plateau in the under threshold distribution may be given, along similar lines as in /43/.

7.3 Dependence of the Excitation Probability on Frequency

An example of dependence of $W_{1.5}$ on ω_0 for fixed $\varepsilon_0 = 0.04$ and different n_0 is shown in Fig. 15. It is here apparent that for high frequencies $\omega_0 > 1$ the excitation probability is significantly less than the corresponding classical one. The reason is that the delocalization threshold (15) increases with the frequency ω_0, so that a majority of points in Fig. 15 belongs to the region of localization. We recall, however, that the estimate (15) is only valid for $\omega_0 > 1$. Indeed, for $\omega_0 < 1$ a dynamical amplification of the classical excitation takes place, as described in section 3.2 (see Fig. 5). From Figs. 5, 15 it appears that for $\varepsilon_0 = 0.04$ the maximum classical excitation is gotten for $\omega_0 \approx 0.7$. Now, as is seen from Fig. 15, the quantum probability of excitation for $n_0 = 30, 45, 66, 100$ is close to the classical value, and even the corresponding distributions on levels (Fig. 16) look rather close to classical results. We interpret this fast excitation in the sense that in the quantum system for this frequency there is a delocalization. Thus numerical experiments show that for sufficiently weak field $\varepsilon_0 = 0.04$ delocalization can take place at a frequency $\omega_0 \approx 0.7$, lower than the Kepler frequency.

The fine structure of the dependence of excitation on frequency is shown in Fig. 17. In the localization region $\omega_0 \approx 1$ one observes an essentially resonant dependence on frequency. For low frequencies $\omega_0 < 0.7$ most resonances disappear and the dependence on ω_0 becomes smoother. An analogous smoothing occurs in the region $\omega_0 \approx 1$, upon increasing n_0 from 30 to 100.

For still lower frequency, $\omega_0 < 0.6$, one falls into the region of classical stability; therefore, excitation ceases for the classical system. Then, the quantum excitation sharply drops, too. Thus, the dependence of the excitation probability on frequency has a threshold character, in that ionization takes place for

$\omega_0 > \omega_c \approx 1$ (7.1)

This estimate for the chaotic threshold ω_c is justified by the fact that for $\omega_0 < 1$ there are no 1st order resonances between the frequency of the external field and the harmonics of the frequencies of the motion of the classical electron /17/; therefore, chaotic excitation for frequency $\omega_0 < 1$ can take place only for so strong fields that higher-order resonances overlap. On the other hand, for very low frequency $\omega_0 \ll 1$ the value of the critical field ϵ_s coincides with that for the classical static field ionization. Notice that the threshold (36) holds only if $\epsilon_0 > 1/50$. Otherwise, the chaotic threshold has to be determined from eq. (3), and is equal to $\omega_c \approx 1/(50\epsilon_0)^3$.

According to the theoretical estimate (24), the diffusive ionization is more effective than direct one-photon ionization. In order to check this prediction we performed a series of numerical experiments, in which the ionization probability from states with $n_0 = 30$ or $n_0 = 66$ was investigated over a broad range of frequencies. The field intensity was so chosen, that direct two-photon ionization was considerably lesser than 1-photon ionization except for intermediate resonances; moreover, $\epsilon_0 < \epsilon_s$, where ϵ_s is the critical intensity for static field ionization. In this situation, the photoeffect is expected to display a threshold dependence on frequency, with negligibly small ionization probability for $\omega_0 < \omega_\phi = n_0/2$.

Such a picture of the photoeffect proved to be incorrect. In Figs. 18, 19 we show the dependence on frequency of the excitation probability W_E above a level $\bar{n}$ after a dimensionless time $\tau = 40\omega_0$ which corresponds to the same physical time for all ω_0's. Computations were made in Sturm base, so that W_E encloses the probability of transition into the continuous spectrum. For $n_0 = 30$, $\bar{n} = 90$; therefore in this case $W_E \approx W_I$. For $n_0 = 66$, we took $\bar{n} = 99$, and then W_E enclosed a significant part of the probability on discrete unperturbed levels. In Figs. 18, 19 the most effective excitation is observed at frequencies well below the 1 - photon threshold. The new threshold value $\omega_c \approx 1$ is close to the corresponding classical value and, as explained above, is

determined by the condition of overlapping of 3rd order resonances. For sufficiently strong field, ω_c appears significantly lesser than 1: for $\varepsilon_0 = 0.1$, $n_0 = 30$, the experimental value for ω_c is ≈ 0.15, and for $\varepsilon_0 = 0.06$, $n_0 = 66$ the threshold is $\omega_c \approx 0.35$.

In the quantum case, however, there is still a small probability of excitation even from the region $\omega_0 < \omega_c$, due to tunneling into the classically forbidden region. In the interval $\omega_c < \omega_0 < \omega_L = (6n_0\varepsilon_0^2)^{3/7}$ delocalization takes place, so that W_E is close to its classical value. For $\omega_L < \omega_0 < \omega_\Phi$ quantum effects lead to the localization of diffusion; therefore, in that region one observes an essentially different excitation picture than in the classical system. A decrease of W_E with ω_0 is observed also in the classical case, due to the decrease of the diffusion rate with ω_0 (see eq. (5)). Indeed, even in the presence of diffusion, the excitation probability above a given level n is nearly zero if at the given observation time τ_E the diffusion has not yet reached this n (i.e. if $\tau_E << (n-n_0)^2/D$). However, in the quantum case, isolated ionization spikes survive in this frequency region due to transitions into the continuum via intermediate resonant levels.

In the frequency region $\omega_0 \approx \omega_\Phi$ the probability W_E sharply increases, because of the possibility of direct one-photon transitions. However, W_E in this region is significantly lesser than for $\omega_0 \approx \omega_c$ when diffusive ionization occurs. In the region $\omega_0 > \omega_\Phi$ numerical data satisfactorily agree with the theoretical formula (22). This agreement indicates that the Sturm base method of integration efficiently describes continuous spectrum effects. See also Fig. (19b).

In Fig. 19 we see that for $\omega_0 \approx 0.43$ the quantum probability of excitation is close to the classical one; again, as in the case of Fig. 15, this means that in this frequency region, for $n_0 = 66$, $\varepsilon_0 = 0.06$, there is quantum delocalization.

Numerical experiments indicate that the threshold value ε_c for

diffusive excitation in this frequency region lies between 0.04 and 0.05. (Fig. 5). In the quantum case, upon varying ϵ_0 from 0.04 to 0.05 the excitation probability changes by about two orders of magnitude. This means that delocalization occurs already at $\epsilon_0 \approx \epsilon_{cl}$, so that the field intensity yielding 10% ionization (which was studied in ref. (26) will be found to agree with classical predictions. In other words, these numerical experiments of ours show that laboratory experiments /12/26/ were performed in that parameter region where 1-dim. delocalization (and a fortiori 2 dim. delocalization) takes place, and this explains the observed agreement with predictions from the classical model.

4.5 Stability of Quantum Diffusion

Even though the "diffusive" ionization, taking place in the delocalized regime, is to some extent similar to the classical diffusion which occurs in the chaotic regime, the quantum system is still short of exhibiting all the statistical properties that would be expected of classical chaos.

The most striking difference is the absence, in quantum dynamics, of the strong instability and of the rapid loss of memory associated with classical chaos. In computer experiments this effect leads to irreversibility. Indeed, even though the exact equations of motion are reversible, nevertheless any, however small, imprecision in solving them, such as, e.g., computer round-off errors, is magnified by exponential instability of orbits to the extent that initial conditions are effaced and reversibility is therefore destroyed.

Investigations aimed at verifying whether an analogous irreversibility would be displayed also by the numerically computed quantum evolution were described in /6/ for the kicked rotator. Here we will present numerical results for time-reversal experiments on the 1 - dimensional H-atom. (Figs. 11, 12). The chosen parameter values lie in the region of delocalization; therefore, up to the moment

of time-reversal (τ = 60) diffusive excitation is going on, both in the quantum and in the classical system. Indeed, the distribution on the quantum levels at τ = 60 is close to the classical one, and is well described by formula (5a). Then, at τ = 60 we reversed the velocities of all particles (N = 1000) in the classical ensemble, and changed the wave function of the quantum atom to its complex conjugate. In both classical and quantum mechanics, the H-atom would be expected to find its way back to the initial state. However, due to the finite computer precision, in the classical case such a return is not observed. The system retraces backward its history just for a few periods of the field, and then, again, diffusive excitation occurs.

Instead, in the quantum case an almost exact reversion of motion is gotten; at time τ = 120 the electron comes back to the initial level. This is even more remarkable on account of the fact that, in order to restore the initial state, some of the total probability had to be called back from the continuum.

The conclusion must be drawn from this exact reversibility, that even though *the quantum diffusion which occurs in the delocalized* regime of the H-atom is by now the most chaotic example of quantum motion hitherto investigated, nevertheless this quantum "chaos" is essentially different from the real chaos of classical dynamics.

5. Experimental Results

A large number of laboratory experiments on hydrogen and alkali atoms in highly excited states have been performed up to now /12/13/22-26/. Additional interest for such experiments has recently arisen in connection with the possibility of chaotic motion in quantum mechanics. It is now possible to perform experiments on microwave ionization on atoms prepared in extended quasi 1-dim. states /23/. Here it is possible to measure the ionization probability identified with the population of levels higher than some sufficiently large n, including continuum; this definition is particularly convenient for comparison with numerical experiments. Also, it is possible to measure the probability distribution on unperturbed levels. This allows, in principle, for a careful comparison of experimental and numerical data.

In particular, very accurate experiments on 1-dim. H-atoms were carried through as described in /23/. The range of parameters for these experiments lies inside the region of low frequency ($\omega_0 \approx 0.2$) and of classical stability, so that the results can not be used as a test for the theory presented in this paper.

A different series of experiments /26/ was performed on 2-d H-atoms. The conditions of these experiments not only lie above the 2-dim. delocalization border, but even above the 1-dim. one. For this reason, our results predict an agreement with classical computations, as indeed was found in /26/. One possible explanation for the not complete agreement obtained is that the experimental values in /26/ migth be above but close to the delocalization border, when one should not expect a better agreement than within a factor 2. To clarify this point we show in Fig. 20 the comparison of numerical 1-dim. quantum and classical ionization probability slightly above the border: there is a strong excitation in both cases, but, unlike strongly delocalized cases, (Fig.11a) here the two results only agree within a 50%.

Since experimental techniques allow for very accurate measurements, it is highly desirable that the conditions of the experiments be defined as precisely as possible; for example it is more convenient to choose a single excited state than a microcanonical distribution. From our point of view, a most important goal for future experiments is to observe and to study the new and unexpected localization phenomenon in classically chaotic situations. For this it is necessary that the frequency ω_0 be increased above $\omega_0 \approx 1$, since in the region $\omega_0 > 1$ a large separation between the classical chaotic threshold ω_c and the quantum delocalization border ω_1 is expected. In the high frequency region it is also possible, by varying the field strength, to observe the transition to delocalization as well as the other phenomena described in the present paper.

Also, in order to give experimental evidence for the "freezing" of the wave packet in localization, it would be desirable to dispose of a control on the interaction time. This latter possibility lies within the capabilities of present day technique/24/.

We would like also to stress that all the phenomena described in this paper should be observable not only in H-atoms, but also in different alkali atoms. In order to produce hydrogen-like states in such atoms, one should take into account that, the unperturbed spectrum for highly-excited alkali atoms is slightly different than in H-atoms, due to quantum defects. However, for values of $l > 3$ this quantum defect is negligible. Since in linearly polarized fields the magnetic quantum number m is a constant of the motion, by exciting states with $m \geq 3$ it is possible to excite states with $l \geq 3$, which correspond very well to the hydrogenic situation. It is then possible to consider also 1-dimensional states by exciting levels with $m \geq 3$, $n_2 = 0$, $n_1 = n - |m| - 1$ and this excitation can be achieved via light-induced resonant transitions. One would then get a situation in which localization and other effects of quantum chaos might be studied.

FIGURES CAPTION

Fig. 1 Ionization probability W_1 as a function of time τ (number of microwave periods) for the case n_0 =30, ω_0= 30, ϵ_0= 0.075. The solid line is drawn according to the analytical expression (22) while the crosses are the results of our quantum numerical computations. The excellent agreement with the theory even for very large frequencies is a check of our numerical computations and shows that Sturm base efficiently takes into account the continuous spectrum.

Fig. 2 Ionization rate versus field intensity for the case n_0=30, ω_0=30, Like in the previous fig. 1, the straight line is drawn according to the theoretical expression (22) and the crosses are results of quantum numerical computations. Here also notice the very good agreement between theory and numerical results.

Fig. 3a Excitation probability $W_{1.5}$as a function of time τ for the case n_0= 66, ϵ_0=0.04, ω_0=2.5. The quantum numerical computations are performed by using: i) the unperturbed base with N=192 basis set eigenstates (solid line); ii) the Sturm base with N= 384 (dotted line); iii) the Sturm base with N= 576 (dashed line). The fairly good agreement of the three curves is a check of the numerical computations. The classical ionization curve is also shown.

Fig. 3b Classical (1) and quantum (2) excitation probability $W_{1.5}$ as a function of time for the same case as in Fig. 3a.

Fig. 4 Quantum probability distributions $\bar{\Pi}(n)$ over the unperturbed states averaged over 60 values of $\tau=\omega t/2\pi$ within the interval $60<\tau<120$. Here n_0=66, ϵ_0=0.04, ω_0=1.5. Three different curves are plotted corresponding to integration in Sturm base with a basis set of N= 384 and N=576 basis functions and integration in unperturbed base with N= 192. The three curves are so close that are not resolved in the graph and this is an additional check on the accuracy of numerical computations.

Fig. 5 Classical ionization probability $W_{1.5}$ after $\tau=40\ \omega_0$ as a function of the microwave frequency for different microwave intensities. Here $W_{1.5}$ is the total probability above the action value $n=1.5n_0$. (x) $\epsilon_0=0.02$; (.) $\epsilon_0=0.03$; (o) $\epsilon_0=0.04$; (Δ) $\epsilon_0=0.05$; ($\cdot$) $\epsilon_0=0.06$.

Fig. 6 Classical (-) and quantum(-) probability distribution $\bar{\Pi}(n)$ averaged over 40 values of τ within the interval $80<\tau<120$. Here $n_0=100$, $\epsilon_0=0.01$, $\omega_0=1.5$. For these parameter values, $\epsilon_0<\epsilon_{cr}<\epsilon_q$ and therefore both classical and quantum packets are localized. Notice the small tunneling through the classical KAM invariant curves.

Fig. 7 Classical (dotted curve) and quantum (solid curve) probability distribution $\bar{\Pi}(n)$ averaged over 40 periods of τ for the case $n_0=66$, $\omega_0=2.5$, $\epsilon_0=0.04$. Fig. 7a average within the interval $80<\tau<120$; Fig. 7b average within the interval $560<\tau<600$. The dashed line in both figures represent the analytical solution (5a) of the Fokker-Planck equation which fairly agree with the classical numerical results. On the contrary, the quantum distribution is localized and do not change significantly by increasing the interaction time with the microwave from 120 to 600. The only difference, as expected, is the slight increases in the peaks of the small multiphoton plateau.

Fig. 8 Second moment $M_2=\langle(n-\langle n\rangle)^2\rangle/n_0^2$ of the classical (solid line) and quantum (dashed line) distribution as function of time $\tau=\omega t/2\pi$ for the same paremeters of fig. 7. The localization of the quantum packet shown in the previous fig.7 leads here to the suppression of the diffusive growth of the moment M_2.

Fig. 9 Normalized average distance $RL=\langle z(t)\rangle/n_0^2$ of the electron from the nucleus as a function of τ for the same case as in Fig. 7. (dotted line) Quantum case; (full line) classical case. Also here the quantum suppression of diffusion is clearly manifest.

Fig. 10 Localization length as a function of field intensity for different parameters values. The dots correspond to numerically measured values

of 1 which are in good agreement with the solid curve given by the analytical estimate (13)

Fig. 11a Classical ( ) and quantum ( ) distribution function $\bar{f}(n)$ averaged over 40 values of τ in the interval $40 < \tau < 80$. Here $n_0 = 100$, $\omega_0 = 1.5$, $\epsilon_0 = 0.08$. Notice the fairly good agreement between classical and quantum numerical results and the analytical solution given by eq. (5a) ( ).

Fig. 11b Probability distribution over the unperturbed states at $\tau = 120$ for the case of fig. 11a, after reversal of velocitiesa at $\tau = 60$. Notice that the quantum system (open lozenges) recovers its initial state to seventeen digits which corresponds to numerical errors. In contrast, the classical motion (solid lozenges) proceeds according to the diffusion equation (5a) (squares).

Fig. 12 Claasical (solid lozenges) and quantum (open lozenges) ionization probability (excitation above the unperturbed level n=150) as a function of time for the case of fig 11b. Notice the perfect specular simmetry of *the quantum curve about the time of reversal* $\tau = 60$.

Fig. 13 Excitation probability at time $\tau = 60$ as a function of the field intensity for different values of n_0 and ω_0. $\tilde{W}_1(\tilde{\epsilon}_0) = W_1^{q}(\epsilon_0)/W_1^{cl}(\epsilon_q^{(1)})$ is the quantum excitation probability at ϵ_0 rescaled to the corresponding classical excitation probability computed at $\epsilon_0 = \epsilon_q^{(1)}$. $\tilde{\epsilon}_0 = \epsilon_0/\epsilon_q^{(1)}$ is field the rescaled field intensity. (Δ) $n_0 = 30$, $\omega_0 = 3$; (.) $n_0 = 45$, $\omega_0 = 1$; ( ) $n_0 = 45$, $\omega_0 = 3$; (•) $n_0 = 60$, $\omega_0 = 1$; (+) $n_0 = 60$, $\omega_0 = 2$; (x) $n_0 = 60$, $\omega_0 = 3$; (o) $n_0 = 100$, $\omega_0 = 3$. The fact that all points coresponding to different n_0 and ω_0 meet at the value $\tilde{W} = 1$ for $\tilde{\epsilon}_0 = 1$ is a numerical verification of our estimate (15); it also verifies that, *in the delocalized regime*, the quantum excitation probability is close to the classical value.

Fig. 14a Quantum probability distribution $\bar{f}(n)$ averaged over 60 periods of τ within the interval $60 < \tau < 120$. Here $n_0 = 60$, $\omega_0 = 2$, and $\epsilon_0 = 0.03$ (fig.14a1); $\epsilon_0 = 0.06$(fig.14a2); $\epsilon_0 = 0.14$ (fig. 14a3).

Fig. 14b Same as Fig. 14a with $n_0=100$, $\omega_0=3$, and $\epsilon_0=0.06$ (Fig. 14b1); $\epsilon_0=0.1$ (Fig. 14b2); $\epsilon_0=0.2$ (Fig. 14b3).

Fig. 15 Excitation probability $W_{1,5}$ as a function of frequency ω_0 at $\tau=40$ for fixed $\epsilon_0 = 0.04$ and for different n_0. (.) $n_0=30$; (Δ) $n_0=45$; (□) $n_0=66$; (+) $n_0=100$. The solid line gives the classical excitation probability. Notice that, by increasing ω_0, the quantum excitation probability becomes much less than the corresponding classical one due to the fact that the delocalization border (eq. 15) increases with ω_0.

Fig. 16 Quantum probability distribution $\bar{f}(\bar{n})$ averaged over 40 periods of τ in the interval $40 < \tau < 80$ for fixed $\epsilon_0=0.04$, $\omega_0=0.7$, and different n_0. Fig. 16a $n_0=100$ (_ . _), $n_0=66$ (- -); Fig. 16b $n_0=45$ (_ . _), $n_0=30$ (- -). The classical probability distribution is also shown(— · —). In order to compare the quantum distributions with different n_0, with the classical one, we have introduced rescaled quantities $\bar{f}' = (n_0/66)\,\bar{f}$ and $\bar{n}' = (66/n_0)\,\bar{n}$. The scaling property of the quantum distribution and the fairly good agreement with the classical motion is due to the delocalization phenomenon.

Fig. 17 Fine structure of the dependence of excitation prpbability $W_{1,5}$ on frequency ω_0 at $\tau=40$ for fixed $\epsilon_0=0.04$. (o) $n_0=45$; (+) $n_0=100$; (.) classical results.

Fig. 18 Ionization probability $W = \sum_{n>\bar{n}} |c_n|^2$ versus field frequency ω_0 after a time $\tau = 40\omega_0$ which corresponds to the same real physical time t for all frequencies. We have set $n_0=66$, $\epsilon_0=0.05$, $\bar{n}=99$. Moreover, quantum theory (□); classical theory (o). Notice that ω_t is here somewhat less than $n_0/2$ because, in our definition of the ionization probability, the contribution of states with $n>\bar{n}$ is also included.

Fig. 19 Same as fig. 18 with $n_0=30$, $\epsilon_0=0.075$, $\bar{n}=90$.

Fig. 20 Classical (.) and quantum (+) excitation probability as a function of time for n_0=66, ϵ_0=0.06, ω_0= 0.43. The quantum system is delocalized but since we are only slightly above the border, the quantum excitation is less than the classical one.

6. Conclusions and recommendations

The study of the 1-dim H atom in a monochromatic field that we have described in the present paper brings into the light a number of facts - some of which were rather unexpected.

These facts concern both the actual physics of atoms in microwave fields, and the general problem of quantum dynamics in the region of classically chaotic motion. Even though the unperturbed eigenfunctions, as well as the matrix elements of the perturbation, can be well approximated by their semiclassical expressions, it may well happen that quantum and classical time evolutions are essentially different, due to the phenomenon of quantum localization of chaos. It is interesting to note that investigations of this phenomenon were prompted by studies on the rotator model /4/. It is a remarkable fact that this phenomenon, originally detected in a somewhat artificial model, has now been shown to exist in a physical system, so that there is a real possibility to observe it in laboratory experiments .

On the other hand, for the H atom also a delocalization regime exists, and our theory allows determination of the threshold for this regime. Above this threshold, the excitation of the quantum system can be approximately described by the classical diffusive excitation. This regime of excitation is much more efficient than the direct 1-photon ionization: therefore a new frequency threshold for the photoelectric effect appears, which is determined by classical border for frequency, $\omega_0 > \omega_c$. Actually there are two different frequency thresholds ω_c and ω_1 , so that strong ionization occurs only for $\omega_c < \omega < \omega_1$. The latter threshold ω_1 is due to quantum localization of classical chaos.

The delocalization phenomenon explains the partial success of classical computations in reproducing experimental results on microwave ionization. At the same time, however, the localization phenomenon sets definite limits to the applicability of classical models, which are due to

quantum localization.

Although a discussion of the two-dim. case was given in sec. 2.2, the bulk of the results presented in this paper were related to the one-dimensional case. While this fact does not certainly affect their conceptual importance, it enforces some caution when comparing them with experiments hiterto performed. Indeed, an analysis of the experiments described in /47/ shows that a three-dimensional theory is required to model them properly. A different series of experiments/23/ is amenable to a one-dimensional description, but here a static electric field ϵ_s collinear with the microwave field was present during the whole time of the experiment. In order to correctly model these experiments we ought to add a term $z\epsilon_s$ in our Hamiltonian. The numerical study of the resulting quantum dynamics presents some technical difficulty, because it seems to call for a finer description of continuous spectrum than allowed by the method exploited here. Perhaps recourse to more sophisticated numerical methods will prove necessary but, in our opinion, the basic qualitative picture of localization-delocalization will not change.

Delocalization is also a challenging subject for future theoretical analysis. This phenomenon has been predicted on the grounds of semiclassical arguments, which are best suited to make contact with classical chaotic behaviour. Nevertheless, it should be possible to understand it in purely quantum terms. A first step in this direction may be provided by a recent result/49/ that a qualitative change occurs in the numerically computed quasi-energy eigenfunctions of the one-dim. problem.

A few concluding remarks are in order concerning the relationship of results described in this paper to the general themes of quantum chaos. As we have seen, diffusive excitation and ionization are brought about in the classical hydrogen atom by the onset of dynamical chaos, which is a regime of extreme instability of trajectories of the electron. A physically relevant question that we have answered above, is whether

the physically observable manifestations of chaos-enhanced ionization and so on - survive also in the quantum domain. However, the more speculative question may be posed, whether also anything of the conceptual setup of classical chaos - instability, irreversibility, and so on - can be translated in a quantum context. An illustration was given in this paper (sec. 3.5) that this is not the case. However similar the quantum evolution may appear to the classical (insofar as the population of levels is concerned) it remains strongly stable, in sharp contrast to the latter. Therefore, even though classical chaos was shown to be relevant in predicting the response of a quantum hydrogen atom to an external microwave field, it must be stressed again that, strictly speaking, no true chaos is possible in quantum mechanics.

We shall now discuss how the results of our investigations modify the general picture of quantum chaos, as we have sketched it in sec. 1. Indeed, we believe that in the light of these findings of ours some previously accepted views must now be modified; at the same time, new developments appear now possible, which hopefully will shed light on some as yet scarcely understood phenomena in atomic physics.

Our study about the possibility of chaotic diffusion in quantum periodically perturbed systems led us to definite predictions on the existence of a localization-delocalization mechanism. Further theoretical analysis and experimental work is required in order that this mechanism may enter the domain of physically ascertained facts, and indeed work is in progress in both directions. Meanwhile, we wish to stress that our theoretical views yield considerable clarification in an otherwise very confused state of affairs. Indeed, judging by current literature and recent international meetings, scientists working on time-dependent problems can be roughly devided in two categories. In the first of these we classify those with a more or less negative attitude in regard of the possibility that some chaotic effects may survive in Quantum Mechanics. It includes mainly people that at some stage of their scientific work became acquainted with the kicked rotator, or with related models, and have therefore a direct experience of the stubborn resistence offered by this quantum object to any attempt at introducing chaos in it. These people usually develop a theoretical attitude according to which the

quantum suppression of dynamical chaos is not just an artefact of a queer, highly non-generic model but has deep roots in the very foundations of quantum Mechanics. Typical representatives of this class were Hogg and Huberman, who even felt justified in dilating the rotor's stability into a general law, according to which any quantum system subject to a periodic perturbation would exhibit a strongly recurrent behaviour, with the only possible exception of non-generic resonant situations.

Even though this contention of Hogg and Huberman [7] turned out to be an erroneus one - we were indeed able to prove that the rotor itself can be nonrecurrent without being resonant [10] - nevertheless it prompted important developments. The claimed impossibility that periodically perturbed quantum systems may follow classical chaotic patterns was assimilated by Fishman, Grempel and Prange [8] to another more firmly established quantum impossibility, namely, that a quantum particle in a disordered static potential may ever escape to infinity. As a matter of fact, it is well known that such a particle will stay localized, due to a complicated interference effect. Fishman, Grempel and Prange were able to establish a formal connection between time dependent problems and localization problems on disordered lattices, that proved very useful.

It is interesting to note that people in this first class who entered the H-atom problem, at least initially were rather skeptical about the possibility that anything like a chaotic ionization may exist in the real quantum H atom, and considered it almost obvious that some more or less severe limitations would be imposed by quantum effects on the chaotic diffusion. (Blumel and Smilanski, [36] Shepelyansky, [11]).

A somewhat specular attitude is displayed by workers who enter Quantum Chaos just because of their involvment in microwave ionization. Being aware of the partial success of classical computations in reproducing experimental data, and relying on the correspondence principle, they hardly realize that a theoretical scheme originally introduced for the exotic kicked rotor provides elements also for a quantum theory of the H atom.

According to our results, both positions are partially justified. The localization-delocalization mechanism provides indeed a key to

understand how quantum limitations of classical chaos can sometimes leave room for seemingly diffusive exitation processes even in quantum dynamics. Much work is now required in order to give firm ground to our theoretical results. In the first place, our theory of the delocalization phenomenon is essentially a semiclassical one. It would be nice to understand this phenomenon in *purely quantum* terms, i.e., by making as little use as possible of the underlying classical diffusive picture. In this way the possibility could be investigated, that a similar quantum instability occurs in different situations for which no classical analog is available-e.g., in problems of nuclear physics.

The best approach towards a purely quantum theory of delocalization is the spectral analysis of the quasi-energy eigenvalues and eigenfunctions. Interesting results in this sense were recently obtained by Blumel and Smilansky [48] who performed a numerical computation of quasi-energy eigenfunctions for several field parameters and were able to detect an abrupt change in their shape across some threshold. We are currently investigating the possible connnections between this phenomenon and delocalization.

Another important question is how our theory should be modified in order to apply also in the realistic case of a 3 dimensional atom. A 3-dimensions numerically solvable quantum model is then needed, allowing for a careful analysis of the localization phenomenon in 3 dimensionas. We have already some theoretical estimates, according to which the qualitative picture should not be different from the 1 dim. case. We are also working on a numerical model, which is still, however, in a preliminary stage.

Insofar as our theory justifies the use of classical concepts under appropriate conditions, it can be considered as a theoretical explanation of the previously detected phenomenon of underthreshold ionization. On the other hand, the localization phenomenon in the hydrogen atom in a microwave field is a relevant prediction of ours that has not yet been subjected to experimental tests. Moreover, according to our views, a scan of the ionization as a function of microwave frequency should expose a big, sharply defined peak in the region of low frequency ! this, also, calls for experimental verification.

In order that a detailed laboratory check can be made, we should include in our model some minor modifications accounting for certain details of the actual experimental setup. For example, in actual experiments hydrogen atoms are submitted to the combined action of the microwave field and of a static electric field. Even though the latter should not essentially modify the localization-delocalization picture, including it into the numerical model requires great care and calls for extreme computer performances.

In drawing a final balance of a three-years activity, we do not certainly feel like stating that the major problems in the solution of which we purported to contribute have been given a final answer whatever.

Nevertheless, we believe that the world-wide research activity on the role of chaos in Quantum Mechanics, in which we have been contributing, is now entering an almost unexplored realm of microphysics, of great potential relevance and immediate physical interest.

7. **Bibliography**

1. Proc. Int. Conf. on Quantum Chaos, Como 1983 (Plenum, 1985). Edited by G. Casati.

2. G.M. Zaslavsky, Phys. Reports 80 (1981), 157.

3. B.V. Chirikov, F.M. Izrailev, D.L. Shepelyansky, Soviet Scientific Review, 2C (1981), 209.

4. G. Casati, B.V. Chirikov, J. Ford, F.M. Izrailev. Lectures Notes in Physics, Springer, 93 (1979), 334.

5. B.V. Chirikov, Phys. Rep. 52 (1979), 263.

6. D.L. Shepelyansky, Physica, 8D (1983), 208.

7. T. Hogg, B.A. Huberman, Phys. Rev. Lett. 48 (1982), 711.

8. S. Fishman, D.R. Grempel, R.E. Prange, Phys. Rev. Lett. 49 (1982), 509; Phys. Rev. A. 29 (1984), 1639.

9. B.V. Chirikov, Ups. Fiz. Nauk. 139 (1983), 360.

10. B.V. Chirikov, D.L. Shepelyansky, Preprint 85-29, INP, Novosibirsk, 1985.

11. D.L. Shepelyansky, Phys. Rev. Lett. 56 (1986),677.

12. J.E. Bayfield, P.M. Koch, Phys. Rev. Lett., 33 (1974), 258.

13. J.E. Bayfield, L.D. Gardner, P.M. Koch, Phys. Rev. Lett. 39 (1977), 76.

14. N.B. Delone, B.A. Zon, V.P. Krainov, Zh. Eksp. Teor. Fiz. 75 (1978), 445.

15. J.G. Leopold, I.C. Percival Phys. Rev. Lett. 41 (1978), 944; J. Phys. B. 12 (1979), 709.

16. B.I. Meerson, E.A. Oks, P.V. Sasorov, Pis'ma Zh. Eksp. Teor. Fiz. 29 (1979), 79.

17. N.B. Delone, V.P. Krainov, D.L Shepelyansky, Ups. Fiz. Nank 140 (1983), 335 (Sov. Phys.).

18. D.L. Shepelyansky, Preprint 83-61, INP, Novosibirsk, 1983; Proc. Int. Conf. on Quantum Chaos 1983 (Plenum, 1983), p. 187.

19. R.V. Jensen, Phys. Rev. Lett., 49 (1982), 1365.

20. R.V. Jensen, Phys. Rev. A. 30 (1984), 386.

21. G. Casati, B.V. Chirikov, D.L. Shepelyansky, Phys. Rev. Lett., 53 (1984), 2525.

22. J.E. Bayfield, L.D. Gardner, Y.Z. Gulkov, S.D. Sharma, Phys. Rev. A, 24 (1981), 138.

23. J.E. Bayfield, L. A. Pinnaduwage, Phys. Rev. Lett. 54 (1985), 313; J. Phys. B, 18 (1985) L49.

24. D. Meschede, H. Walter, G. Mueller, Phys. Rev. Lett. 54 (1985), 551.

25. H. Rinneberg, J. Neukammer, G. Joensson, H. Hieronymus, A. Koenig, K. Vietzke, Phys. Rev. Lett. 55 (1985), 382.

26. K.A.H. van Leeuwen, G.V. Oppen, S. Renwick, J.B. Bowlin, P.M. Koch, R.V. Jensen, O. Rath, D. Richards, J.G. Leopold, Phys. Rev. Lett. 55 (1985),2231.

27. R.V. Jensen, Phys. Rev. Lett. 54 (1985), 2657.

28. L.D. Landau, E.M. Lifshitz, Quantum Mechanics, Moscow, Nanka, 1974.

29. J.G. Leopold, D. Richards, J. Phys. B 18 (1985), 3369.

30. L.D. Landau, E.M. Lifshitz, Mechanics, Moscow, Nauka, 1973.

31. J.N. Bardsley, B. Sundaram, Phys. Rev. A, 32 (1985), 689.

32. L.D. Landau, E.M. Lifshiftz. Field Theory, Moscow, Nauka, 1973, p. 236.

33. S.P. Goreslavsky, N.B. Delone, V.P. Krainov, Zh. Eksp. Teor. Fiz. 82 (1982), 17 89; preprint PhIAN USSR N33; Moscow, 1982.

34. L.V. Keldysh. Zh. Eksp. Teor. Fiz. 47 (1964), 1945 (Sov. Phys. JEPT 20 (1965), 1307).

35. E.V. Shyryak. Zh. Eksp. Teor. Fiz. 71 (1976), 2039.

36. R. Blumel, U. Smilansky Phys. Rev. A, 32 (1985), 1900.

37. A.K. Dhar, F.M. Izrailev, M.A. Nagarajan. Preprint 83-162, INP, Novosibirsk, 1983.

38. R. Bluemel, U. Smilansky, Phys. Rev. Lett. 52 (1984), 137; Phys. Rev. A, 30 (1984) 1040.

39. H. Bateman, A. Erdelyi, Higher Transcendeantal Functions V.1. New York, MC Graw - Hill Book Company, INC, 1953.

40. D.A. Jones, J.G. Leopold, I.C. Percival J. Phys. B, 13 (1980), 31.

41. F. Fabre, G. Petite, P. Agostini, M. Clement, J. Phys. B, 15 (1982),

1353.

42. P. Kuit, J. Kimiman, H.G. Muller, M. J. van der Wiel, Phys. Rev. A, 28 (1983), 248.

43. Z. Deng, J. H. Eberly, Phys. Rev. Lett. 53 (1984),1810.

44. D.E. Khmelnitskij, Pis'ma Zh. Eksp. Teor. Fiz. 32 (1980), 248.

45. G. Casati, B.V. Chirikov, I. Guarneri, D.L. Shepelyansky, Phys. Rev. Lett. 57(1985) 823.

46. G. Casati, B.V. Chirikov, I. Guarneri, D.L. Shepelyansky, Phys. Rev. Lett. 56 (1986) 2437.

47. P.M. Koch, in *Fundamental aspects of quantum theory*, V. Gorini and A. Frigerio eds., Plenum Press, (1987).

48. R. Blumel and U. Smilansky, submitted to Phys. Rev. Lett.

49. R. Blumel and U. Smilansky, preprint.

50. J.N. Bardsley and M.J. Comella, preprint.

51. Shortly before the definitive redaction of this paper, some new papers appeared in preprint form, reporting about further computational efforts in this sense. /49/50/.

8. Appendixes

Appendix I : Quasi Classical Matrix Elements in Parabolic Coordinates.

We shall here get the expression for the z coordinate in parabolic action-angle variables $(n_1, n_2, m, \lambda_1, \lambda_2, \psi)$. To this end we introduce the parabolic coordinates ξ,η,ψ:

$$\begin{aligned} x &= \sqrt{(\xi\eta)}\cos\psi \\ y &= \sqrt{(\xi\eta)}\sin\psi \\ z &= (\xi-\eta)/2 \end{aligned} \qquad (I.1)$$

In these coordinates the unperturbed Hamiltonian takes the form:

$$H = 2\xi/(\xi+\eta)\, p_\xi^2 + 2\eta/(\xi+\eta)\, p_\eta^2 + 1/(2\xi\eta)\, p_\varphi^2 - 2/(\xi+\eta) \qquad (I.2)$$

The transformation to action-angle variables $(n_1,n_2,m,\lambda_1,\lambda_2,\psi)$ is achieved by separation of variables in the Hamilton -Jacobi equation for which we refer to standard textbooks (see e.g. 30). Here we just recall that the generating function of this transformation is found to be:

$$S(n_1,n_2,m,\xi,\eta,\psi) = \int^{\xi} P_\xi\, d\xi' + \int^{\eta} P_\eta\, d\eta' - m\psi \qquad (I.3)$$

where the canonical momenta P_ξ, P_η , P_φ are given by/30/:

$$\begin{aligned} P_\xi &= [E/2 + \beta_1/\xi - m^2/4\xi^2]^{1/2} \\ P_\eta &= [E/2 + \beta_2/\eta - m^2/4\eta^2]^{1/2} \\ P_\varphi &= m \end{aligned}$$

$$\beta_{1,2} = (n_{1,2} + |m|/2)/n \qquad n = n_1 + n_2 + |m| \qquad E = -1/2n^2$$

Then the angle variables λ_1, λ_2

$$\lambda_{1,2} = \partial S/\partial n_{1,2} \tag{I.4}$$

can be obtained by differentiating (I.3) and computing the integrals. The procedure is greatly simplified by the introduction of the auxiliary angles χ_1,χ_2 defined by

$$\begin{aligned} \xi &= -2n^2 \mu_1 \sin \chi_1 + 2n (n_1 + |m|/2) \\ \eta &= -2n^2 \mu_2 \sin \chi_2 + 2n (n_2 + |m|/2). \end{aligned} \tag{I.5}$$

where the parameters μ_1,μ_2 are given by:

$$\mu_{1,2} = [n_{1,2} (n - n_{2,1})/n^2]^{1/2}$$

In this way we get the following result:

$$\begin{aligned} \lambda_1 &= - \mu_1 \cos \chi_1 - \mu_2 \cos \chi_2 - \chi_1 \\ \lambda_2 &= - \mu_1 \cos \chi_1 - \mu_2 \cos \chi_2 - \chi_2 \end{aligned} \tag{I.6}$$

From (I.5) we get the following expression for z:

$$z = 1/2 (\xi-\eta) = n^2(\mu_2 \sin \chi_2 - \mu_1 \sin \chi_1) + n (n_1 - n_2) \tag{I.7}$$

The coordinate z can be expanded in a double Fourier series in the angles λ_1,λ_2 with coefficients $z_{k_1k_2}$ given by:

$$z_{k_1k_2} = \int d\lambda_1 \int d\lambda_2 \, z \, e^{-i(k_1\lambda_1 + k_2\lambda_2)}$$

We now substitute (I.7) for z in this integral, and change integration variables to χ_1, χ_2 by using (I.6). Thus we find:

$$z_{k_1 k_2} = n^2 \int_0^{2\pi} d\chi_1 \int_0^{2\pi} d\chi_2 \, D(\chi_1, \chi_2) \, (\mu_2 \sin \chi_2 - \mu_1 \sin \chi_1) \, e^{-i(k_1\lambda_1 + k_2\lambda_2)} + n\,(n_1 - n_2)\,\delta_{0k_1}\,\delta_{0k_2} \qquad (I.8)$$

where $D(\chi_1, \chi_2) = \partial(\lambda_1,\lambda_2)/\partial(\chi_1,\chi_2) = 1 - \mu_1 \sin \chi_1 - \mu_2 \sin \chi_2$ is the Jacobian determinant for the transformation $(\lambda_1, \lambda_2) \rightarrow (\chi_1, \chi_2)$.

Evaluating the double integral in (I.8) yields formulas (1d) in the text.

Appendix II: Solution of the Fokker-Planck equation.

In order to solve Eq. (4) with the boundary condition $\partial f/\partial n\big|_{n=\bar{n}} = 0$, we shall first perform some change of variables. First of all, putting $\bar{\tau} = \epsilon_0^2 t/\omega_0^{7/3}$, $y = n/n_0$, the Fokker-Planck equation takes the form:

$$\partial f(y,\bar{\tau})/\partial\bar{\tau} = \partial/\partial y \, (y^3 \partial f/\partial y)$$

Now let's change again variables to $z = y^{-1/2}$ and let's introduce a new function $g(z,\bar{\tau})$ according to $f = z^2 g$. This function g must then satisfy:

$$\partial g/\partial\bar{\tau} = (1/4)\,\partial^2 g/\partial z^2 + (1/4z)\partial g/\partial z - (1/z^2)\,g$$

and its Laplace transform $\hat{g}(z,s)$ must satisfy the equation:

$$\partial^2\hat{g}/\partial z^2 + (1/z)\,\partial\hat{g}/\partial z - (4/z^2 + 4s)\,\hat{g} = -4g(z,0).$$

A further change of variables to $w = 2\sqrt{s}\,z$ yields:

$$\partial^2\tilde{g}/\partial x^2 + (1/x)\,\partial\tilde{g}/\partial x - (1+4/x^2)\,\tilde{g} = -(1/s)\,g(x,0) \qquad \text{(II.1)}$$

By the same changes of variables we find that, in order that f satisfies the boundary condition $\partial f/\partial n\big|_{n=\bar{n}} = 0$, $\tilde{g}$ must satisfy:

$$\partial\tilde{g}(x,s)/\partial x\big|_{x=\bar{x}} = -(2/x)\,\tilde{g}(\bar{x},s)\ ,\ \text{where}\ \bar{x} = 2(s\,n_0/n)^{1/2} \qquad \text{(II.2)}$$

The general integral of eq. (II.1) can be written as

$$\tilde{g} = A\,I_2(x) + B\,K_2(x) + \bar{g}$$

where I_2, K_2 are.... , A ,B are numerical constants and $\bar{g}$ is a particular integral that can be determined e. g. by Lagrange's method:

$$\begin{aligned}\tilde{g} = {} & I_2(x)\,[A - (1/s)\int_0^x x'g(x',0)\,K_2(x')dx'] + \\ & + K_2(x)\,[B + (1/s)\int_0^x x'g(x',0)\,I_2(x')dx'\end{aligned} \qquad \text{(II.3)}$$

The constants A,B can then be chosen so that the boundary condition (II.2) is satisfied. Indeed, upon substituting (II.3) into (II.2) we get:

$$\begin{aligned}\tilde{g}(x,s) = {} & [\,K_1(\bar{x})\,I_2(x)/I_1(\bar{x})]\,(1/s)\int_0^{\bar{x}} g(x',0)I_2(x')x'dx' + \\ & + I_2(x)\,(1/s)\int_{\bar{x}}^{x} g(x',0)K_2(x')x'dx' + K_2(x)\,(1/s)\int_0^{x} g(x',0)I_2(x')x'dx'\end{aligned} \qquad \text{(II.4)}$$

Since $f(n,0) = \delta(n-n_0)$, we must choose $g(x,0)$ in the form $\delta(4s/x^2 - 1)$. Then the asymptotics of (II.4) for $s \to \infty$ and fixed y has the form:

$$g(x,s) \sim (4s/x)^{1/4}\,(1+2\sqrt{s})\,[\exp[-\sqrt{s}(1+\ln 2\sqrt{s} - \ln 2\sqrt{s})] +$$

$$+ \exp[2\sqrt{s}(x/2\sqrt{s}-1)]\}$$

whence it follows

$$\tilde{r}(y,s) \underset{s\to\infty}{\sim} 1/(2\, y^{3/4}\sqrt{s})\,\{\exp[2\sqrt{s}(1+1/\sqrt{y}-2/\sqrt{y})]+$$

$$+\exp[2\sqrt{s}(1/\sqrt{y}-1)]\}$$

Eq. (5a) in the text easily follows from the last formula.

Appendix III: Estimate for the Delocalization Border.

Let's evaluate the 2nd moment of the distribution over the levels: $M_2 = \langle(\Delta n)^2\rangle = \langle(n-\langle n\rangle)^2\rangle$. From the diffusion equation we get approximately

$$d/d\tau\ \langle(\Delta n)^2\rangle \approx \langle D\rangle = a n_0^2 \langle(n/n_0)^3\rangle \qquad \text{(III.1)}$$

where $a = 2\,\epsilon_0^2 \omega_0^{-7/3}$. The equation for the 1st moment gives

$$d\langle n\rangle/d\tau = (3\, a\, n_0/2)\,\langle(n/n_0)^2\rangle \qquad \text{(III.2)}$$

In order to solve (III.1) and (III.2) we will use a rough approximation, namely, we will substitute for n its mean value $\langle n\rangle$. Doing so, and *performing the integration*, we obtain

$$\langle n\rangle = n_0[1-3a\tau/2]^{-1}$$

$$\langle(\Delta n)^2\rangle = n_0^2[(1-3a\tau/2)^{-2}-1]/3$$

The localization condition $r^2 = a^2\langle(\Delta n)^2\rangle = a^2 l^2$ gives an equation for

τ, the least root of which determines the localization length l:

$$(n_0^2/3)\,[(1-3\tau a/2)^{-2}-1] = \tau^2/\alpha^2 \qquad \text{(III.3)}$$

$$l = \tau/\alpha$$

A straigthforward manipulation gives then formulas (13), (14).

Appendix IV: A Method for computing Hypergeometric functions.

The numerical computations of matrix elements in (32) ? presents some technical difficulty since a direct expansion of hypergeometric functions in series of powers of $-4nn_0/(n-n_0)^2$ doesn't give correct values of B_{ns} for $n\sim s \sim 100$ due strong cancellations of different terms and finite computer precision. Therefore in order to compute the hypergeometric function F we used a different method based on the recursion formulas between values of F for three consecutive values s-1, s, s+1 (see, e.g./39/). The method is essentially as follows:

We take two values of F for s=0, s=1 and then we recurrently determine all F up to $s=n_s \approx n$. After that we take two arbitrary values for F_m and F_{m+1} for s =m and s=m+1 where $m >> s_{max}$ was chosen (for example $m \approx 5\, s_{max}$) and recurrently determined values of F for $n_s-10< s < m$. These latter values of F differ from the actual ones only by a numerical factor c_F. The value of this constant was obtained by comparison with F computed for $s< n_s$. For different values $s< n_s$ the constant c_F was obtained with a precision $\approx 10^{-10}$. After taking into account this constant factor we got precise values of F for $0<s<s_{max}$, which didn't change upon changing the arbitrary values F_m , F_{m+1} .

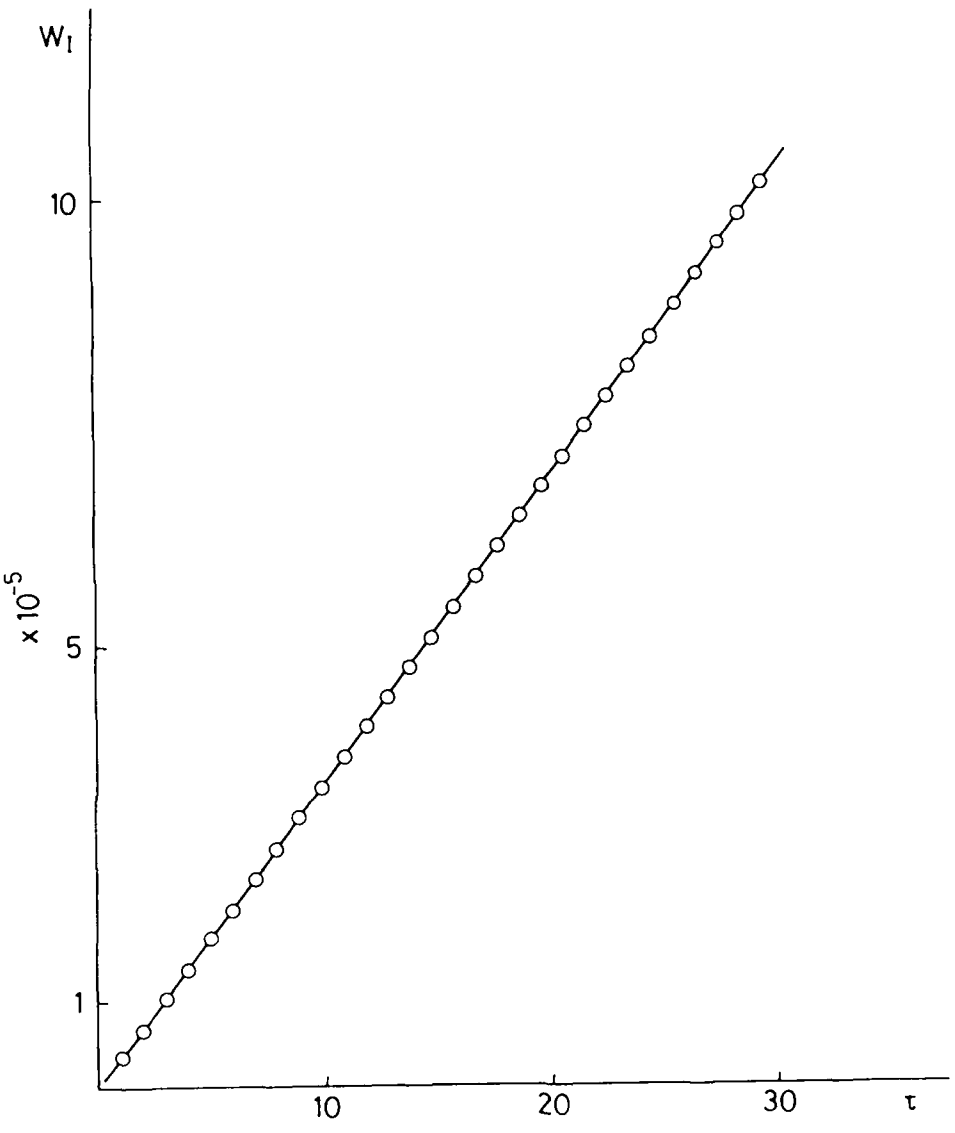

FIG. 1

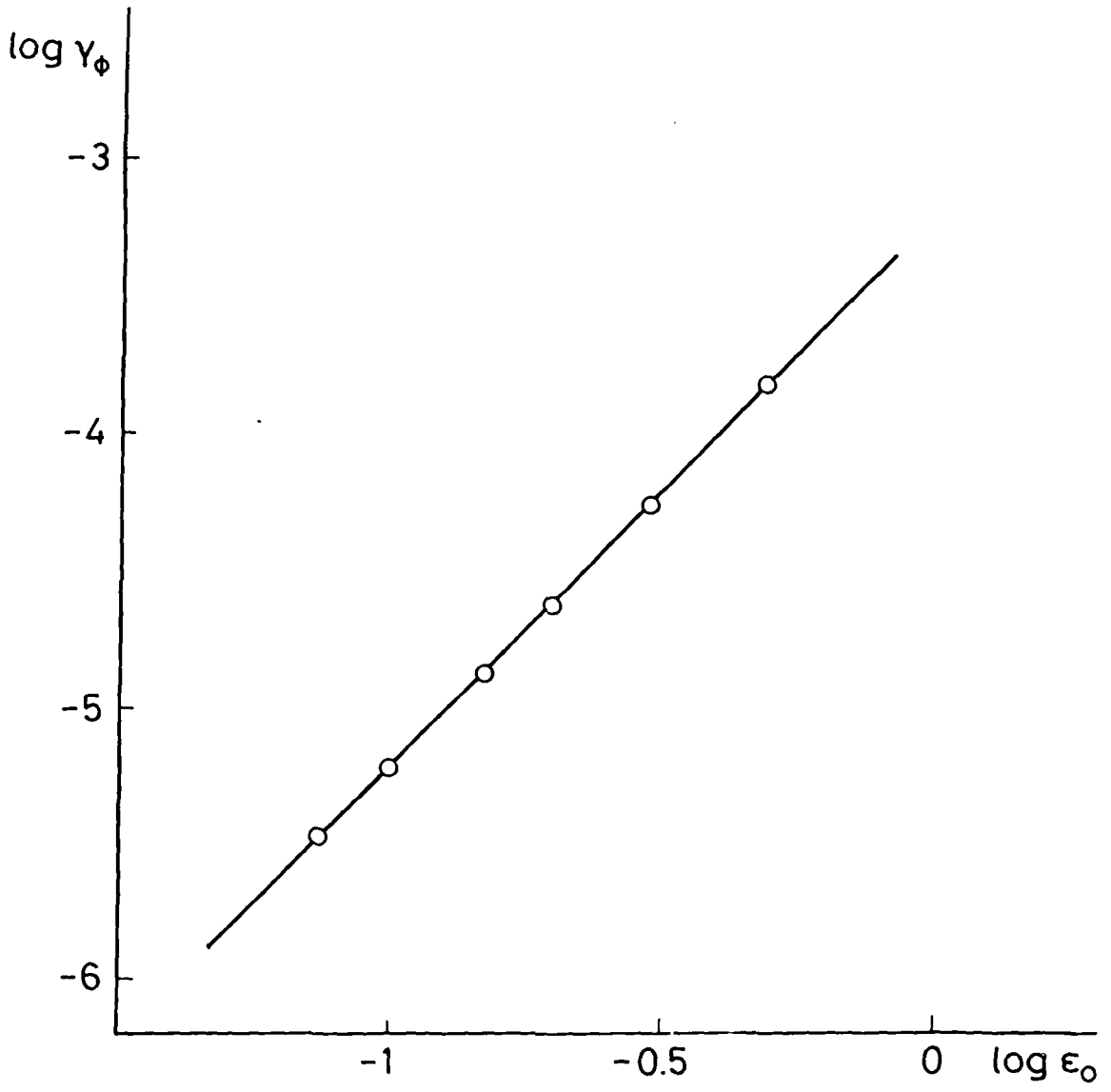

FIG. 2

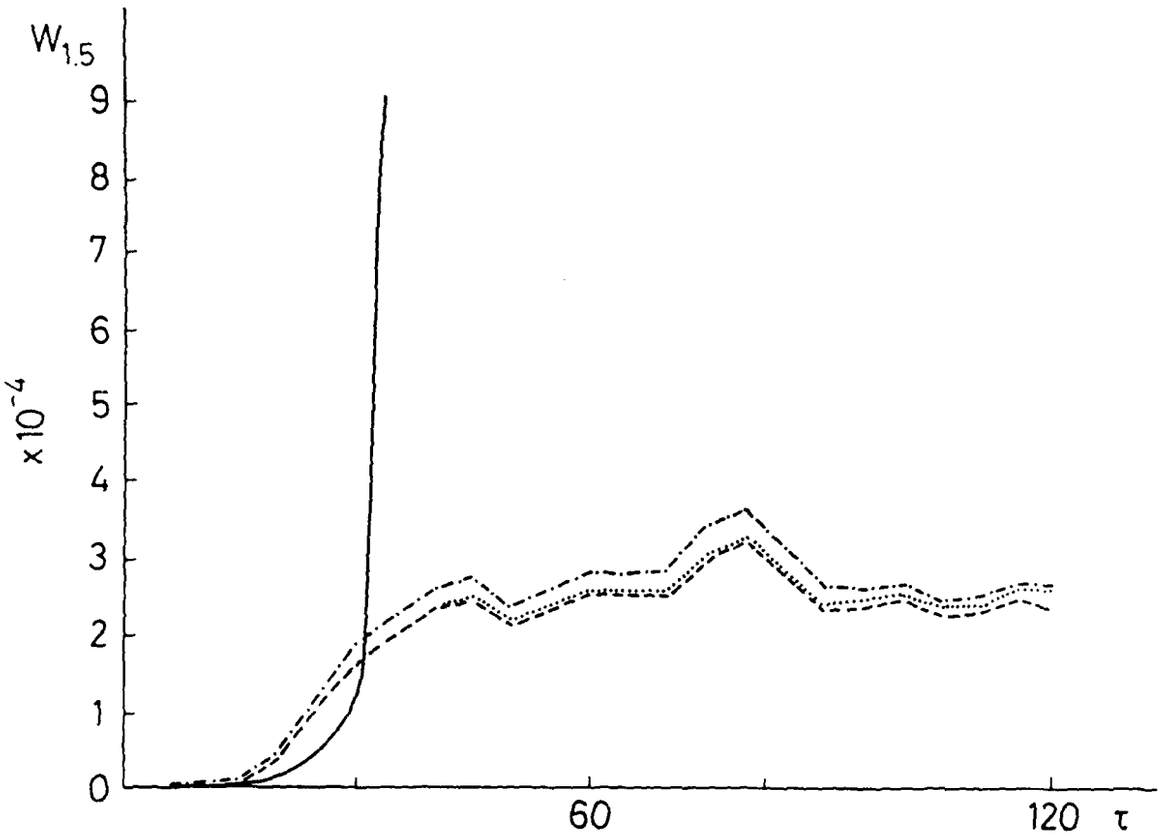

FIG. 3a

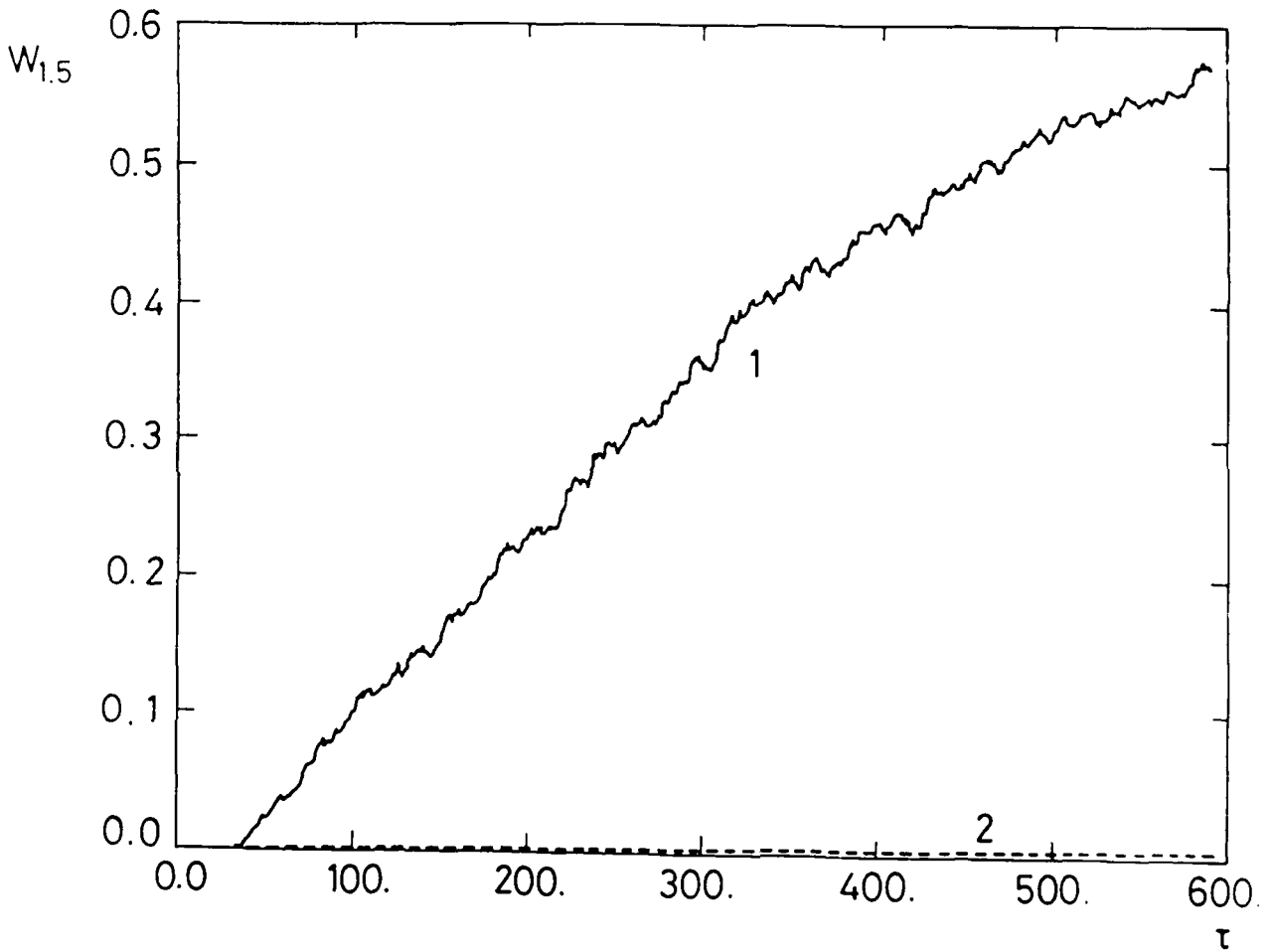

FIG. 3b

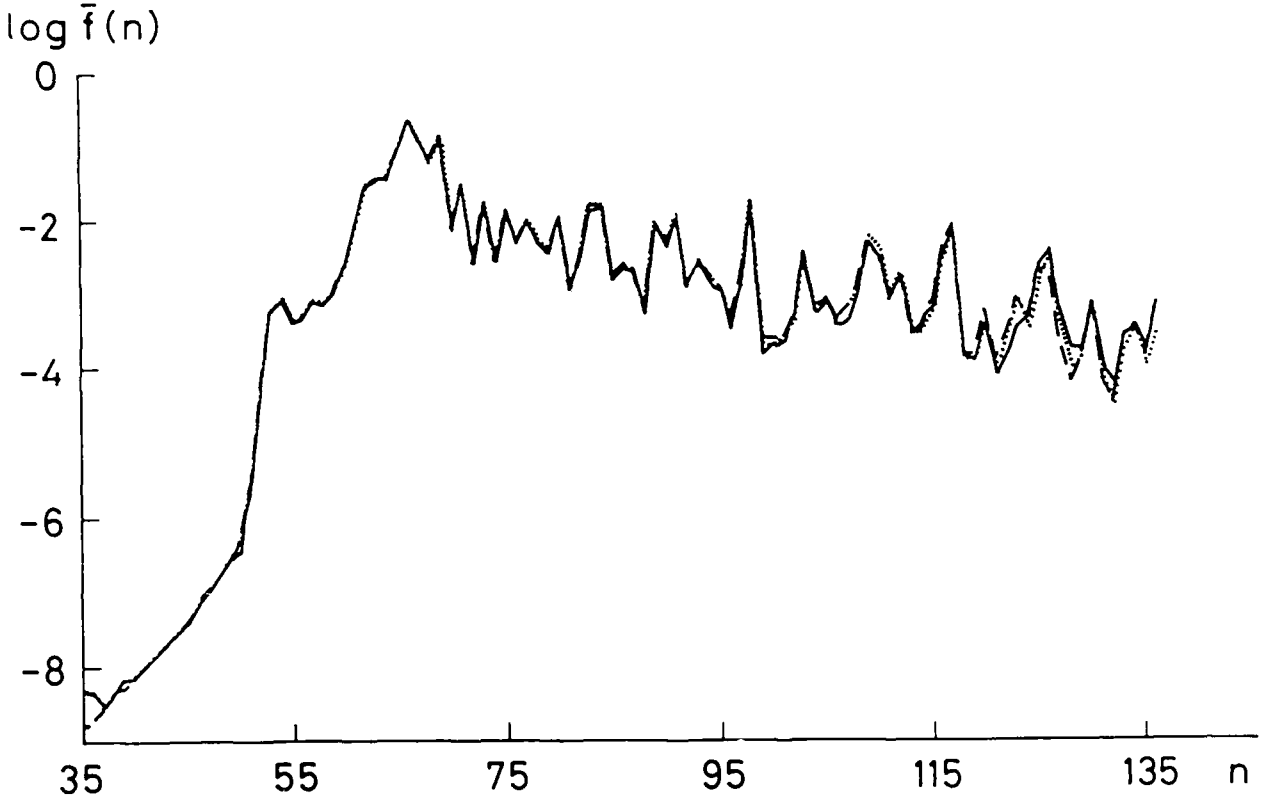

FIG. 4

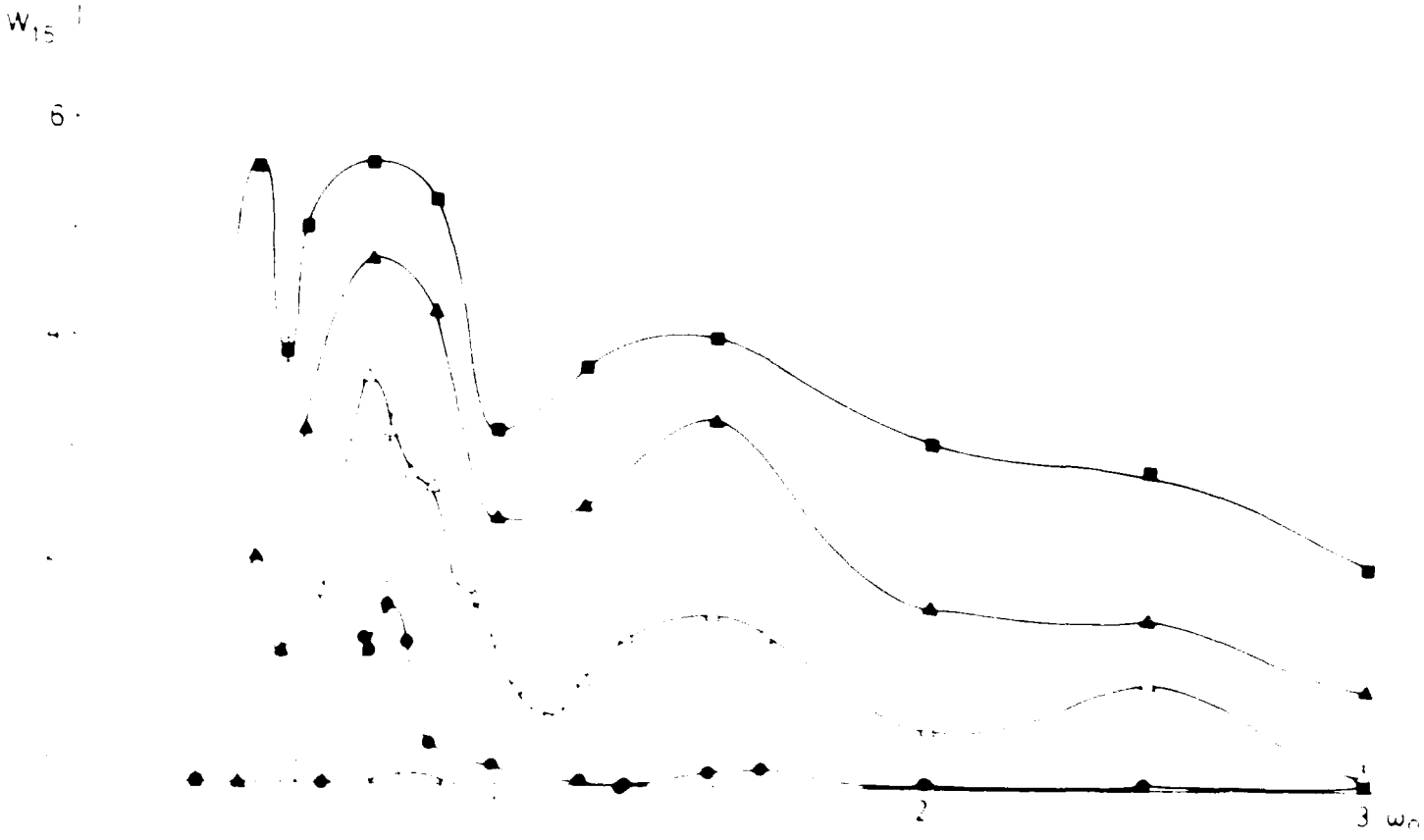
W_{15}
6
2
3 ω_n

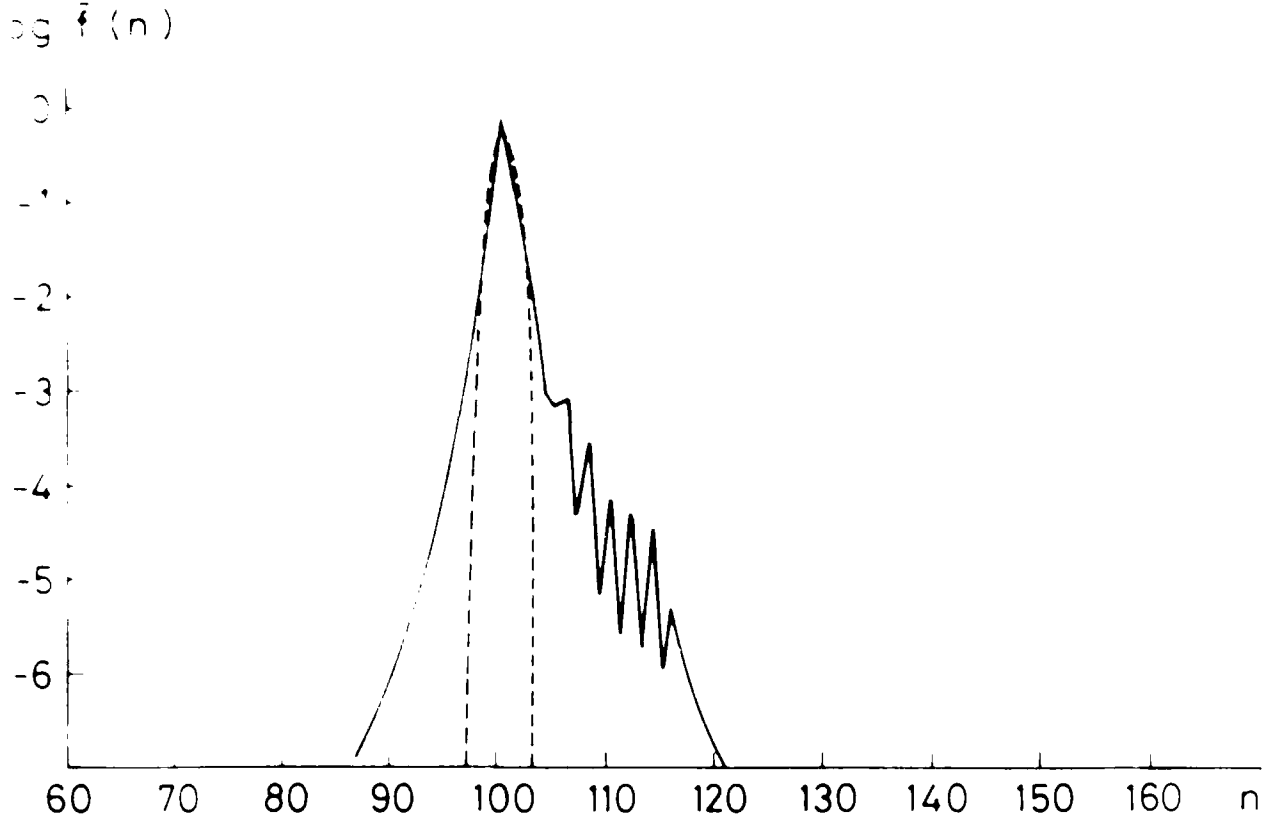
log f (n)
-2
-3
-4
-5
-6
60
70
80
90
100
110
120
130
140
150
160
n

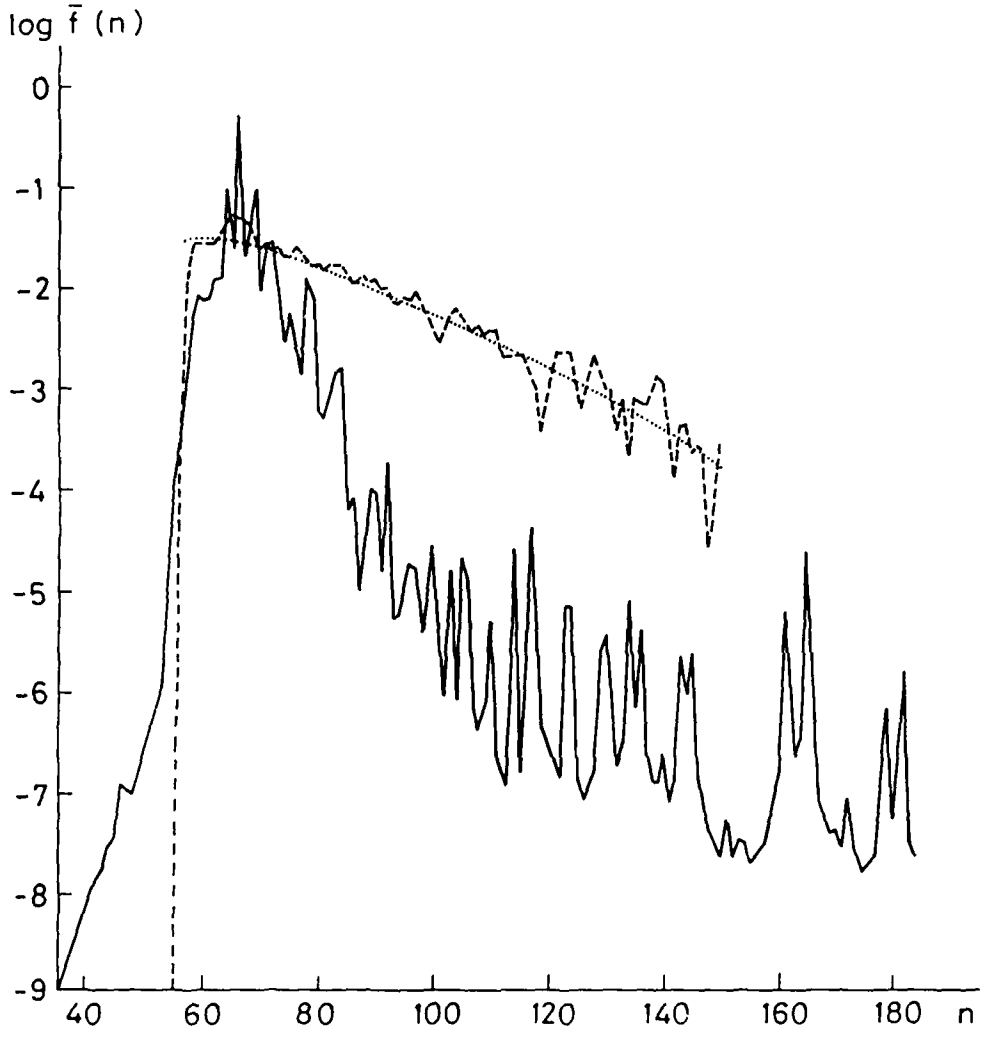

FIG. 7a

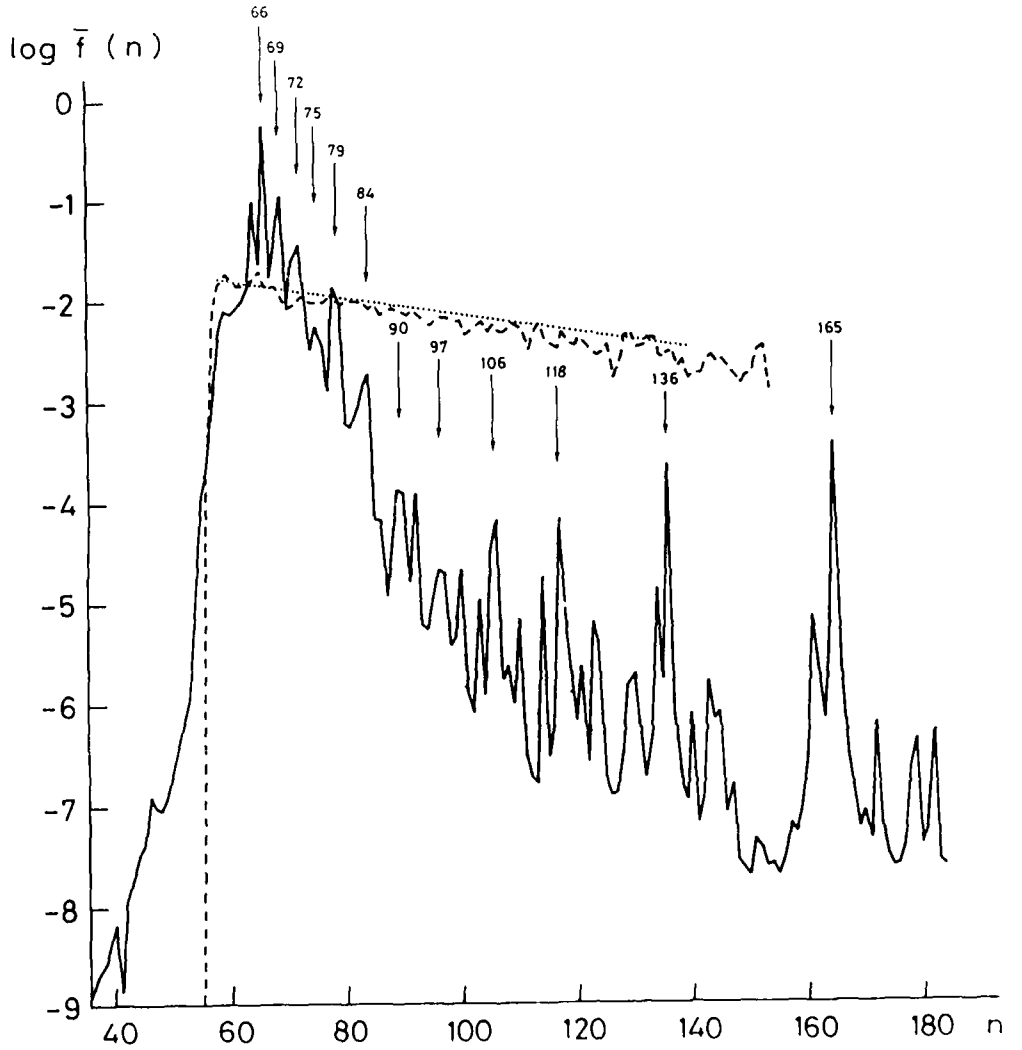
log $\bar{f}$ (n)
0
-1
-2
-3
-4
-5
-6
-7
-8
-9
40
60
80
100
120
140
160
180
n
66
69
72
75
79
84
90
97
106
118
136
165

FIG. 7b

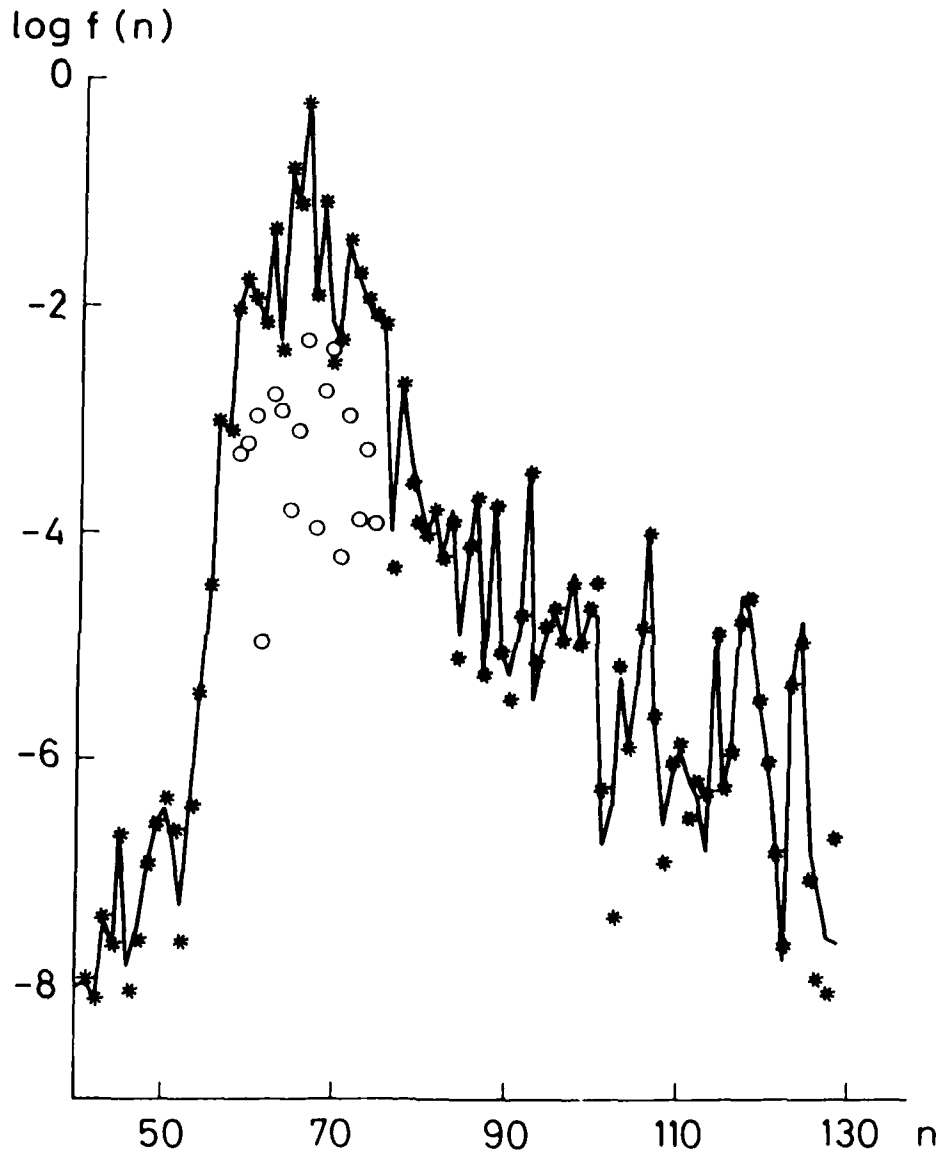

FIG. 7c

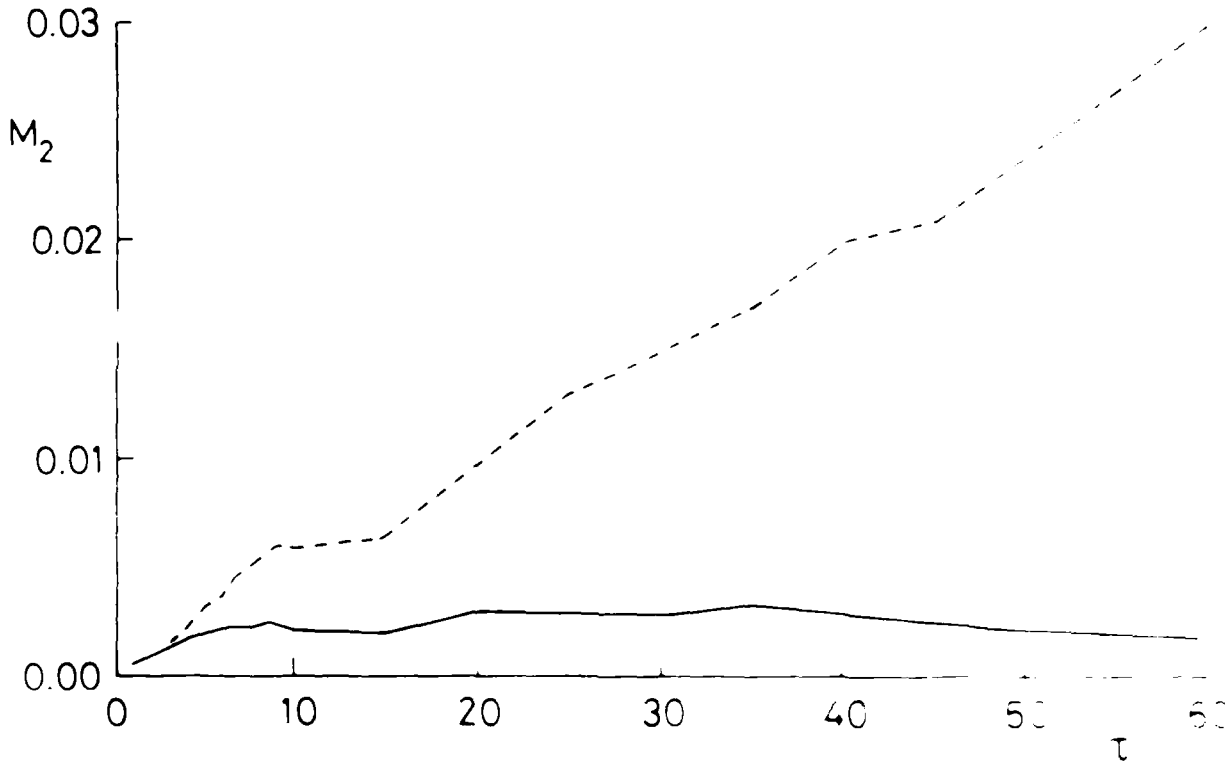
0.03
M_2
0.02
0.01
0.00
0
10
20
30
40
τ

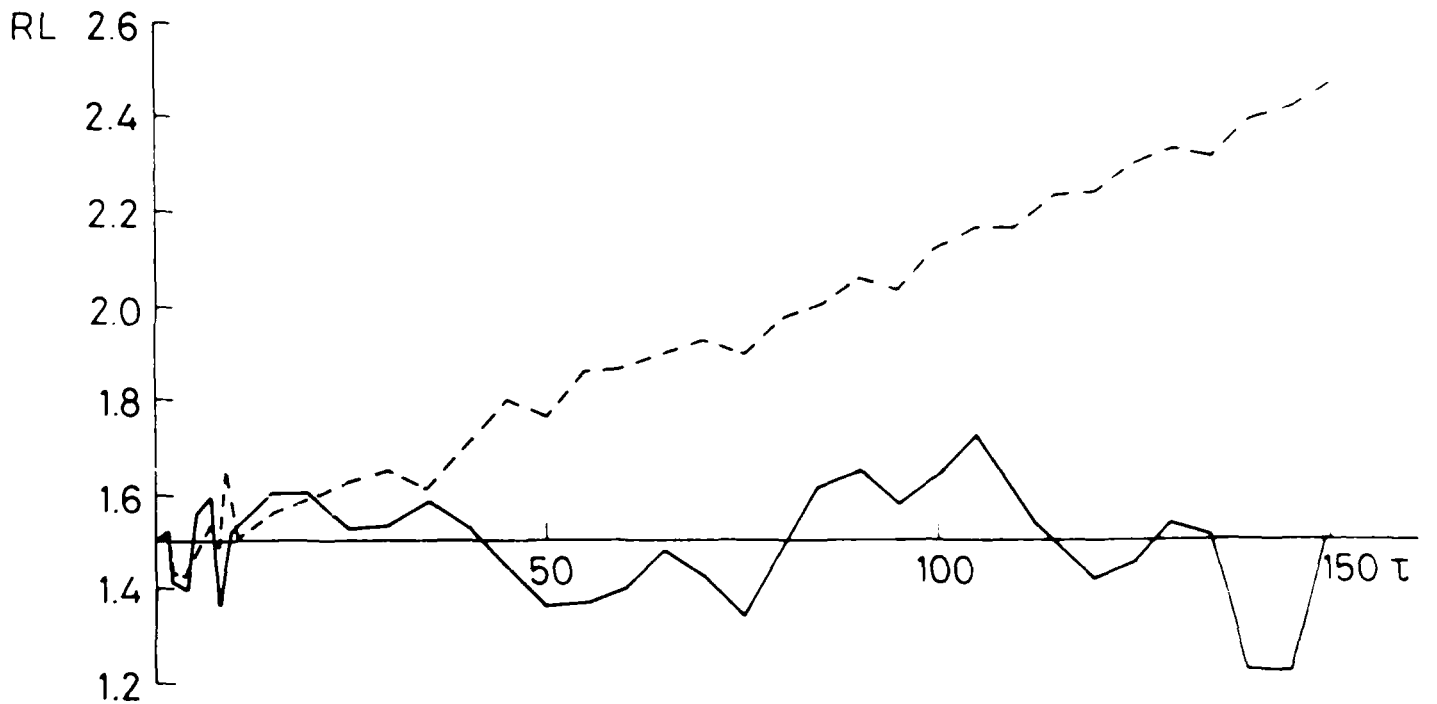
RL
2.6
2.4
2.2
2.0
1.8
1.6
1.4
1.2
50
100
150 τ

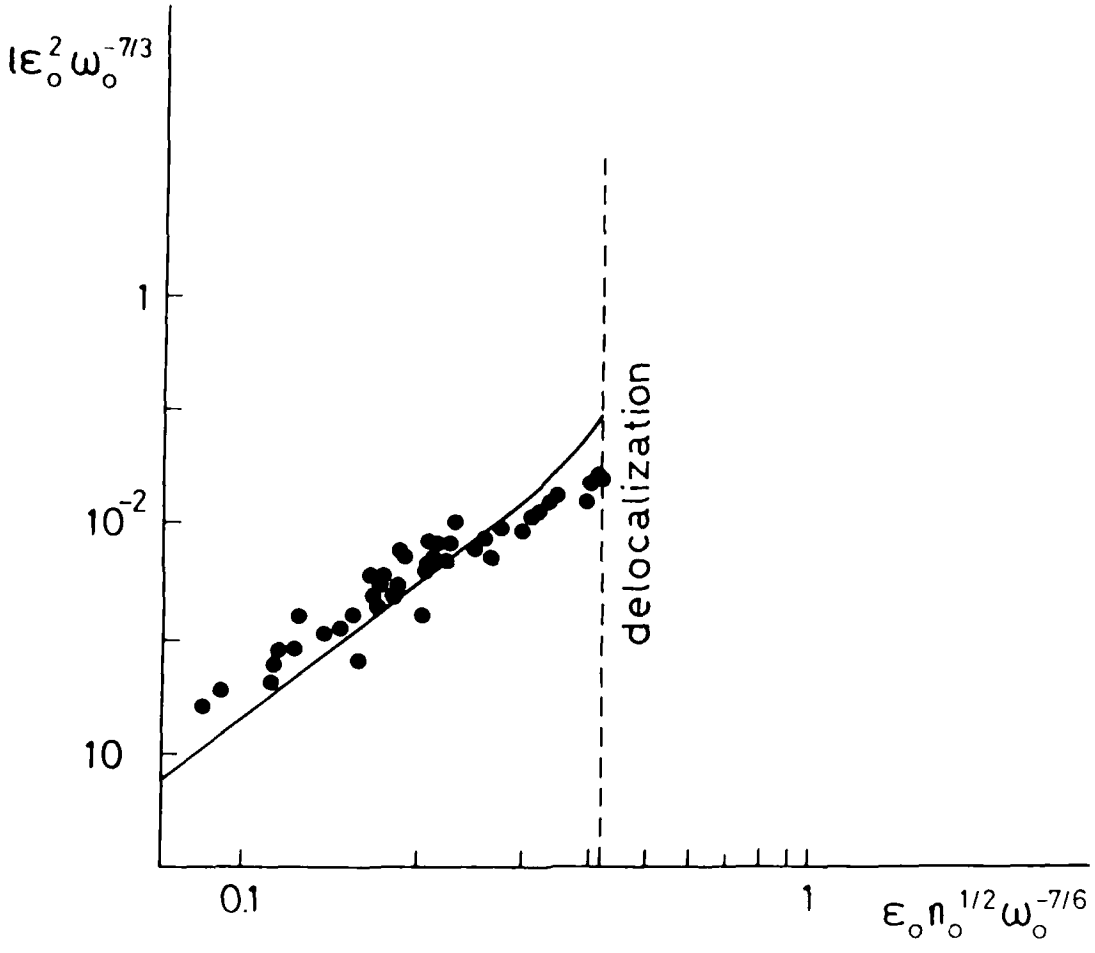
$I\varepsilon_o^2\omega_o^{-7/3}$
1
10^{-2}
10
delocalization
0.1
1
$\varepsilon_o n_o^{1/2}\omega_o^{-7/6}$

FIG. 10

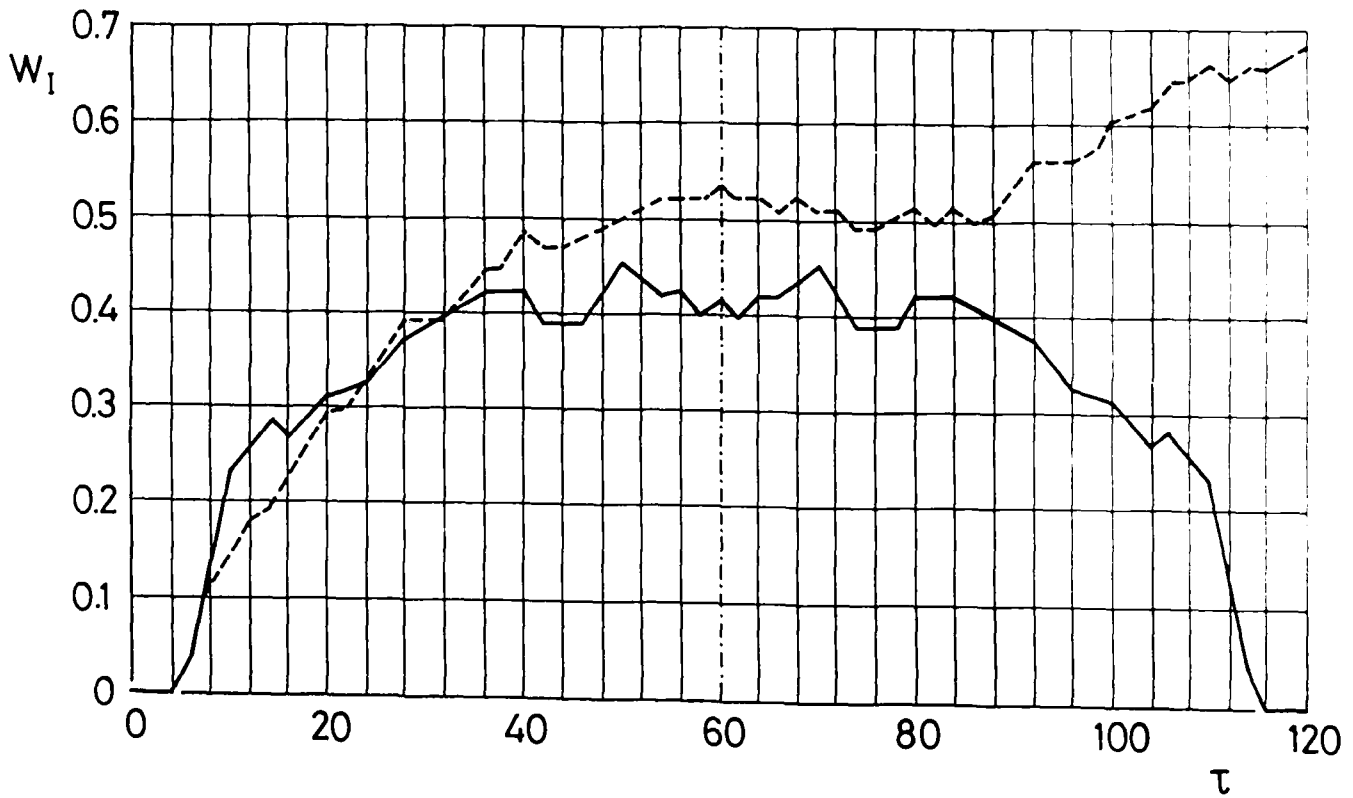

FIG. 12

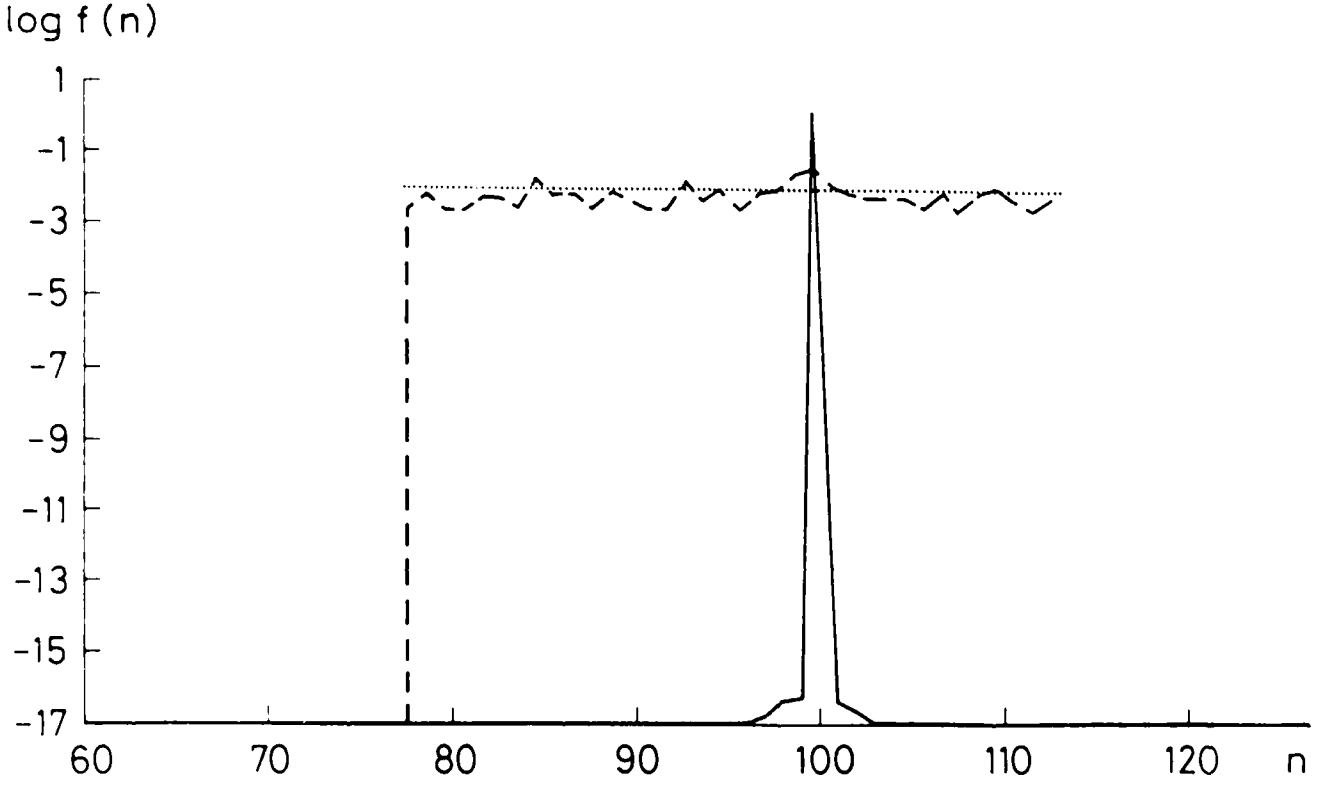

FIG. 11b

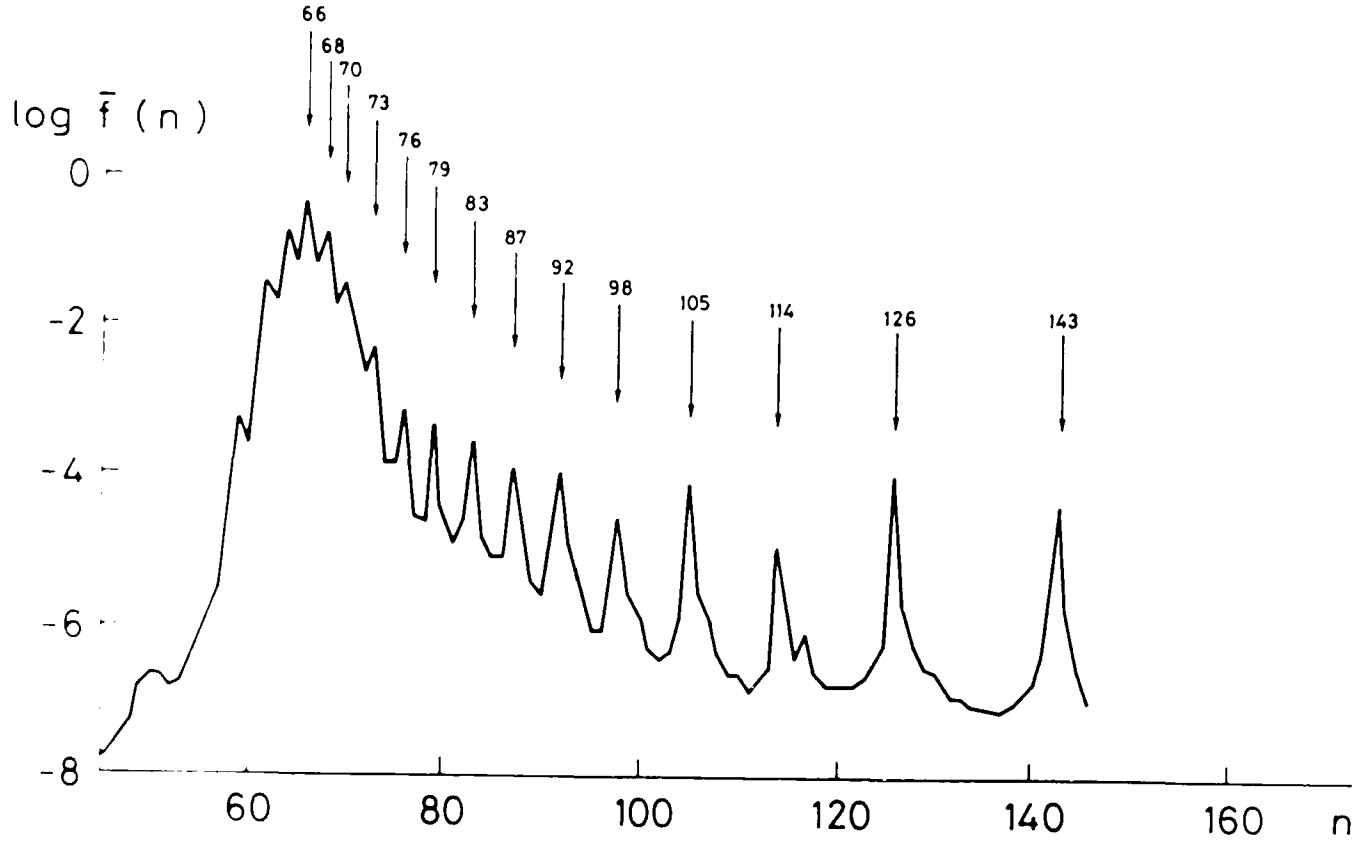
log $\bar{f}$ (n)
0
-2
-4
-6
-8
66
68
70
73
76
79
83
87
92
98
105
114
126
143
60
80
100
120
140
160
n

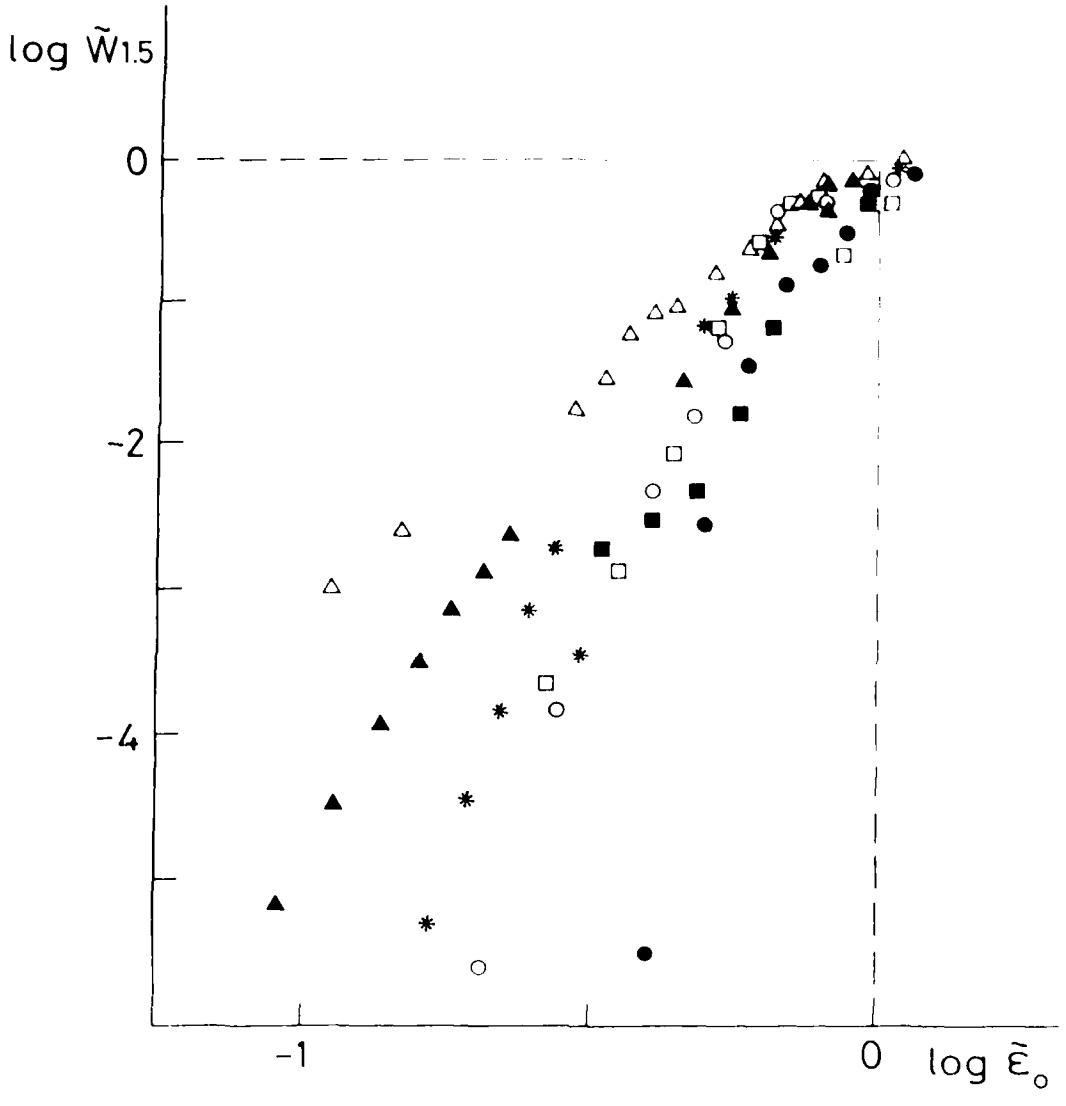
log $\tilde{W}_{1.5}$
0
-2
-4
-1
0
log $\tilde{\varepsilon}_o$

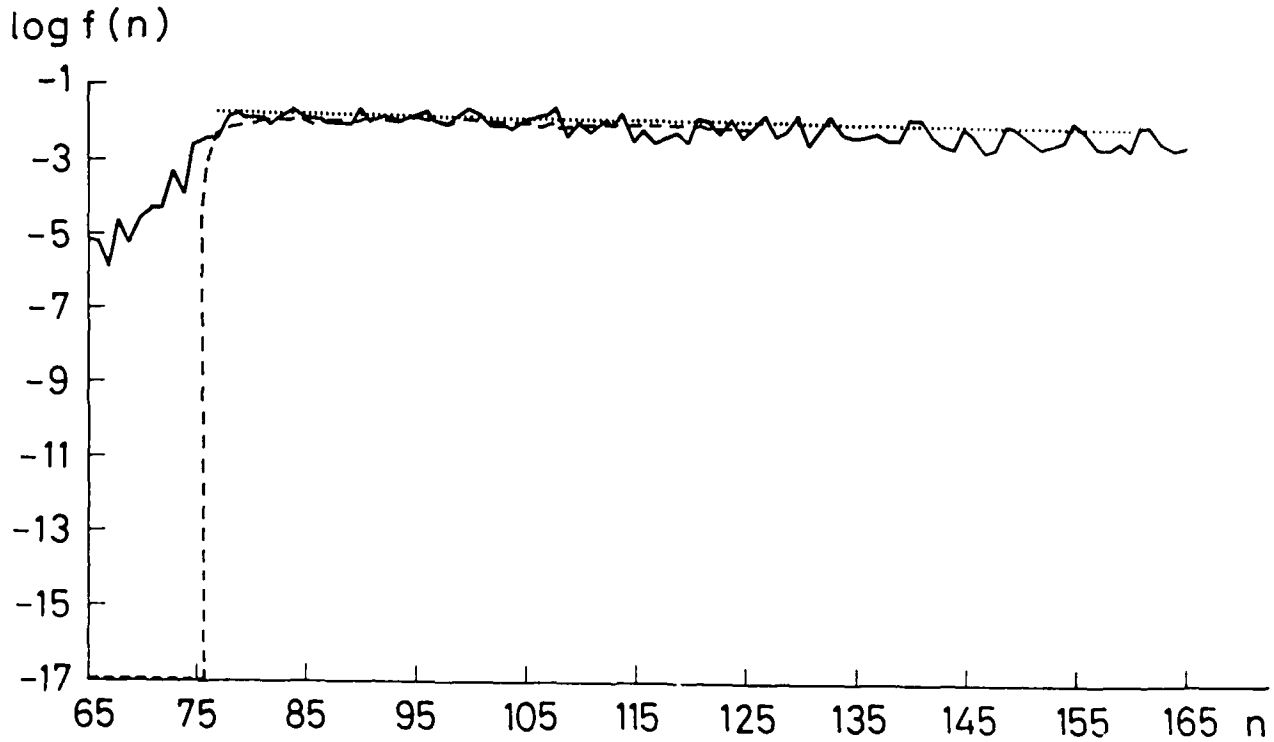

FIG. 11a

AD-A178 299 CHAOTIC BEHAVIOUR IN QUANTUM DYNAMICS(U) CENTRO DI CULTURA SCIENTIFICA A VOLTA COMO (ITALY) G CASATI ET AL. DEC 86 R/D-4183-PH DAJA45-83-C-0050 2/2

UNCLASSIFIED F/G 20/10 NL

END

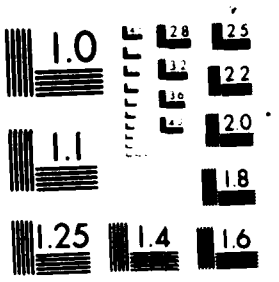
1.0
1.1
1.25
1.4
1.6
1.8
2.0
2.2
2.5

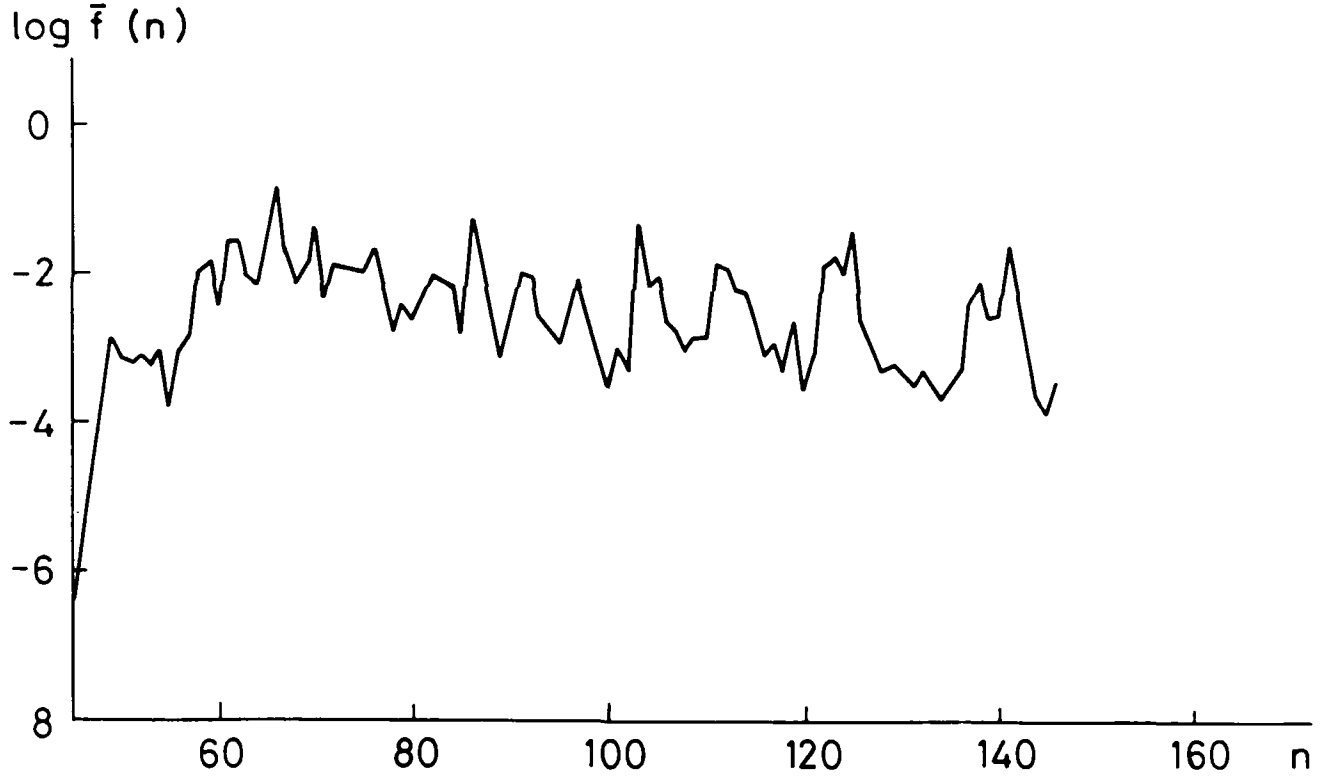

FIG. $14a_2$

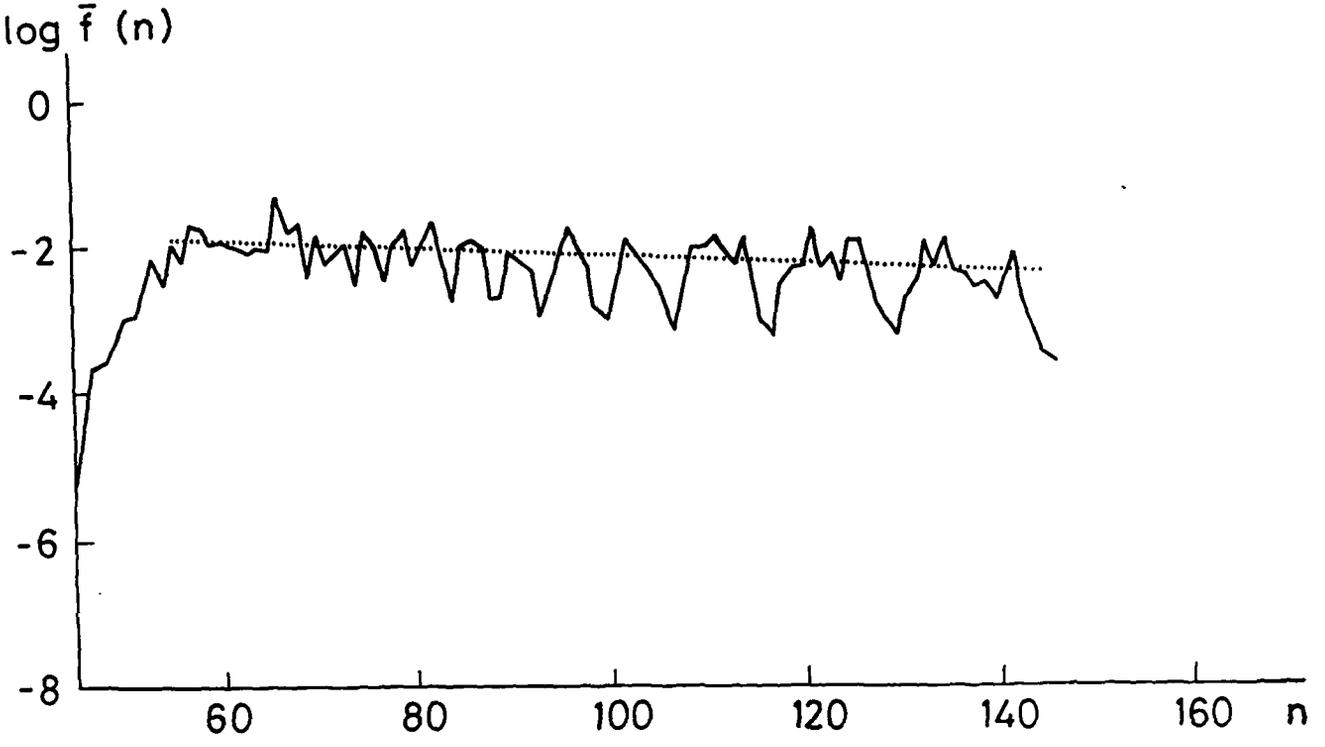

FIG. $14a_3$

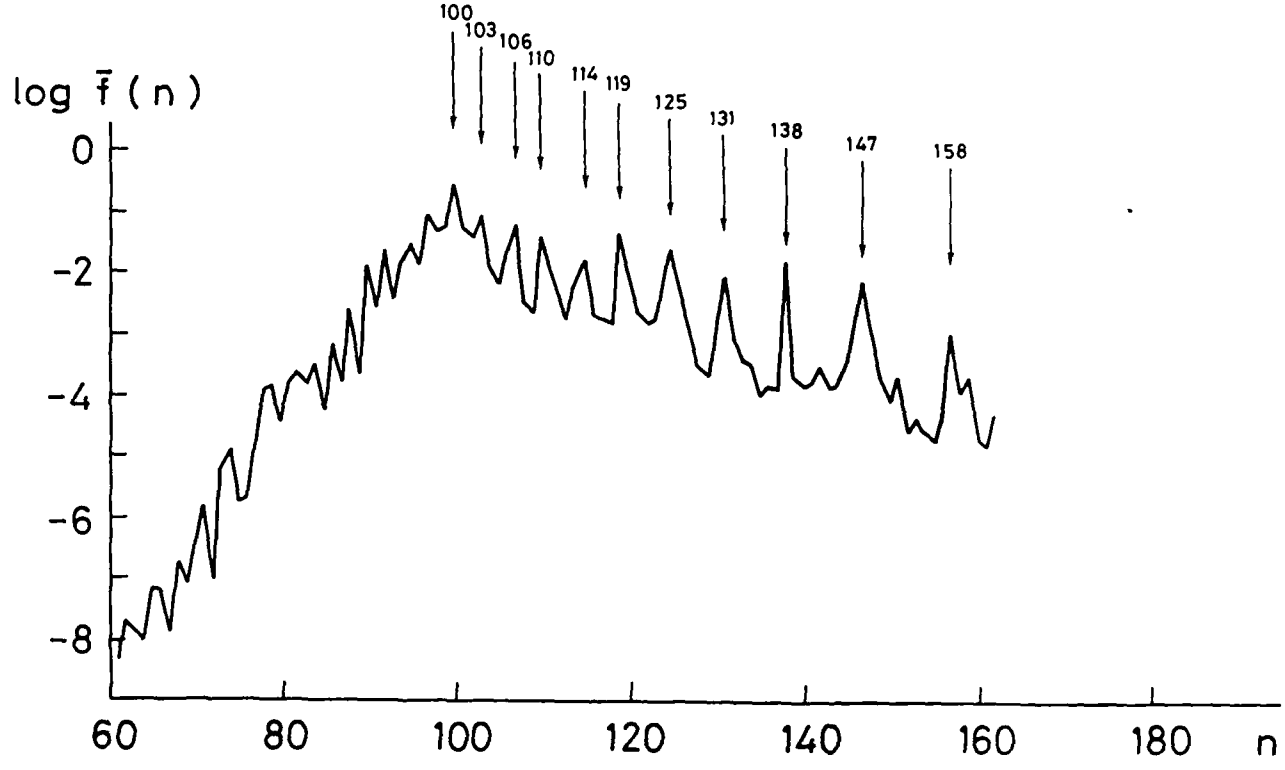
log $\bar{f}$ (n)
0
-2
-4
-6
-8
60
80
100
120
140
160
180
n
100
103
106
110
114
119
125
131
138
147
158

FIG. 14b$_1$

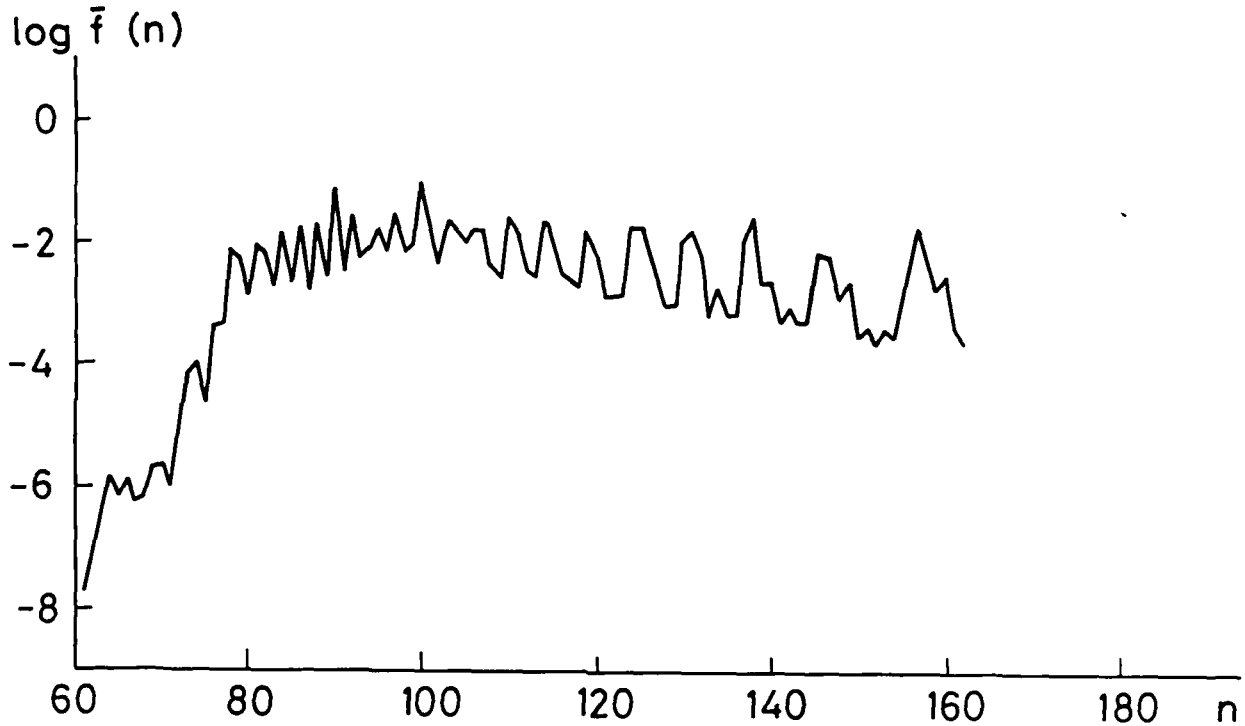

FIG. $14b_2$

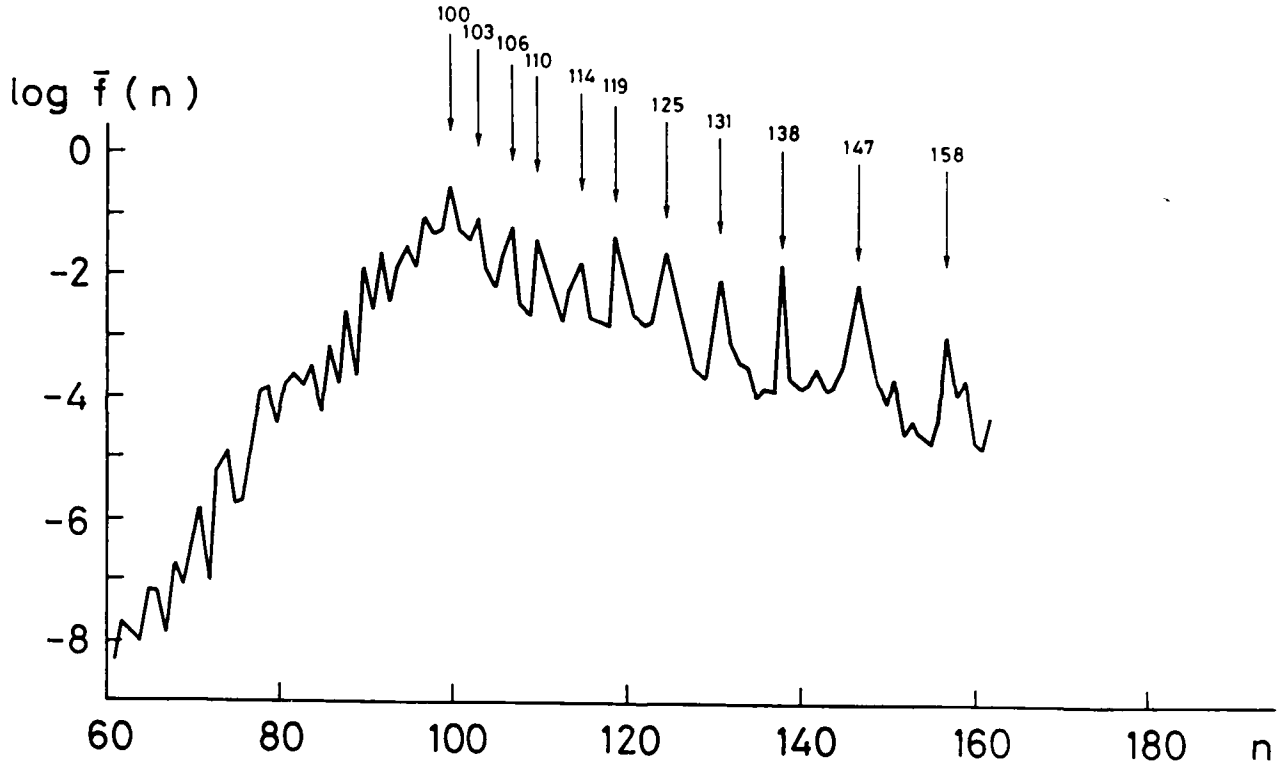
log $\bar{f}$ (n)
0
-2
-4
-6
-8
100
103
106
110
114
119
125
131
138
147
158
60
80
100
120
140
160
180
n

FIG. $14b_1$

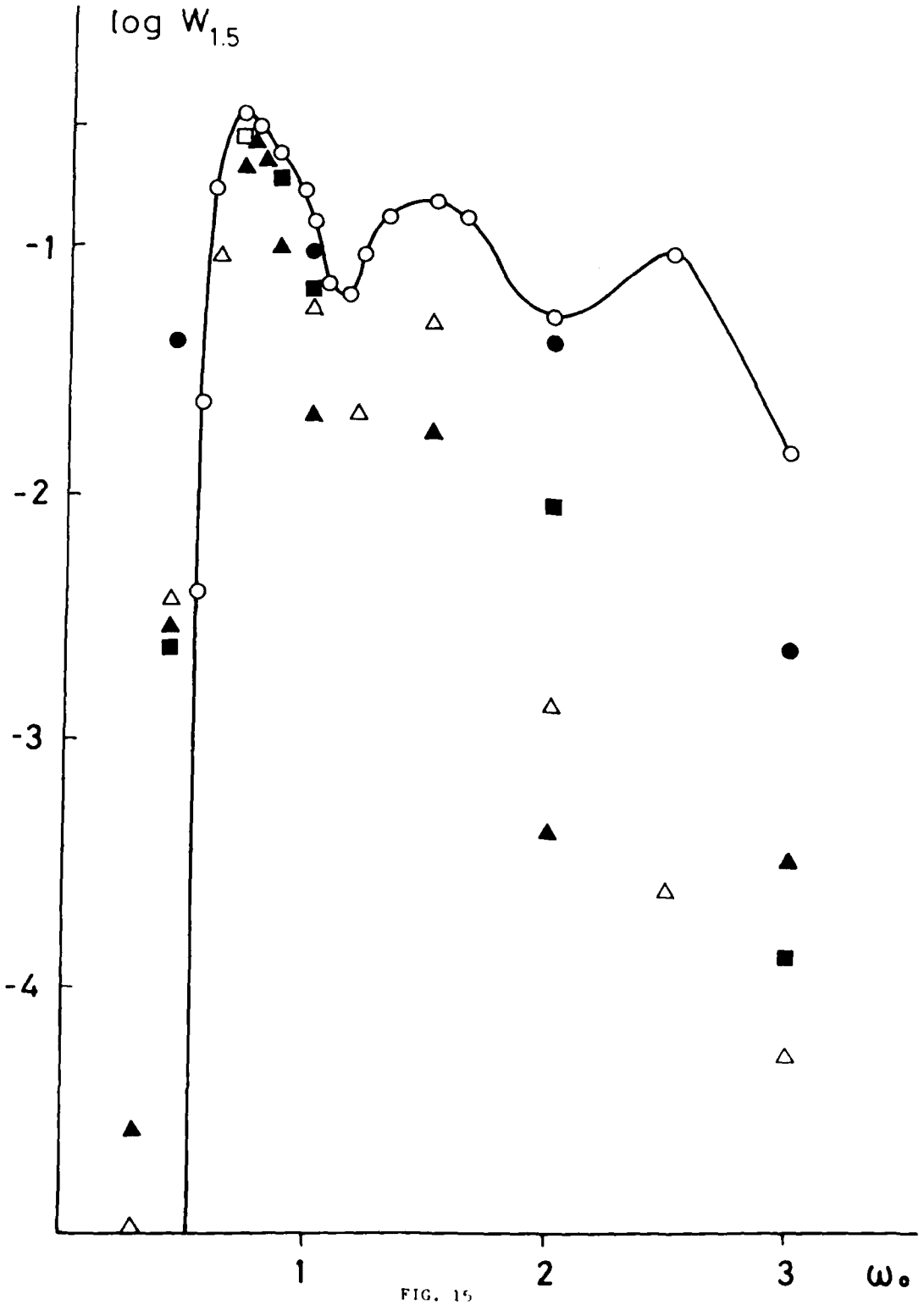

FIG. 15

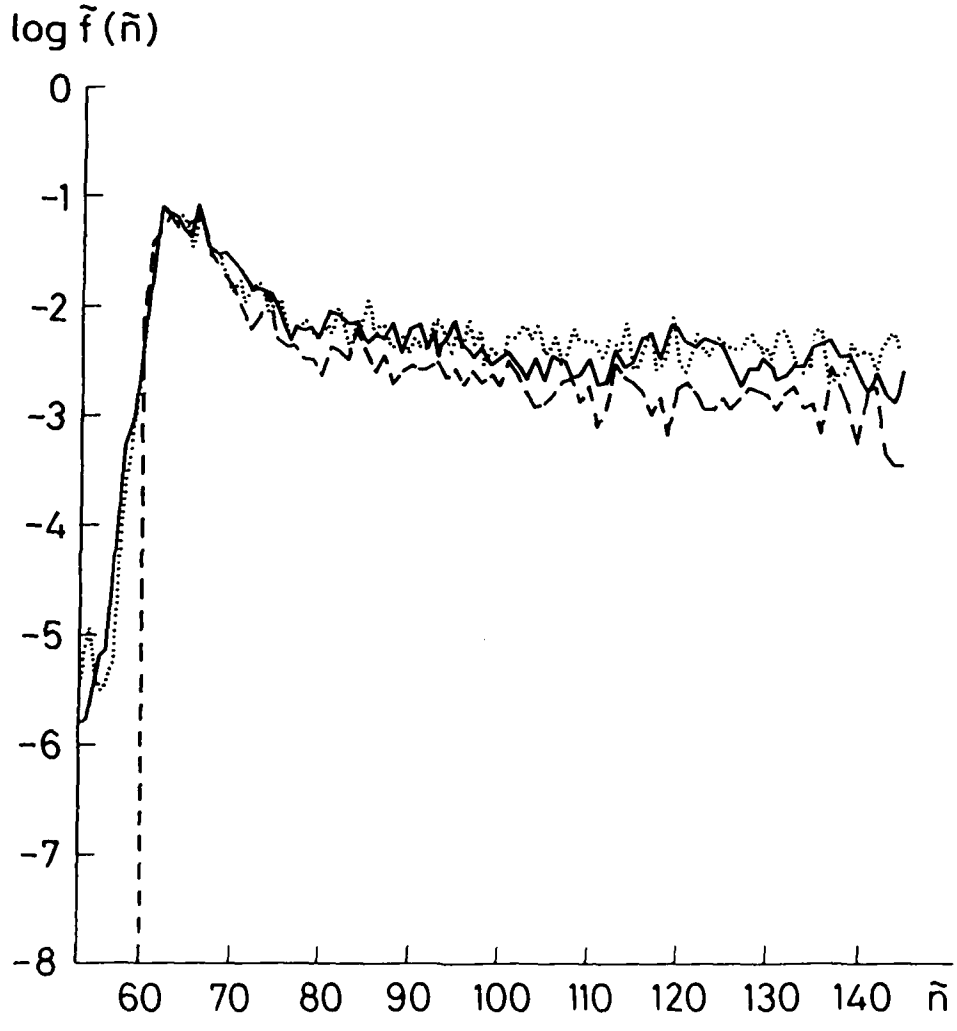

FIG. 10a

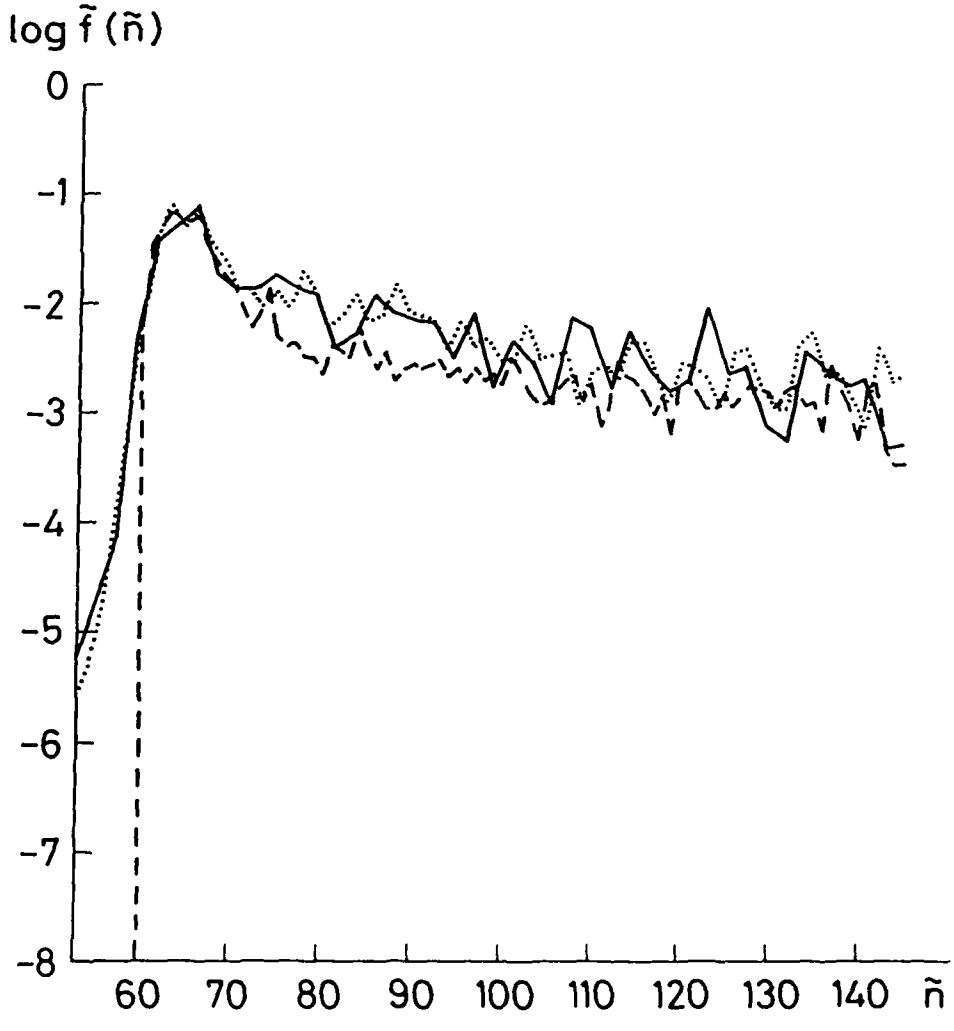

FIG. 16b

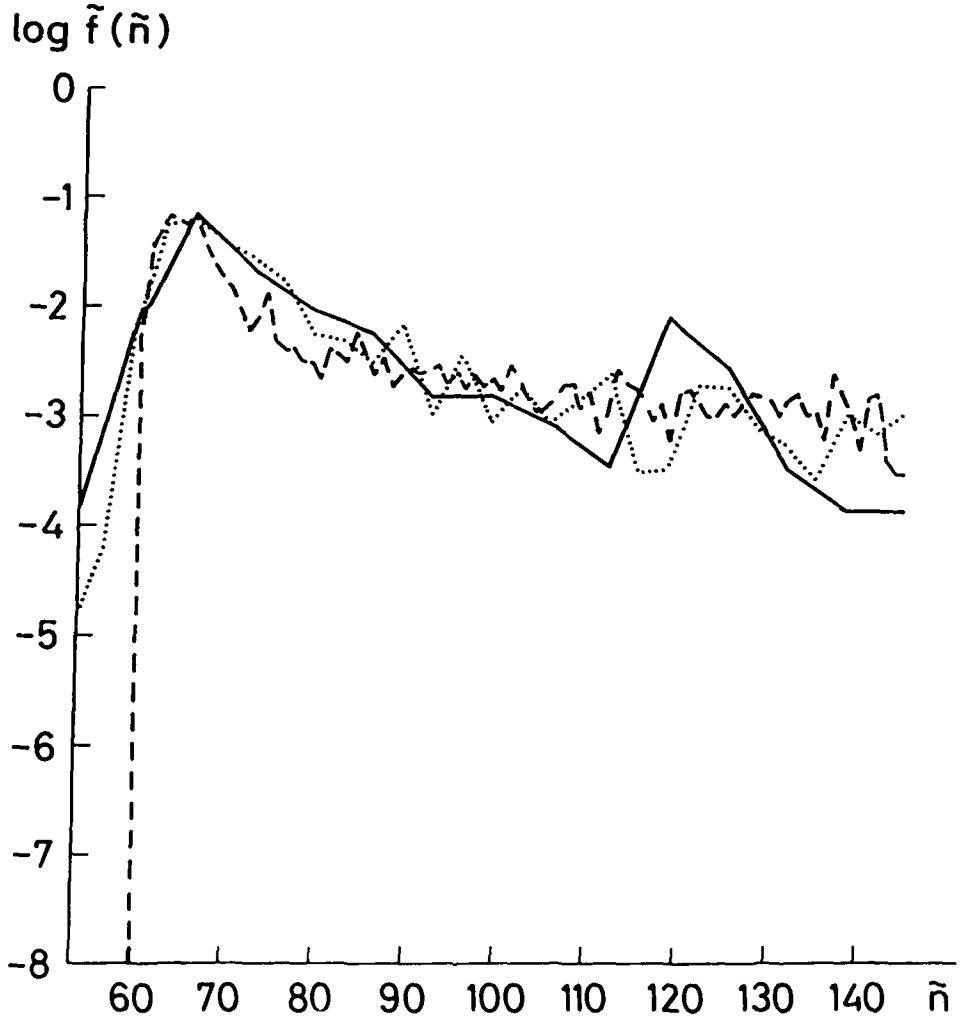

FIG. 16c

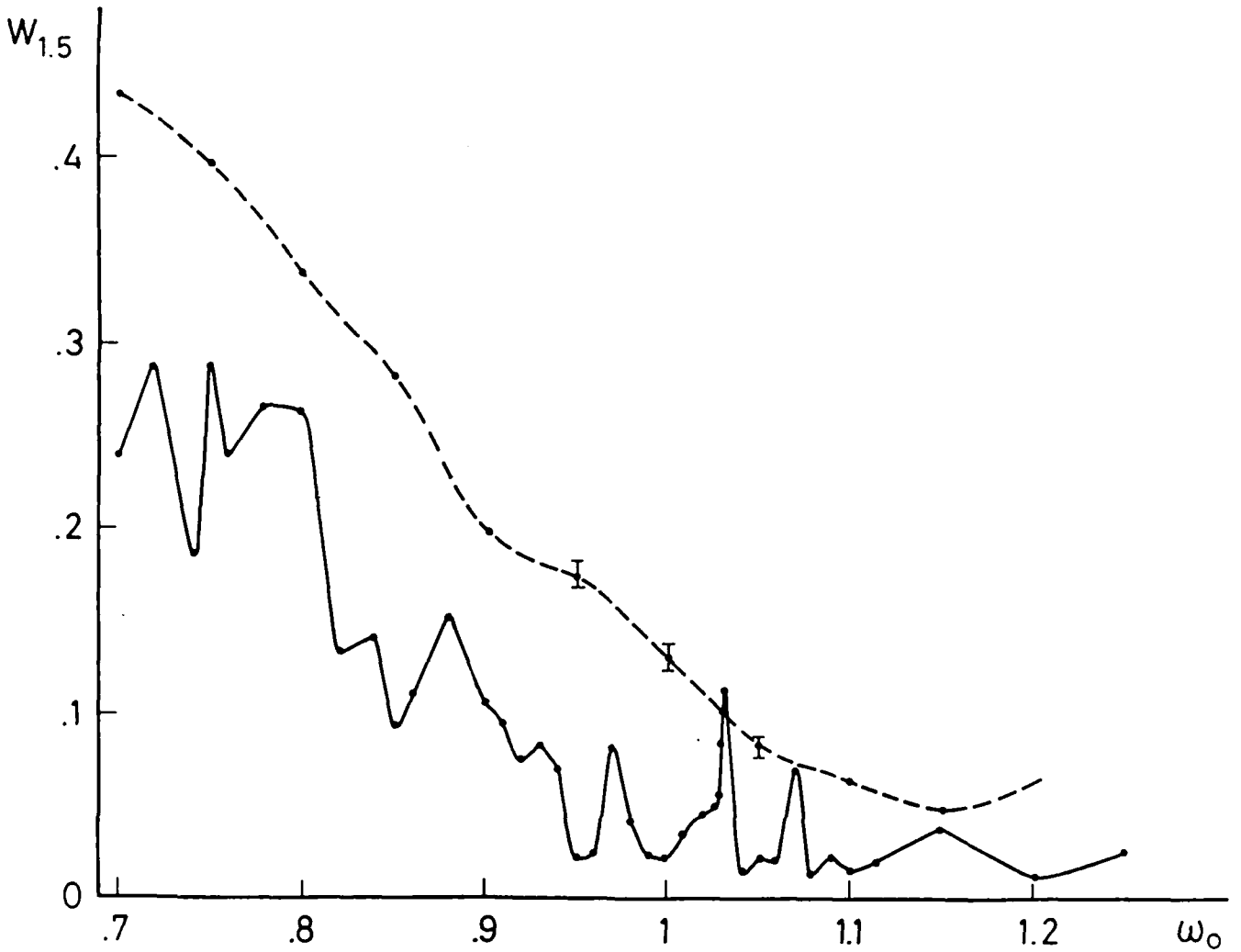

FIG. 17

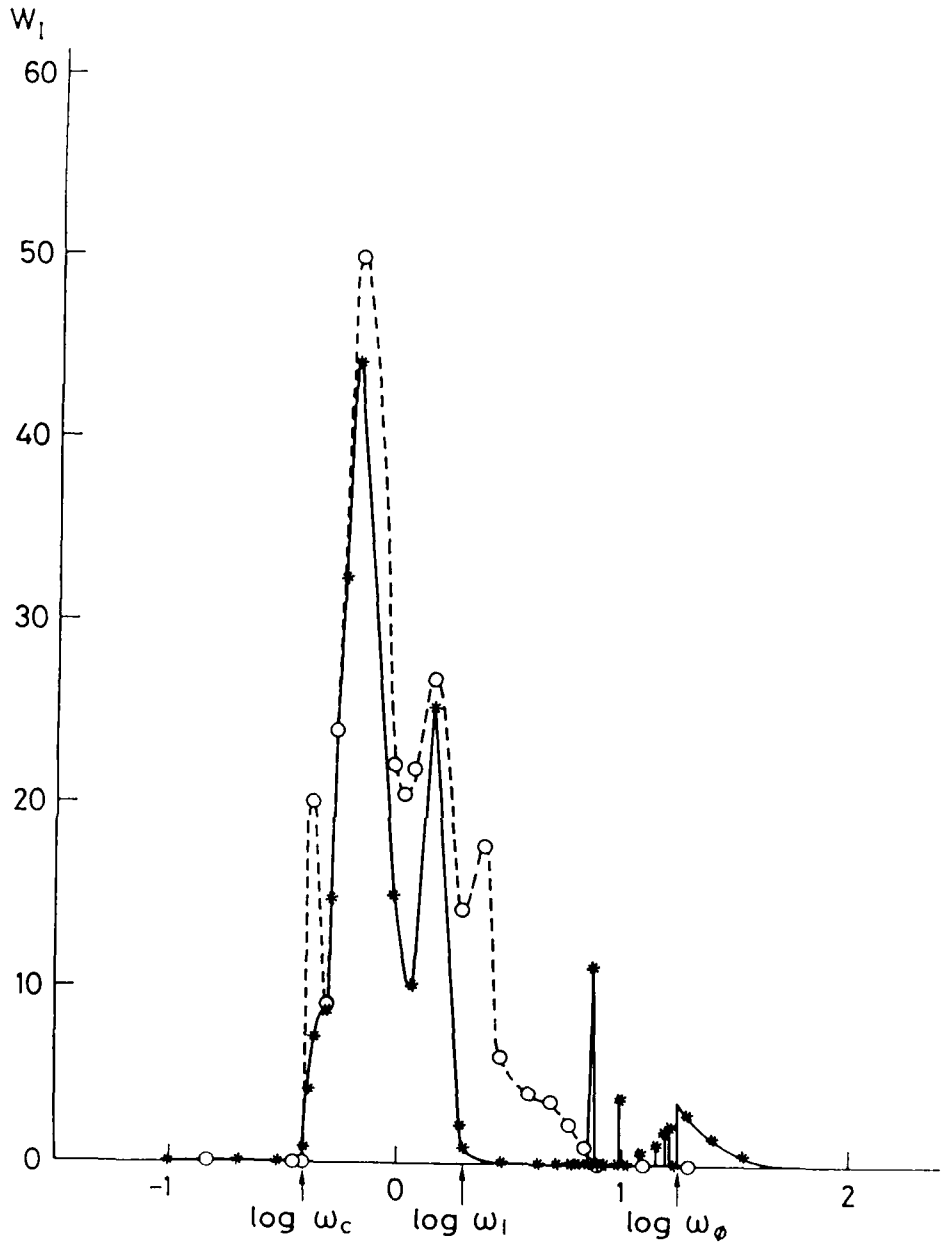
W_I
60
50
40
30
20
10
0
-1
0
1
2
log ω_c
log ω_I
log ω_ϕ

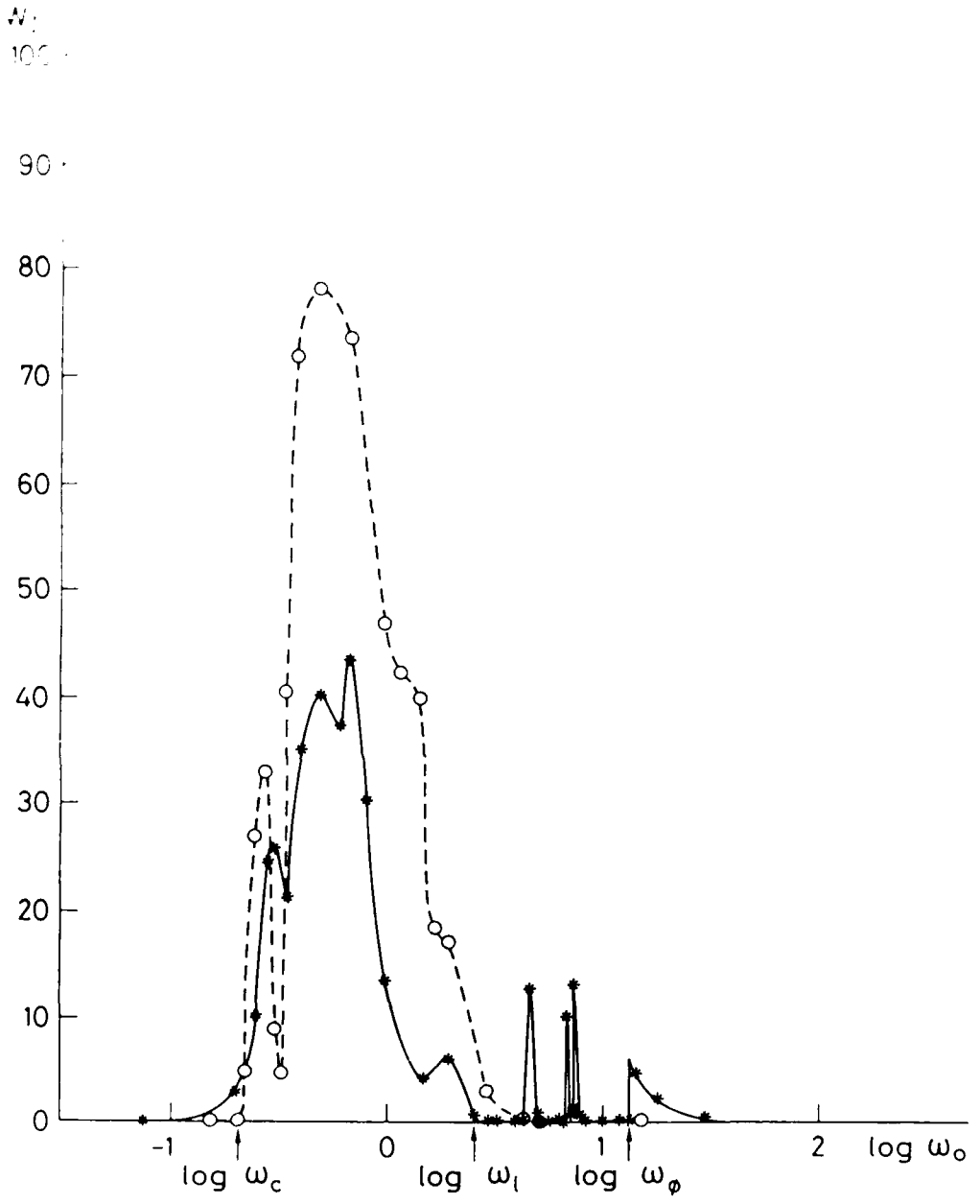

FIG. 19

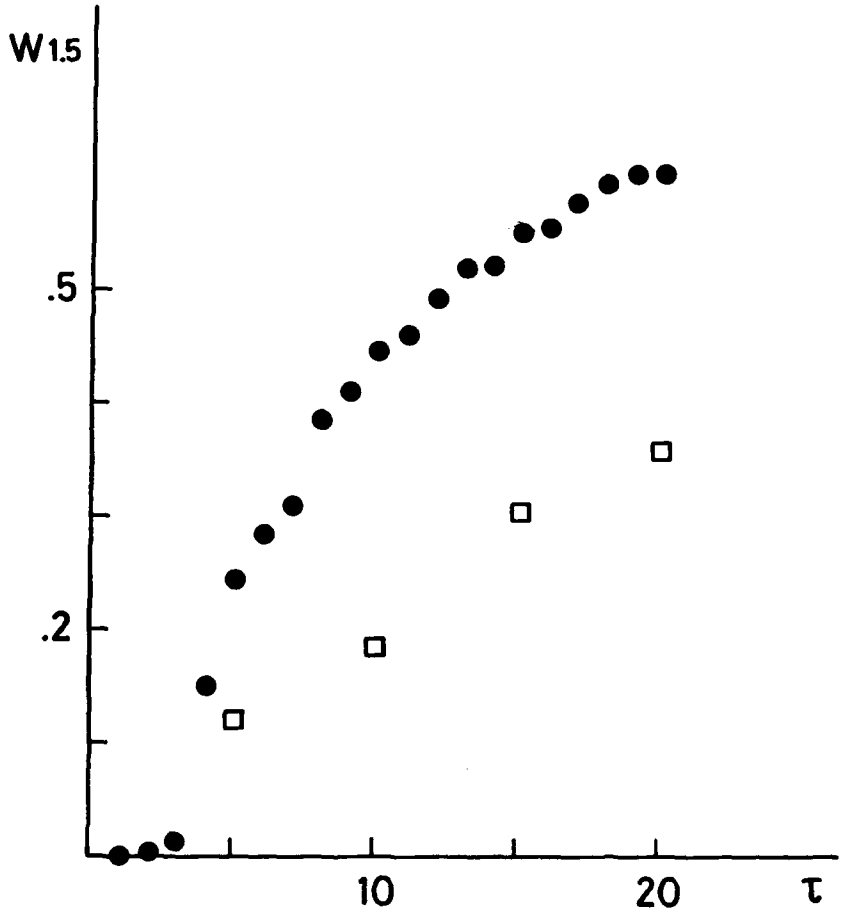

FIG. 20

END

DATE
FILMED

4-87